

RICE UNIVERSITY

Enhanced WLAN Performance with New Spectrum at 60  
GHz and Visible Light

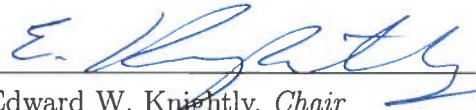
by

Sharan Naribole

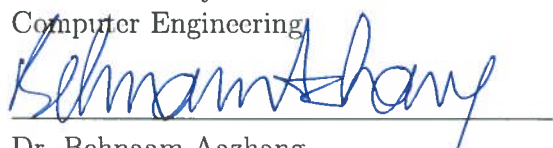
A THESIS SUBMITTED  
IN PARTIAL FULFILLMENT OF THE  
REQUIREMENTS FOR THE DEGREE

Doctor of Philosophy

APPROVED, THESIS COMMITTEE:



Dr. Edward W. Knightly, *Chair*  
Sheafor-Lindsay Professor of Electrical &  
Computer Engineering



Dr. Behnaam Aazhang  
J.S. Abercrombie Professor of Electrical &  
Computer Engineering



Dr. T.S. Eugene Ng  
Professor of Computer Science and Electrical & Computer Engineering



Dr. Lin Zhong  
Professor of Electrical & Computer Engineering

HOUSTON, TEXAS  
MAY 2018

## ABSTRACT

Enhanced WLAN Performance with New Spectrum at 60 GHz and Visible Light

by

Sharan Naribole

To enhance the WLAN operation at sub-6 GHz, research has been directed towards utilizing new spectral bands including millimeter waves (60 GHz) and visible light spectrum. The 7-14 GHz unlicensed band at 60 GHz can enable multi-gigabit rate applications including live HD video streaming, virtual reality, etc. Visible light communication (VLC) is a key emerging energy-efficient communication technology that dual purposes LED-based lighting infrastructure for both illumination and communication. Although both these bands have the potential to enhance WLAN performance, each of them possesses unique physical properties that hinder some existing services readily available in sub-6 GHz bands. First, the strong directionality required at 60 GHz precludes serving all clients in a multicast group with a single transmission and instead is comprised of a sequence of beam-formed transmissions that together cover all multicast group members. I design, implement, and experimentally evaluate scalable directional multicast (SDM) as a technique to address the challenges imposed by directional communication for a scalable multicast service at 60 GHz. Second, the wide coverage and relatively high transmit power realized by the VLC downlink to satisfy the illumination objective is problematic to realize on the uplink. I design, analyze, and implement

LiRa, a Light-Radio WLAN that fuses light and radio capabilities in an integrated system design without requiring mobile devices to emit light or infrared. I design an uplink control channel for LiRa that is Wi-Fi compliant, has a controllable impact on airtime taken from legacy Wi-Fi clients, and efficiently scales with increasing VLC user population. Third, contention-based uplink radio access might lead to significant degradation in airtime efficiency and energy efficiency as the time spent *awake* by the radio is dependent on the network traffic conditions. I design and evaluate LiSCAN, a VLC uni-directional control channel that enables virtual full-duplex contention-free operation of uplink radio access. My analysis shows that LiSCAN can provide significant improvements in the radio airtime efficiency, the sessions delivered with pre-defined service quality requirements and energy savings.

## ACKNOWLEDGEMENTS

A great number of people have contributed to the production of this dissertation. I owe my gratitude to all those people who have made this dissertation possible and because of whom my PhD experience has been one that I will cherish forever.

My deepest gratitude is to my advisor, Dr. Edward Knightly. I have been amazingly fortunate to have an advisor who gave me the freedom to explore on my own, and at the same time the guidance to recover when my steps faltered. Dr. Knightly taught me how to question thoughts and express ideas. His patience and support helped me overcome many crisis situations and finish this dissertation. I hope that one day I would become as good an advisor as Dr. Knightly has been to me.

I would also like to express my gratitude to the members of my committee, Dr. Behnaam Aazhang and Dr. Lin Zhong, and Dr. Eugene Ng for their time and effort in reviewing my work, and for their invaluable support throughout my PhD thesis.

A special thanks to Rice Network Group (RNG) members Adriana, Xu, Yasaman, Kumail, Ryan, and Riccardo for providing invaluable guidance and inspiration to succeed in my PhD defense. I would like thank the rest of the RNG group members and department friends for reviewing my work and providing excellent feedback during the practice sessions.

Many friends have helped me stay sane through these two years particularly the extended 8-monkeys group and rock climbing/biking group.

Their support and care helped me overcome setbacks and stay focused on my graduate study. I greatly value their friendship and I deeply appreciate their belief in me. I am also grateful to the Indian Students at Rice (ISAR) organization that helped me adjust to a new country.

Most importantly, none of this would have been possible without the love and patience of my family. My immediate family to whom this dissertation is dedicated to, has been a constant source of love, concern, support and strength all these years. I would like to express my heart-felt gratitude to my family. My extended family has aided and encouraged me throughout this endeavor. I warmly appreciate the generosity and understanding of my extended family.

# Contents

---

<b>Abstract</b>	ii
<b>Acknowledgements</b>	iv
<b>1 Introduction</b>	1
1.1 Scalable Directional Multicast at 60 GHz (SDM) . . . . .	2
1.2 VLC with Wi-Fi Uplink . . . . .	4
1.3 VLC Uni-directional Control Channel . . . . .	6
<b>2 SDM: Scalable Directional Multicast in Highly-Directional 60 GHz WLANs</b>	11
2.1 Design Overview . . . . .	11
2.2 Scalable Multicast Training . . . . .	16
2.3 Scalable Multicast Beam Grouping . . . . .	23
2.4 SDM Implementation and Data Collection . . . . .	29
2.5 Experimental Evaluation . . . . .	38
<b>3 LiRa: a WLAN architecture for Visible Light Communication with a Wi-Fi uplink</b>	46
3.1 LiRa Architecture . . . . .	46
3.2 A Scalable Feedback Channel for Light . . . . .	50
3.3 LiRa Implementation . . . . .	55
3.4 Experimental Evaluation . . . . .	61

<b>4 LiSCAN: Visible Light Uni-Directional Control Channel for Uplink</b>	
<b>Radio Access</b>	<b>76</b>
4.1 Background . . . . .	76
4.2 LiSCAN Architecture . . . . .	77
4.3 LiSCAN Design . . . . .	80
4.4 LiSCAN Simulation Framework . . . . .	87
4.5 LiSCAN Evaluation . . . . .	90
<b>5 Related Work</b>	<b>95</b>
5.1 Scalable Directional Multicast at 60 GHz . . . . .	95
5.2 Visible Light Communication WLAN with Wi-Fi Uplink . . . . .	97
5.3 VLC Uni-Directional Control Channel for contention-free radio access	99
<b>6 Summary</b>	<b>101</b>
<b>References</b>	<b>103</b>
<b>7 Appendix</b>	<b>110</b>
7.1 Appendix A . . . . .	110

## List of Figures

---

1.1	Radio awake time on sensor. . . . .	8
2.1	(a) An indoor conference room scenario where multicast group 1 comprising of clients A, B and C wins the contention and the AP selects two beams for the data transmission. (b) The different stages of our multicast timeline model for the scenario considered in (a). . . . .	12
2.2	An example codebook tree construction. . . . .	18
2.3	A basic traversal. . . . .	19
2.4	Imperfect codebook traversal. . . . .	20
2.5	SDM's sibling training to address non-monotonicity. . . . .	22
2.6	(a) 60 GHz system signal and control flow. (b) Map of the room used for data collection. . . . .	30
2.7	(a) The correlation in peak directions for different AP beamwidth at a fixed client location and orientation. (b) The diversity in the peak directions for different client orientations at a fixed location with 7 degree horn at the AP. . . . .	32
2.8	Indoor measurements of receiver rotation. The receiver was placed between 1 to 5 meters from the transmitter in steps of 1 meter. <i>Not drawn to scale.</i> . . . . .	33
2.9	Radial translation of the receiver to characterize the effect of transmitter-receiver beam misalignment. The transmitter is fixed at 0 degree azimuth while the receiver moves and constantly points at the transmitter. <i>Not drawn to scale.</i> . . . . .	34

2.10	(a) Measured signal strength loss when the receiver rotates its beam away from the transmitter while remaining in the center of the transmit beam (2 meter distance). (b) Radial translation of the receiver to characterize the effect of transmitter-receiver beam misalignment. The transmitter is fixed at 0 degree azimuth orientation while the receiver moves and constantly points at the transmitter. . . . .	34
2.11	Monotonicity. . . . .	37
2.12	Deviation from Best Beam from exhaustive search. . . . .	38
2.13	Training Overhead. . . . .	41
2.14	Beam Grouping Efficiency. . . . .	41
2.15	Beam Group Computation time. . . . .	43
2.16	Throughput incorporating the overhead in training and beam grouping. . . . .	43
3.1	Example LiRa scenario. . . . .	47
3.2	LiRa's protocol stack and data flow. . . . .	49
3.3	Simplified LiRa timeline illustrating the combination of ASMA trigger to the AP, trigger message transmitted by the AP and uplink VLC ARQ feedback transmissions. . . . .	51
3.4	VLC single high range sensor. . . . .	56
3.5	VLC receiver array with 4 photo diodes. . . . .	57
3.6	Smart LED-based experiment setup. . . . .	57
3.7	Illustration of experimental setup for VLC measurements. . . . .	58
3.8	Radio link Implementation Setup . . . . .	59
3.9	Downlink coverage provided by LiRa as a function of client rotation. (a) Roll axis (b) Pitch axis. . . . .	63
3.10	Uplink coverage experiments (a) Setup where IR stands for infrared. (b) pureLiFi client unit. . . . .	64
3.11	Uplink throughput of pureLiFi versus orientation angle. . . . .	65
3.12	ASMA's trigger time impact on response delay. . . . .	66
3.13	Wi-Fi traffic impact on LiRa's response delay: 1 flow and 3 flows. . .	68
3.14	Computed airtime used by LiRa for varying access delay between expiration of the trigger timer and transmission of the feedback trigger message: (a) zero delay (b) 1.3 ms delay. . . . .	70
3.15	LiRa's feedback trigger time impact on Wi-Fi throughput degradation using over-the-air measurements. . . . .	72

3.16	Response Delay performance of Per-Client Contention in different Wi-Fi channels.	73
3.17	Wi-Fi throughput degradation comparison between LiRa and Per-Client Contention model.	74
4.1	802.11 contention-free period timeline.	77
4.2	Example LiSCAN scenario.	78
4.3	LiSCAN architecture and polling traffic flow.	79
4.4	LiSCAN contention-free period timeline.	80
4.5	Mean channel access delay vs traffic burst arrival rates for varying sensor ratios.	91
4.6	Aggregate throughput vs traffic burst arrival rates for varying sensor ratios.	92
4.7	Mean energy consumption per active sensor in LiSCAN vs traffic burst arrival rates for varying sensor ratios	93
4.8	Mean energy consumption per active sensor vs traffic burst arrival rates for varying ratios of sensors with traffic.	94

## **List of Tables**

---

2.1	Description of notations used in the problem formulation and algorithms description . . . . .	24
4.1	802.15.7 frame timing and data rates. . . . .	85

## CHAPTER 1

# Introduction

---

To enhance the WLANs operating at sub-6 GHz bands, research has been directed towards utilizing new spectral bands including millimetre waves (60 GHz) and visible light spectrum. First, unlicensed access in the 7-14 GHz wide band available at 60 GHz has the potential to enable gigabit rate applications [1, 2]. Second, visible Light Communication (VLC) is a key emerging communication technology that dual purposes LED-based lighting infrastructure for both illumination and communication. In particular, ceiling-mounted luminaries can modulate lighting in a manner unnoticeable to the human eye (i.e., flicker free) for reception at mobile devices fitted with low-cost photo diodes integrated with their casing surfaces. The proliferation of VLC-enabled luminaries promises not only support for low-rate IoT applications [3, 4] but also Gigabit rate wireless networking [5, 6].

Although both these bands have the potential to possess enhance WLAN performance, each of them possesses unique physical properties that hinder some existing services readily available in sub-6 GHz operation. The gigabit rate communication enabled at 60 GHz [7] makes it ideal for new broadcast scenarios including high-definition video streaming in hotspots, conferences, smart classrooms and also wireless 3D multi-player gaming [8, 9]. Unfortunately, the increased path loss (over 20 dB) at

60 GHz severely limits the data rate and range when an omnidirectional broadcast is performed as in legacy bands. In contrast to 60 GHz communication, VLC has inherent broadcast capability as the AP can broadcast data over multiple LED luminaires. Unfortunately, the wide coverage and relatively high transmit power realized by the downlink to satisfy the illumination objective is problematic to realize on the uplink: even if a mobile client is fitted with infrared LEDs, providing wide aperture long-range transmission is ill-suited to mobile devices' form factor and energy constraints [10, 11]. Hence, the VLC is restricted to a uni-directional downlink channel.

In this thesis, I address the above challenges in 60 GHz and VLC that hinder services readily available in legacy bands. I design, experiment and evaluate novel system architectures and protocols to enhance WLANs leveraging the new spectrum capabilities. The thesis contributions are as follows:

## 1.1 Scalable Directional Multicast at 60 GHz (SDM)

Because using the widest possible beam at 60 GHz severely limits the data rate and range, the AP needs to partition the multicast group into multiple subsets and select an appropriate beam and data rate to serve each subset. Our objective is to maximize the throughput delivered to multicast groups incorporating the overhead in beam training and the subsequent selection of the **beam group**, or group of beams covering all of the group's clients for data transmission. Each beam is defined via a multi-level codebook in which the codebook level corresponds to beamwidth and the codes within a level span different directions [12, 13]. In particular, we propose **Scalable Directional Multicast (SDM)**, the first 60 GHz multicast protocol to incorporate overhead in training and beam grouping, and make the following contributions:

**Scalable Training.** Beam training enables the AP to obtain per-client per-beam RSSI measurements for the multicast group members. To ensure that beam

---

training only occurs when necessary, SDM precedes each multicast transmission with a multicast group announcement and a short packet exchange with each client. Training is only invoked if a group member fails to respond. To limit overhead, we utilize a tree-based codebook structure that links the beams of different levels based on their spatial similarity.

In an idealized propagation environment with line of sight (LOS) to the AP for all codebook entries, one could simply find the strongest beam at each level from client feedback and use only its children for the next level training. For a general scenario, SDM’s key strategy is to first perform training at the finest beam level, thus ensuring every client is reachable and has at least one beam with high directivity gain. Then, SDM performs a pruned tree traversal up the tree in wider beam levels. For the pruned set of beams to be used for each level’s training, SDM selects the parents of the strongest beams of the previous level. In this way, SDM obtains sufficient, but not exhaustive, training that we will show enables near-optimal beam grouping.

**Scalable Beam Grouping.** Using the training information, SDM next selects the beam group. First, we formulate an optimization problem of minimizing the data sweep time, i.e., the time taken to transmit a fixed number of bits via sequential generation of the beams in the beam group using the Modulation and Coding Scheme (MCS) for each beam as determined by the beam training. We show that performing exhaustive search over all possible combinations of beams and clients incurs overhead of order  $O(c^{K-1}N^{\frac{N}{2}+1})$ , where  $N$  is the multicast group size,  $K$  is the number of levels and  $c$  is the average ratio of beamwidth between two neighboring levels. Second, we present SDM’s beam grouping algorithm. The key strategy is to begin with an initial solution consisting of only the finest beams that provide high directivity gain. Then, when beneficial, SDM iteratively replaces the finest beams with wider beams in descending order of each wide beam’s improvement ratio over the initial solution. By

considering only the reachable client subset for each codebook, SDM searches over a reduced space of order  $O(KN^3)$  which our experiments show closely track exhaustive search.

**SDM Implementation & Experimental Evaluation.** We implement the key components of SDM in software and use a mechanically steerable 60 GHz RF-frontend combined with the software-defined radio platform WARP [14] for transmissions and training. We validate the significance of imperfect codebook traversal in realistic indoor environments using over-the-air measurements. As a baseline for comparison, we consider sequential unicast. Namely, because the IEEE 802.11ad standard [15, 16] does not define a multicast protocol, providing a multicast service could be realized via sequential unicast transmissions, i.e., generation of beams directed to individual clients of the multicast group. While such an approach can provide high signal strength at the clients, the total transmission time increases linearly with group size. To assess SDM, we collect training information in a typical indoor conference room setting for different client locations and codebook trees. Our results show that SDM consistently outperforms sequential unicast. Moreover, SDM provides over 1.8x throughput gains with up to 45% reduction in training overhead and 12x reduction in beam grouping overhead vs. exhaustive search and grouping.

## 1.2 VLC with Wi-Fi Uplink

Even when a high-speed VLC downlink is available for both unicast and broadcast services, the key challenge of not having a reliable uplink is still present. To address this challenge, we make the following contributions:

**Light-Radio WLAN (LiRa).** We present the design of LiRa, a **Light-Radio WLAN** that fuses light and radio links on a frame-by-frame basis at the MAC layer. Unlike commercial systems [17], LiRa does not require uplink infrared transmission

by the mobile client, and instead employs a radio uplink, seamlessly integrating with legacy Wi-Fi. We describe the hardware and software architecture of LiRa along with the network deployment scenario and protocol stack.

**AP-Spoofed Multi-client ARQ.** A key challenge of LiRa is realizing a radio feedback path via Wi-Fi for both acknowledgements of VLC data transmissions to control ARQ and client transmission of control information such as signal strength reports, needed for luminary selection and adaptation of modulation and coding schemes. In legacy Wi-Fi, the ACK is **protected** by the same NAV that protects the ACK’s associated data. Thus, a legacy Wi-Fi ACK does not separately compete for access to the medium and its transmission time is part of the duration-field that specifies the time for other stations to defer [18]. Due to LiRa’s co-existence with legacy Wi-Fi, there might be an ongoing transmission in the Wi-Fi channel that prevents a client from sending feedback immediately after VLC data reception. Consequently, LiRa cannot employ the 802.11-style two way DATA-ACK handshake for downlink VLC data as such an approach would incur severe ACK delays, orders of magnitude greater than SIFS, and would consume excessive resources on the RF network.

Thus, we design AP-Spoofed Multi-client ARQ (ASMA) as a mechanism to minimize the impact of VLC control frames on legacy Wi-Fi traffic, while providing sufficient feedback for the visible light downlink. ASMA relies on three principles: First, the AP triggers VLC ARQ feedback as opposed to a traditional ACK being triggered by the reception of a certain number of bytes or frames (ACK and block ACK respectively). Moreover, VLC ARQ feedback information is opportunistically aggregated up to the time of the trigger. Second, we spoof the AP’s 802.11-compliant trigger message with a sufficient NAV duration (time commanding other stations to defer) to enable **multiple** clients to transmit feedback. To avoid each of those clients independently contending, we equip the trigger message with a transmission

order such that the clients can sequentially transmit during the protected NAV time. Third, the AP contends to transmit the trigger command after a configurable **feedback trigger time** which can be set to balance feedback responsiveness with airtime used in legacy Wi-Fi.

**LiRa Implementation and Evaluation.** We implement LiRa and ASMA on a software defined radio [19] and perform an extensive set of experiments using a mix of LiRa components and commercial systems as baselines. By employing Wi-Fi for the uplink, LiRa’s uplink is not subject to rotational outages. For comparison, we perform measurements of uplink coverage using a state-of-the-art commercial system [17] and show that its infrared uplink is subject to deep rotational fades yielding zero throughput with rotation beyond  $\pm 15^\circ$  in comparison to perfect alignment. While [17] is intended for desktop platforms, it would require a bulky array of infrared LEDs. Next, we evaluate ASMA’s ability to obtain channel access in a busy Wi-Fi environment and evaluate the impact of the feedback control channel on fully backlogged Wi-Fi traffic. As a baseline, we implement a feedback control channel termed Per-Client-Contention (PCC) in which each VLC client must independently transmit its feedback via encapsulated Wi-Fi. We collect over-the-air measurements of the feedback delay and find that in a typical WLAN scenario, ASMA reduces response delay by a factor of 15 compared to PCC and reduces the impact of feedback messages on legacy Wi-Fi throughput from an excessive value of 74% for PCC to 3% for ASMA.

### 1.3 VLC Uni-directional Control Channel

Sensors have become a leading solution in many important applications such as industrial automation, smart buildings, telemedicine, etc. A Wireless Sensor Network (WSN) typically consists of a large number of small, low-cost sensor nodes distributed in the target area for collecting data of interest. The data flow in such networks is

mainly in the uplink direction from the sensors to the AP. These sensors are often powered with batteries, therefore energy-efficiency is extremely important. To reduce the energy consumption, the key idea of numerous power management mechanisms used in existing works is based on alternating the sensor between two states: awake and sleep. As illustrated in the Figure 1.1, the radio is turned on only when there is backlogged traffic at the sensor. There are ongoing transmissions on the radio band and the yellow arrow represents the timestamp at which the sensors queue got a new data frame for transmission. Accordingly, the sensor takes part in the contention-process and transmits its data as shown by the green data frame. After the transmission, the radio can be turned off. Due to the contention process, the time for which sensor is awake is dependent on the network traffic conditions. This uncontrollable access delay might also lead to failed QoS requirements for sensors related to safety e.g., alarms, gas leak detection, etc.. Moreover, as the radio is turned on for the duration of access delay, significant energy would be consumed from the sensor during this period.

In an ideal scenario, the AP has perfect knowledge of when the sensors would generate traffic. In such a scenario, the AP can trigger[20] a sensor to turn on its radio only when the sensor has backlogged traffic and transmit immediately without contention. The trigger message can be achieved by a low-power radio on the sensor which can then wake up the primary radio for the data transmission. In this manner, the sensor can save its energy which was previously consumed by the contention-based access. Unfortunately, the sensor data generation might be bursty and the AP lacks the traffic information about each sensor [21, 22]. : (a) whether it is backlogged and (b) if it is backlogged, what is the size of backlogged data. Therefore, transmitting a trigger message does not guarantee a data transmission in the uplink as the sensor might not have any backlogged data. And instead, such control triggers to hundreds

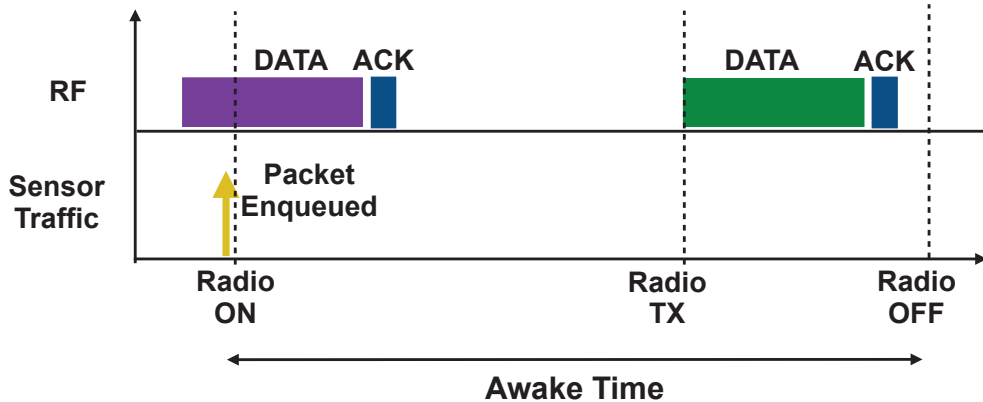


Figure 1.1: Radio awake time on sensor.

of sensors might consume significant airtime over the radio band. This inefficiency increases for bursty traffic and with increase in sensor size.

In this paper, our objective is to maximize the throughput delivered to the AP incorporating the channel access delay and the radio energy consumption. We define this access overhead as the radio airtime spent idly without data or corresponding acknowledgement transmissions. To achieve the objective, we propose LiSCAN, a visible light communication (VLC) uni-directional control channel for contention-free uplink radio access and make the following contributions:

#### **VLC Uni-Directional Control Channel for Concurrent Transmissions.**

Our key strategy for reducing the access delay and energy consumption is to transfer the AP's polling to an out-of-band channel. In such a system, the AP doesn't need an ongoing uplink data transmission over radio to end before transmitting poll to next sensor in schedule. Moreover, the AP's radio module can be turned on only for the data transmission. Due to the severe spectrum scarcity in Wi-Fi bands [23, 24], sensors' antenna, and power limitations [25], utilizing an additional radio channel exclusively for polling control becomes infeasible. In contrast, LiSCAN utilizes VLC for uni-directional out-of-band control. First, VLC is well-suited for energy-efficient operation by dual purposing LED-based lighting infrastructure for both illumination

---

and communication. In particular, ceiling-mounted luminaries can modulate lighting in a manner unnoticeable to the human eye (i.e., flicker free) for reception at sensors fitted with low-power wake-up VLC receivers that consume negligible power in the order of tens of microwatt [26, 27]. Second, the wide coverage and relatively high transmit power realized by the VLC downlink to satisfy the illumination objective is problematic to realize on the uplink: even if a sensor is fitted with infrared LEDs, providing wide aperture long-range transmission is ill-suited to sensors’ form factor and energy constraints [10, 11]. Therefore, in LiSCAN, the sensors transmits any backlogged data over radio leading to a uni-directional polling system wherein polls are transmitted over VLC and data is transmitted over radio.

We integrate the VLC and radio bands at the MAC layer [20] to enable concurrent near-zero latency communication across the two bands. Similar to 802.11 PCF, in LiSCAN, the AP begins contention-free period by gaining access to both RF and VLC channels. To enable simultaneous poll transmission and data reception at the AP, in LiSCAN, the AP exclusively transmits polls over VLC (*light-poll*) and is in receive mode (RX) over radio. To minimize the airtime lost in RF while transmitting light-poll to first sensor in schedule, our key strategy is to *align* both transmissions such that light-poll to first sensor in schedule ends SIFS duration after the end of CFP start beacon.

**Pipelined Polling for Overhead Minimization.** In 802.11 PCF, a significant part of the polling overhead includes the airtime spent in poll transmission and wait time during which no other transmission is allowed to take place (81.8%). To minimize this overhead, first, we transmit light-poll for next sensor immediately after polling the current sensor. To avoid collisions arising out of data transmissions from multiple sensors, LiSCAN simply aborts transmission of the ongoing light-poll for next sensor upon AP’s detection of data transmission from the current sensor. Second, after a

successful reception of a data frame, the AP transmits the ACK over VLC instead of radio to eliminate the overhead from the AP’s radio switching from receive to transmit mode and back. Third, if the light-poll to next sensor in schedule was aborted due to an ongoing data transmission, our goal is to minimize the radio airtime spent idly during the retransmission of this light-poll. We achieve this objective by aligning the end of light-poll retransmission with the AP’s ACK transmission.

**Pre-emptive Interference Avoidance.** In 802.11 PCF, when the AP doesn’t detect an uplink data transmission due to channel fading/interference, it continues transmitting polls based on the schedule. This might lead to severe performance degradation and radio airtime lost due to collisions at the AP. In LiSCAN, when AP doesn’t detect an uplink data transmission, it fully transmits the light-poll to next sensor in schedule without abortion. To avoid collisions at the AP, upon hearing the light-poll to next sensor, the sensor currently transmitting data will abort its ongoing transmission. In this manner, LiSCAN reduces the airtime spent in collisions at the AP.

**LiScan Experimental Evaluation.** We implement LiSCAN in ns-3 network simulator and analyze LiSCAN’s performance under varying traffic conditions including varying sensor sizes and bursty traffic parameters. Our key metrics for analysis include the radio airtime overhead, throughput and channel access delay (delay between packet generation at sensor and corresponding over-the-air uplink transmission). For the sake of equity and fairness, we compare LiSCAN and alternative strategies under the same network conditions.

## SDM: Scalable Directional Multicast in Highly-Directional 60 GHz WLANs

---

### 2.1 Design Overview

In this section, we present an overview of SDM’s design. First, we discuss the network model considered in this paper. Second, we describe the beam group quality test conducted by SDM to test whether training is necessary. Third, we describe the training period conducted by SDM to update clients’ signal strength information if the beam group quality test fails. Lastly, we describe the beam grouping for data transmission using the training information.

#### 2.1.1 Network Model

We consider a highly directional environment in which both the AP and the clients are equipped with antenna arrays capable of generating a fixed set of transmission and reception beams of different beamwidths [28]. This fixed set of beams is defined by a codebook in which each beam corresponds to a particular entry in the codebook including a combination of weights assigned to the antenna elements. We can adjust

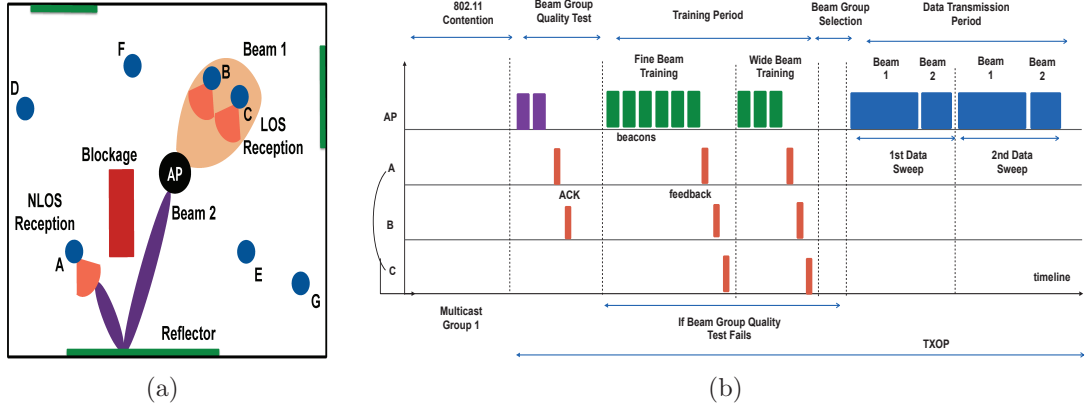


Figure 2.1: (a) An indoor conference room scenario where multicast group 1 comprising of clients A, B and C wins the contention and the AP selects two beams for the data transmission. (b) The different stages of our multicast timeline model for the scenario considered in (a).

beamwidth and steer the beam using discrete phase shifts of the antenna weights [13, 12]. We consider that each antenna array utilizes a single RF chain and can generate only a single beam at a time [29]. Most state-of-the-art 60 GHz systems employ a single RF chain [30] and at most 2 RF chains for the entire antenna array [31, 32, 33]. This is inspite of a possibly increased number of antennas in comparison to legacy MIMO systems. The key reason for limited RF-chains is the increased power consumption arising out of operating over a multi-GHz bandwidth channel. This RF chain limitation prevents the simultaneous transmission of finest beams each directed at a different client in a MIMO fashion for multicast service.

We consider a network with unicast clients and multiple multicast groups, with each group comprising of multiple clients. For example, a multicast group could represent a particular TV content. When the clients request multicast service either during the association phase or as a separate request, we place the client in the corresponding multicast group and inform the client about its group number. Otherwise, we list it as a unicast client. In Fig.2.1(a), clients A, B and C are in multicast group 1, clients D and E are in multicast group 2 and clients F and G are unicast clients.

Like 802.11, a multicast transmission begins with a group announcement when the AP wins contention to serve a multicast group (group 1 in Fig. 2.1(b)). Next, we describe the SDM's functioning in the different stages of the timeline.

SDM comes into effect once the AP wins the contention for a multicast group. The control and data frames transmitted during multicast TXOP as shown in Fig. 1(b) will include a NAV to defer clients not part of this multicast group from taking part in contention. In this manner, SDM can be integrated with 802.11ad operation.

### 2.1.2 Beam Group Quality Test

Except for the first transmission, a beam group will have previously been established for the prior transmission. If there was negligible client and environmental mobility since the last transmission, the same beam group can be used again for the current data transmission without performing any beam training nor a new beam grouping. Because the AP is oblivious to such mobility, to learn if the existing beam group can be used or not, SDM tests the existing beam group via transmitting a short data packet on each beam using its corresponding data rate as shown in Figure 2.1(b). In these packets, SDM includes information about the multicast group selected for data transmission and a pre-assigned order for clients to send ACKs.

If the AP receives an ACK from every client of the multicast group, then SDM uses the existing beam group. However, if this test fails, SDM will find a new beam group. In Figure 2.1(b), the AP fails to receive an ACK from client C and consequently SDM invokes beam training.

### 2.1.3 Training Period

If the beam group quality test fails, SDM conducts training that provides it with the clients' latest signal strength information for the AP's different beams. In order

to provide the AP with latest signal strength information for finding the best beam group, we consider every client in the multicast group takes part in the training even if a client successfully receives the beam group quality test packet. Alternatively, a network controller can invoke only the clients that fail the beam group quality test to participate in training. The key concept of training is that the AP transmits a beacon at the base rate (MCS 0 in [34]) using a particular beam from the codebook followed by a feedback packet from every client consisting of the received power measure of the transmitted beacon. Because different beams correspond to different levels, SDM conducts the training of each level separately. For simplicity, two-level training is illustrated by the wide beam training and fine beam training in Fig. 2.1(b). The training beacons include information about the multicast group selected for data transmission and the time the clients outside the multicast group should defer.

To limit feedback overhead, the AP transmits beacons with all selected beams of a particular level before receiving feedback from each client. A client's feedback includes the received power measures for the different beams. Although a beacon might be detected at the client as it is transmitted at the base rate, the power measure might be lower than the minimum required for a data transmission (MCS 1 in [34]). To minimize collisions, SDM pre-assigns the feedback order and this information is included in the training beacons. We consider the AP to be in quasi-omni reception mode during the feedback period.

If a client requests for both unicast and multicast services, it is possible that the AP serves the client with different beams for both the services. This is because the finest level beam would be used for the unicast service to provide the highest data rate to the client. In contrast, for the multicast service, SDM might use a wider beam to serve this client if this wider beam can also serve other client(s) and improve the multicast performance. In terms of overhead, the feedback obtained from client in

finest level beam training in SDM can be used to select the optimal beam for future unicast transmissions to the client and vice versa. This leads to a overall reduction in the training overhead.

#### 2.1.4 Beam Group Selection and Data Transmission

Given the training information, SDM next finds the beam group to be used for data transmission. Each beam is defined by its codebook entry, the clients that it serves and the data rate used for transmission. This leads to a sequential generation of beams one after the other which we define as a *data sweep*. As the AP sends the same data for all beams in the beam group, a client receiving the same packet via more than one beam doesn't increase its throughput. The data sweep consists of only data transmission and no control overhead. As the AP takes part in contention for data transmission to this multicast group, we consider the AP has fully backlogged traffic for the duration of transmission opportunity (TXOP) period analogous to frame aggregation in unicast communication. Fig. 2.1(b), depicts two data sweeps during the data transmission period. As many clients might be served by the multicast data transmission, we consider the TXOP to begin after the beam grouping selection by the AP. Alternatively, a network controller might include the beam group quality test, beam training and beam grouping computation within the TXOP duration. However, that might lead to a significantly reduced airtime for the data transmission.

Acknowledgements of data reception from every client in a multicast group might lead to significant control overhead especially in large group sizes. This is because ACKs need to be sent in a scheduled manner to avoid collisions at the AP and this is to be performed for multiple data sweeps in a single data transmission. To eliminate this control overhead, SDM doesn't include any ACKs from the clients during the

multicast data transmission. The AP selects the highest MCS for each beam such that every client served by the beam receives the data reliably. If a client is mobile, then the beam group quality test in SDM would fail for that client the next time AP wins contention for transmission to the clients multicast group. This would lead to re-training and selection of a new beam for the mobile client before the next data transmission period thereby addressing mobility. Additionally, existing beamwidth and rate adaptation protocols [35, 36] for unicast mobility can be applied on top of SDM to address mobility of high mobile clients.

## 2.2 Scalable Multicast Training

In this section, we firstly introduce the concept of multi-level codebook-based beamforming and the codebook tree architecture as a useful means to reduce the training overhead. Secondly, we describe the training strategy that minimizes overhead in ideal indoor environments followed by its challenges in a general setting. To address these challenges, we present SDM’s training protocol.

### 2.2.1 Multi-level codebook-based beamforming

As discussed in Section 2.1, we consider the AP and the clients are equipped with antenna arrays capable of generating a fixed set of beams of discrete beamwidths. In Fig. 2.1(b), the AP uses two levels of transmission beamwidth indicated by wide beam and fine beam. In general, we consider a multi-level codebook at the AP of  $K$  levels of beamwidth such that at each level, the beams are uniformly spread out  $360^\circ$  around the AP. We consider the AP and clients are operating at the maximum transmission power as defined by the IEEE 802.11ad standard [16] and the range achieved by a beam pattern is dependent on the directivity of the main lobe. For

multicast, multiple beamwidth levels provide flexibility in selection of a beam used to serve multiple clients simultaneously in order to reduce the total transmission time. Beamwidth decreases with increasing codebook level with the 1st level representing the widest beams. If  $\phi(k)$  represents the beamwidth in radians of the beam in the  $k$ th level codebook, the number of beams  $M(k)$  at  $k$ th level is given by  $\lceil \frac{2\pi}{\phi(k)} \rceil$ .

Exhaustive training that would require every beam in the entire codebook for sending the training beacons has overhead  $O(KN + y^K)$ , where  $y$  represents the average ratio of the number of beams of two neighboring beamwidth levels. This overhead would have a significant impact on multicast throughput scalability. Next, we show how the codebook tree architecture can be used to reduce training overhead.

### 2.2.2 Codebook Trees for Partial Traversal

To scale group size with limited training overhead, we leverage the clients' feedback information after each codebook level training to select only a partial set of beams to be used in the next level training. We need to establish a relationship between the beams or codebook entries of different levels. As the number of codes increases with codebook level, we establish an edge between beam  $p$  of level  $k$  to the set of beams in level  $k + 1$ , each of which has the highest spatial correlation with  $p$  in comparison to any other beam of level  $k$ . The formation of such a graph results in a tree structure termed a *codebook tree* [12, 13]. Fig. 2.2 shows an example codebook tree construction in which beam  $\psi_A$  of level  $k$  has beam  $\psi_B$  of level  $k + 1$  as its child in the codebook tree.

To obtain such a relationship, for every beam, we initially find the array form for every directions among a discrete set of directions around the AP (Equation 2.1(a)). Then, an array form vector is constructed for every beam (Equation 2.1(b)). For a beam in level  $k + 1$ , the correlation of its array form vector is computed with that

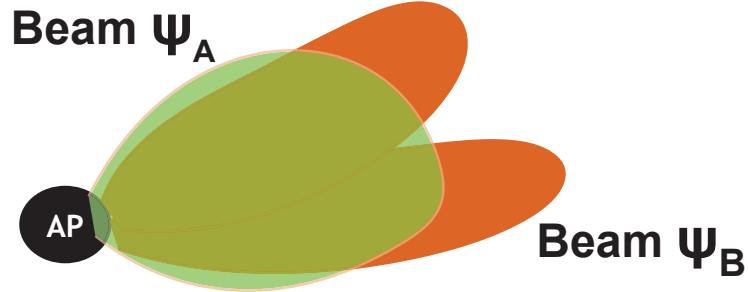


Figure 2.2: An example codebook tree construction.

of every beam in level  $k$  (Equation 2.1(c)). We select the beam in level  $k$  with the highest correlation as its parent in the codebook tree.

$$AF(\psi, \theta) = \sum_{u=1}^U w(u) e^{j2\pi/\lambda(u-1)d\cos(\theta)} \quad (2.1a)$$

$$G(\psi) = [AF(\psi, 0), \dots, AF(\psi, 2\pi - 360/2\pi)]^T \quad (2.1b)$$

$$\text{Correlation} = |G(\psi_A)^H G(\psi_B)| \quad (2.1c)$$

**Basic Traversal.** Firstly, we define a client to be *reachable* at level  $k$  if there exists at least one beam used for training in that level such that its received power measure is greater than or equal to the minimum required for data transmission (MCS 1 in [34]). We define this beam as the *primary beam* at level  $k$  for this client. A basic traversal of the codebook tree represents the network state in which every client is reachable at all levels and the primary beam of any level is a child of the primary beam of the previous wider level.

In the basic traversal, the key strategy is to, at each level, find the union set of beams that provided the strongest beacon to the clients. Then, we use only their

children in the codebook tree for the next finer level training. An example of basic traversal is illustrated for a three level codebook tree in Fig. 2.3. The training begins with the widest beams all of which are used for sending beacons. From the next level onwards, we select a partial set of beams based on the client's feedback information.

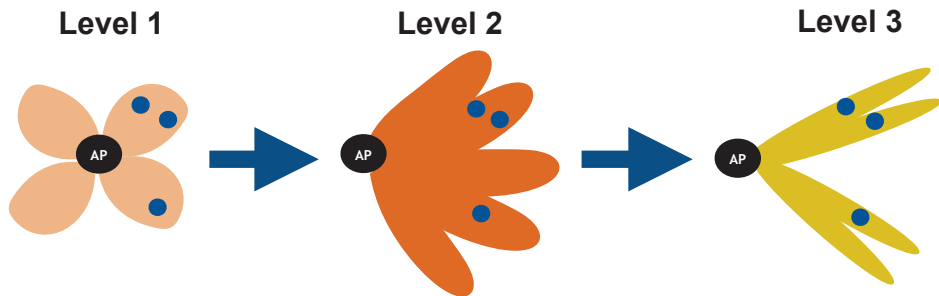


Figure 2.3: A basic traversal.

**Challenges in Real Environments.** There are two main challenges that exist in realistic indoor environments that make the basic traversal fall back to exhaustive training.

(i) *Unreachability:* A client's distance from the AP might be such that it is unreachable at a wider beamwidth level training due to the reduced directivity gain. In this case, none of the beams of this level can be used for serving data to this client. As there is no primary beam obtained for a client in a wider codebook level, the AP can't select a pruned set of beams for finer level training in order to reduce the training overhead.

(ii) *Non-monotonicity:* The codebook tree might be fixed for the AP's antenna array and is independent of the environment the AP is deployed. Due to presence of temporary reflectors and blockage elements in the environment, if a client that was reachable at a finer level through a non line-of-sight (NLOS) path might be unreachable at a wider level or vice-versa. Moreover, although the codebook tree forms edges between beams across adjacent levels still the crest of a wide beam can

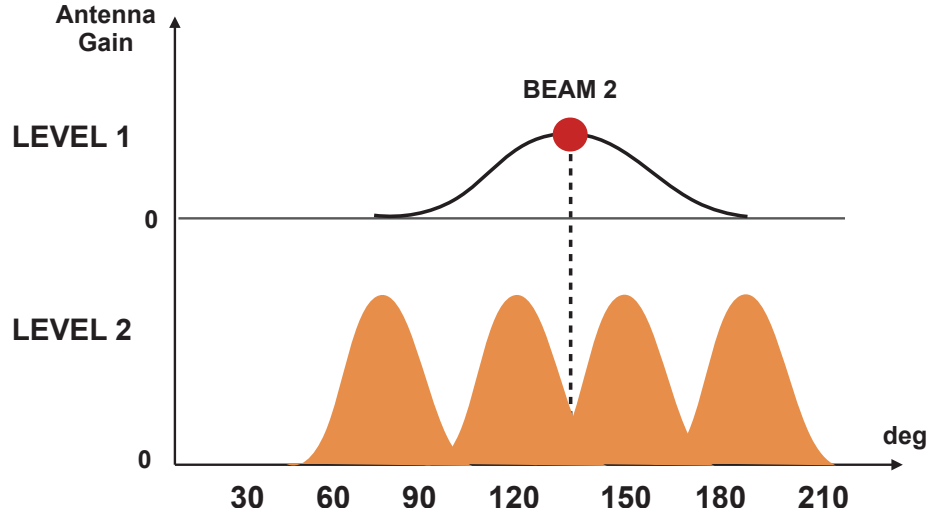


Figure 2.4: Imperfect codebook traversal.

correspond to the trough of a wide beam and vice versa as illustrated in Figure 2.4. Using over-the-air measurements collected using our 60 GHz testbed, we validate the significance of this challenge in typical conference room environments (Section 2.4).

In the worst case, both of the above challenges lead to the AP falling back to the exhaustive training which has significant overhead. To address the scalability of training with the presence of the above challenges in realistic indoor settings, we next present SDM’s training protocol.

### 2.2.3 SDM’s Training Protocol

The key concepts of SDM’s training protocol are as follows:

(i) *Descending order Traversal*: Due to the high directivity gain provided by the beams of the finest beam level, every client is reachable by at least one of those beams. Otherwise, the client wouldn’t be able to associate with the AP. Transmission via only finest level beams represents a *sequential unicast* beam grouping. If we performed an ascending order traversal, as in the basic traversal, then only a partial

set of beams might be used in the finest level training leading to incomplete information in comparison to an exhaustive approach or a strategy in which only the finest level is trained. Thus, an only-finest-beams solution using ascending order traversal information might be worse than alternative approaches.

In contrast, with descending order traversal, as we begin with training for all finest beams, we ensure any beam grouping algorithm would generate at least the sequential unicast solution. Therefore, SDM's key strategy is to perform descending order traversal. SDM selects the parents of the primary beams found for the clients in a codebook level training as the beams to be used for the next lower level and wider beam level training.

If a client cannot be reached by the AP using any of the finest level beams, that means the client's beam is severely misaligned or suffering from severe blockage. In such scenarios, we assume the client side beam adaptation follows the 802.11ad standard procedure wherein the Beacon Header Interval period is used for sector level sweep between the AP and the client. In general, all the clients that request for services adapt their beams in the Beacon Header Interval period.

(ii) *Sibling training*: If any client reachable in the previous level training is found to be unreachable in the current level training, SDM performs additional training in this level. Ideally, for each client that was reachable in the previous level, the parent of its primary beam in the previous level should be the primary beam in the current codebook level. However, if it is not, we include in the additional training the sibling of the expected ideal beam for each unreachable client if this beam wasn't already used in the initial training. Similar to the initial training, the AP sends a beacon using each selected beam for the additional training except that the feedback period has only the unreachable clients provide the feedback.

If a client is not reachable even after this additional training, we do not consider

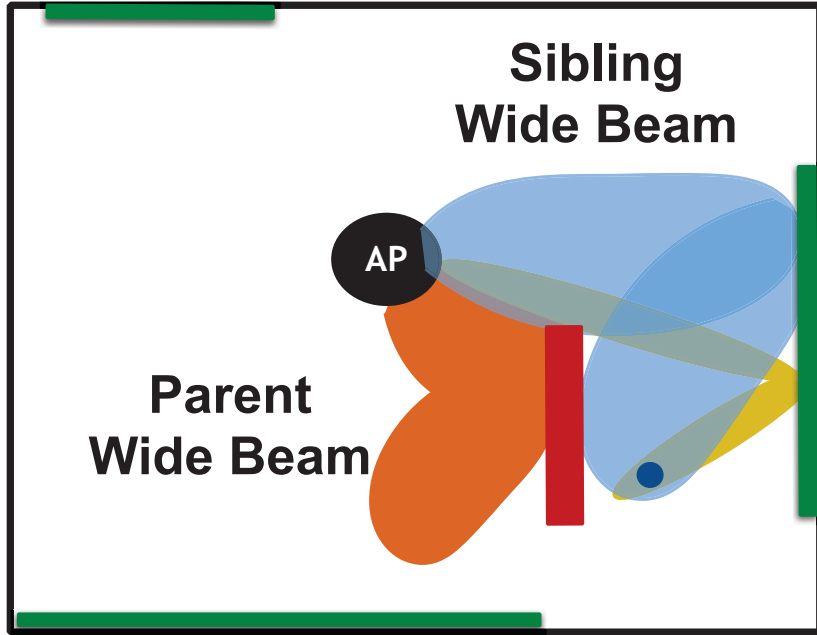


Figure 2.5: SDM’s sibling training to address non-monotonicity.

this client in selecting the set of beams for the next level training. In the worst case, this client might not be reachable in the training of any of the remaining levels. However, as this client was reachable in the finest beam level in which all beams were used for training, there exists at least one beam that can be used for data transmission to serve each client.

An example of SDM’s traversal is illustrated for a single client in Fig 2.5 in which the client that was reachable by a finest level beam through a NLOS path was found to be unreachable by its parent beam in the neighboring wide beam level. Then, additional training utilizing the sibling is performed before proceeding to the wider beam levels. At the end of training period, for each client we have a 2-dimensional training vector of all beams used in the training and their corresponding power measures. In the next section, we describe how the beam group is selected using this training information.

## 2.3 Scalable Multicast Beam Grouping

Using the training information, we next select the beam group for data transmission as shown in Fig. 2.1(b). First, we formulate an optimization problem of minimizing the data sweep time. Secondly, we present SDM’s beam grouping algorithm. Table 2.1 provides a comprehensive list of notations used in this section.

### 2.3.1 Problem Formulation

The training information consists of each client  $c$ ’s training vector that maps a beam  $\psi(i, j)$  to its corresponding power measure  $P(i, j, c)$ . For beams not used in the training or not reachable at the client, the power measure is zero watts. As discussed in Section 2.1, the data transmission occurs in a sweep of the selected beams with each beam transmitting the same data and the total time of a sweep is called the data sweep time. SDM’s objective of beam group selection is to minimize this data sweep time.

As we send the same data from each selected beam, a client receiving the same packet from more than one beam doesn’t increase its throughput. Therefore, we need to judiciously find  $S(i, j)$ , the set of clients to be served by a beam  $\psi(i, j)$  in the final beam group so that none of the clients in this set are also assigned to another beam in the beam group. As each client is assigned to a single beam, the number of beams in the optimal beam group ranges from one beam to at most  $N$  beams where  $N$  is the number of clients. The client assignment determines the data rate  $R(i, j)$  that can be used by the beam for successful reception at its serving clients. Mathematically, we select the data rate by

$$R(i, j) = \text{MCS}\left(\min_{c \in S(i, j)} P(i, j, c)\right), \quad (2.2)$$

where  $\text{MCS}()$  outputs the highest data rate that can be used for transmission given the power measure. For determining which client is best served by which beam, for each  $\psi(i, j)$ , we find the set of clients  $C_{th}(i, j) \in \mathbb{U}$  that have a power measure greater than  $P_{min}$ , the minimum required for data transmission (MCS 1).

$\mathbb{U}$	set of multicast group clients
$N$	number of clients $\in \mathbb{U}$
$K$	number of levels
$\psi(i, j)$	$i$ th beam in $j$ th level
$P(i, j, c)$	power measure of client $c$ for $\psi(i, j)$
$C_{th}(i, j)$	$\{c \mid P(i, j, c) \geq P_{min}\}$
$S(i, j)$	clients $\in \mathbb{U}$ assigned to be served by $\psi(i, j)$
$R(i, j)$	data rate selected from 802.11ad MCS table for $\psi(i, j)$ for successful reception at clients $\in S(i, j)$
$\mathbb{B}$	Beam group for data transmission
$B$	number of beams in a beam group
$\mathbb{I}$	initial solution beam group solution using only finest beams
$T(G)$	Data sweep time of beam group $G$
$\text{WIR}(G)$	WIR of a set of wide beams $G$ when finest beams serve clients not served by beams $\in G$
$C_W$	clients served by wide beams in a beam group selection

Table 2.1: Description of notations used in the problem formulation and algorithms description

Let  $\mathbb{B} = \{(\psi(i_1, j_1), S(i_1, j_1)), \dots, (\psi(i_B, j_B), S(i_B, j_B))\}$  be a beam group composed of  $B$  beams. We express the optimization problem as follows:

$$\min_{B, i_1, \dots, i_B, j_1, \dots, j_B, S(i_1, j_1), \dots, S(i_B, j_B)} \sum_{b=1}^B \frac{1}{R(i_b, j_b)} \quad (2.3a)$$

$$\text{s.t. } \bigcup_{b=1}^B S(i_b, j_b) = \mathbb{U} \quad (2.3b)$$

$$S(i_b, j_b) \subseteq C_{th}(i_b, j_b), \quad 1 \leq b \leq B. \quad (2.3c)$$

Equation 2.3(a) represents the cost function of the optimization proportional to the data sweep time with the search space being the beams in the codebook and corresponding client assignment to each beam. Equation 2.3(b) ensures each client in the multicast group is assigned to at least one beam that serves it. Equation 2.3(c) ensures that each client assigned to a beam received a power measure  $> P_{min}$  from this beam during beam training.

### 2.3.2 SDM's Beam Grouping Algorithm

Here, we describe the key steps of SDM's beam grouping algorithm.

**1. Initial Solution:** Using the training information, we begin with an initial solution composed of only finest level beams representing a sequential unicast solution. For simplicity of explanation, we assume each client is served by a distinct finest beam although our analysis is applicable to a more general setting. Let this initial solution be denoted by  $\mathbb{I} = \{(\psi(i_1, K), c_1), \dots, (\psi(i_N, K), c_N)\}$  consisting of  $N$  beams of the finest level  $K$  and  $c_1, \dots, c_N$  represent the clients.

We observe that  $\mathbb{I}$  will not be the best solution if there exists at least one beam  $\psi(i^*, j^*)$  with a client assignment  $S(i^*, j^*)$  such that

$$\frac{1}{R(i^*, j^*)} < \sum_{b=1}^{N^*} \frac{1}{R(i_b, K)}, \quad (2.4)$$

where for simplicity we consider  $S(i^*, j^*)$  corresponds to the clients served by the first  $N^*$  beams  $\in \mathbb{I}$ . Equation (2.4) means that the transmission time using  $\psi(i^*, j^*)$  for clients  $\in S(i^*, j^*)$  is smaller than serving them with the finest beams. In a general

scenario, Equation (2.4) could be satisfied for multiple such client assignments which are a subset of  $C_{th}(i^*, j^*)$  for the same beam and multiple of such beams could exist.

**2. Wide Beam Improvement Ratio and Hashmap:** To obtain the best solution, we need to exhaustively traverse every combination of a *wide beam* (any beam not belonging to the finest codebook level) and its client assignment. Unfortunately, this exhaustive search has a significant overhead because we consider every combination of every wide beam in the codebook and every possible client assignment out of the clients in the multicast group. The number of wide beams in the codebook tree is order  $O(c^{K-1})$ . The total number of client assignments for a given wide beam is order  $O(N^{\frac{N}{2}})$  and WIR computation for every combination of wide beam and client assignment is order  $O(N)$ . Overall, the complexity of exhaustive wide beam search results in the order  $O(y^{K-1}N^{\frac{N}{2}+1})$ , where  $y$  represents the average ratio of the number of beams of two neighboring beamwidth levels.

To overcome this infeasible overhead, SDM's key strategy is to have a unique client assignment for each wide beam. SDM utilizes only the client set  $C_{th}(i, j)$  of a beam  $\psi(i, j)$  as its client assignment. By selecting  $C_{th}(i, j)$  for the client assignment, we are allowing this pattern to serve every client that it reached in training thereby reducing the total number of beams in the beam group. We identify every beam  $\psi(i^*, j^*)$  that improves upon  $\mathbb{I}$  when this is the only beam added to  $\mathbb{I}$  along with removal of finest beams that were serving clients  $\in C_{th}(i^*, j^*)$ . Let this modified beam group be denoted by  $\mathbb{B}^*$ . To rank all such beams in order of their improvement over  $\mathbb{I}$ , we define the metric *wide beam improvement ratio* (WIR) expressed mathematically as

$$\text{WIR}(\{\psi(i^*, j^*)\}) = \frac{T(\mathbb{I})}{T(\mathbb{B}^*)} \quad (2.5)$$

where  $T(x)$  is the data sweep time of beam group  $x$ . SDM stores the information in

---

an initially empty hashmap that takes  $\text{WIR}(\{\psi(i^*, j^*)\})$  as the value and  $(\psi(i^*, j^*))$  as its key. SDM utilizes separate chaining technique [37] to store multiple values having the same key. After complete traversal of the codebook tree using the training information, SDM obtains a hashmap of wide beams that can improve the data sweep time.

If the hashmap is empty at the end of this step, then there exists no wide beam that can improve upon the initial solution of only finest beams. In that case, the sequential unicast is the best solution based on the training information provided and SDM terminates the algorithm.

**3. Beam Group Selection:** In this step, SDM finds the final beam group solution in an iterative manner. The initial solution is the only finest beams solution. SDM initializes an empty set  $C_W$ , that represents the clients served by wider beams. In each iteration, SDM’s key strategy is to select the key from the hashmap with the largest WIR as it corresponds to the maximum improvement possible over the initial solution. SDM adds the corresponding beam  $\psi(i, j)$  to the final beam group solution and the clients  $\in C_{th}(i, j)$  to  $C_W$ .

As the clients newly added to  $C_W$  need not be served by any other beam, we delete every key from the hashmap that has any client  $\in C_W$  as a part of the corresponding beam’s client assignment. Also, we remove the finest beams serving clients  $\in C_W$  from our beam group solution. Thus, every beam added to the final beam group solution is serving a different client subset. The iterative mechanism terminates when every client of the multicast group is part of  $C_W$  or if the hashmap becomes empty due to the key deletion after each iteration. If any client is absent from  $C_W$  after this iterative procedure, then we serve such clients using the finest beams still present in the solution since the first iteration. In this manner, SDM finds the beam group for data transmission.

SDM's final beam group might be composed of a mixture of wide beams and finest beams based on the training information provided. Let SDM's beam group solution be composed of a set of  $Z$  wide beams defined by  $G = \{(\psi(i_1, j_1)), \dots, (\psi(i_Z, j_Z))\}$  along with finest beams serving the clients not served by the wide beams. Then, we derive (Appendix A) the resultant WIR of this beam group to be

$$\text{WIR}(G^*) = \frac{1}{\left( \sum_{a=1}^Z \frac{1}{\text{WIR}(\{\psi(i_a, j_a)\})} \right) - (Z - 1)} \quad (2.6)$$

**4. Complexity.** SDM's initial solution computation is order  $O(N^2)$  involving finding the clients served by the same finest beam followed by data rate selection. Next, using SDM's training information, the number of wide beams traversed is order  $O(KN)$ . For each wide beam, finding the unique client assignment ( $O(N)$ ) followed by calculation of WIR ( $O(N)$ ) thus amounting to  $O(N^2)$  complexity. Therefore, the complexity of wide beam search using SDM is order  $O(KN^3)$ . Hash map traversal in Step 3 of SDM's beam grouping after each iteration involves testing whether the new beam has in its client assignment any client that is already served. This procedure amounts to overhead of order  $O(KN^4)$ . Once a valid beam is found during an iteration, adding it to the beam group and selecting its data rate involves order  $O(N)$  complexity. Therefore, the time complexity of SDM's beam grouping is order  $O(KN^4)$ .

In this manner, SDM provides an efficient beam group based on the training information. Next, we describe our implementation of SDM and the data collection from a typical 60 GHz indoor scenario.

## 2.4 SDM Implementation and Data Collection

We implement SDM and perform over-the-air data collection to evaluate its key components. In this section, first, we describe the implementation of the 60 GHz system. Second, we describe the methodology of data collection. Last, we analyze the monotonicity of the codebook tree traversal using our collected measurements.

### 2.4.1 SDM Implementation

Our SDM implementation consists of one set of transmitter and receiver modules that are capable of communicating in the 57-64 GHz unlicensed band with up to 1.8 GHz modulation bandwidth via the VubiQ platform [38]. These modules accept and output I/Q baseband signals. For this paper, we use the transmitter module as the AP and the receiver module as the client. In order to streamline the measurement process, we integrate these modules with two WARP v1 boards according to the flow outlined in Figure 2.6(a).

One computer running MATLAB, WARP-Lab [39], and the VubiQ control panels control the entire system. Using WARPLab, we generate a random set of binary data and modulate it using BPSK with a modulation bandwidth of 10 MHz (WARP v1 is capable of a transmission bandwidth of up to 20 MHz with a sampling rate of 40 MSps). WARPLab then sends the digital samples to the AP, where the WARP analog daughtercard converts these samples into single-ended analog I/Q signals. These signals are passed to an evaluation board with the ADL5565 differential amplifier [40], which removes the analog daughtercard's DC offset and converts the single-ended signals into differential signals. This differential I/Q is then passed to the AP's VubiQ module where it is upconverted to 60 GHz for over-the-air transmission. The client's VubiQ module then receives this transmission and downconverts it back to analog I/Q baseband. We pass the differential signal to an off-the-shelf 15 MHz

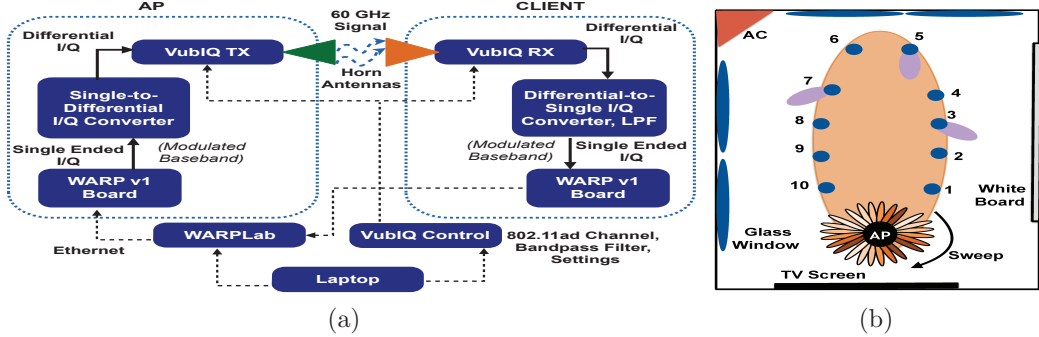


Figure 2.6: (a) 60 GHz system signal and control flow. (b) Map of the room used for data collection.

low pass filter (LT6600-15) to clean up the baseband signal. These signals are then sampled to by the client's WARP board and processed/demodulated in WARPLab.

Directional transmission and reception is achieved by using MI-WAVE's WR-15 60 GHz gain horns. To emulate the different beamwidth levels in a codebook tree, we use 7 degrees, 20 degrees, and 80 degrees gain (antenna) horns. To collect received power measures at different client locations and for different receive antenna orientations, we use a mechanical motor, DC microstep driver and a commercial motion control setup [41] to steer the beams with sub-degree accuracy.

We implement an 60 GHz WLAN trace-driven emulator that is fed the over-the-air signal strength traces as inputs. Parameters and frame times are incorporated from the 802.11ad standard. We use the Single Carrier (SC)-PHY (MCS 1-12) defined in 802.11ad MCS table which is the only modulation in the first generation of chip sets.

#### 2.4.2 Data Collection

Depending upon the client's location and the objects in the environment, the client might not be reachable from the AP for a particular codebook level. Even if the client is reachable, then its primary beam for this codebook level will vary with it's location and the reception path could either be a LOS or NLOS path. Using our 60

---

GHz system, we collect signal measures for a rich topology of client distributions in an indoor conference room setting illustrated in Figure 2.6(b). As we are interested in capturing the signal strength variations with separation distance and beam misalignment for different beamwidth levels, the 20 MHz signal bandwidth provided by the WARP is sufficient. This is because the frequency diversity of the 2 GHz channel at 60 GHz impacts the signal strength in the same manner for the different beamwidth levels. The room is composed of different reflectors including a white board, large TV screen and glass windows.

We fix the AP location at one end of the conference table. We place the client's location in 10 different positions. To emulate blockage, for each client position, we use 3 different orientations uniformly spaced in an angular range of 60 degrees. One of the orientations provides a LOS path to the AP from each client position whereas the other two represent client's receive beams for forced NLOS paths. We select the 20 degrees horn for the client's receive antenna as it provides an efficient trade-off between receiver sensitivity of 7 degrees and receive capture area of 80 degrees. For each client position and orientation, we perform a 360 degrees sweep of the AP in steps of 5 degrees. To emulate the multi-level codebook structure, we conduct the AP's sweep using 7 degrees, 20 degrees, and 80 degrees horns. At each point of AP's sweep, we take RMS baseband measurements to estimate the received signal strength. We normalize the signal strength measurements based on the maximum observed in the entire data set as shown in Fig. 2.7.

Fig. 2.7(a) provides the normalized signal strength for client position 8 in Fig. 2.6(b) for a fixed orientation and different AP beamwidths. We observe that the peaks for different beamwidths are correlated independent of the path being a LOS path or NLOS path. Fig. 2.7(b) provides the normalized signal strength for same client position but for different orientations when the AP sweeps with 7 degrees horn.

We observe the diversity in the signal strength peaks for different client orientations.

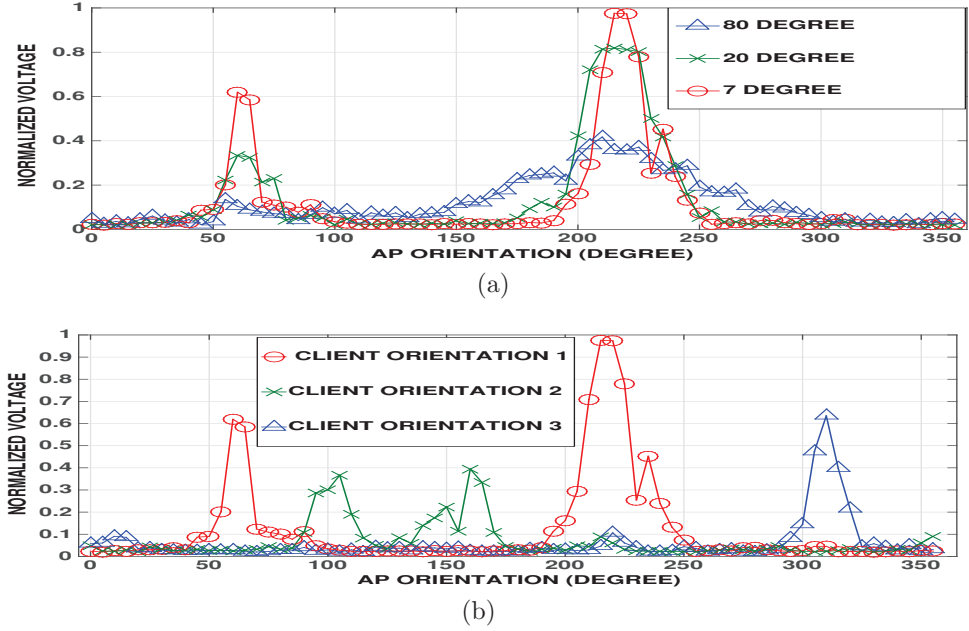


Figure 2.7: (a) The correlation in peak directions for different AP beamwidth at a fixed client location and orientation. (b) The diversity in the peak directions for different client orientations at a fixed location with 7 degree horn at the AP.

### 2.4.3 Beam Misalignment Analysis

To obtain the highest possible data rate, the AP and client should both beamform such that the center of their target resides in the center of their beam. However, in actuality, beam misalignment degrades performance. To analyze the effect of these non-idealities on the measured signal strength at the receiver, we utilize our 60 GHz testbed.

We collect traces indoors in an 8 x 3.5 meter room. The VubiQ boards are placed at a height of 1 meter in the center of the room as shown in Figure 2.8. The transmitter (AP) is placed on one end of the room and transmits longways down the room with the 7 degrees antenna horn. The receiver (client) is placed in the center of the transmitter's beam 1 meter away. We take baseband RMS measurements to

estimate the received signal strength when the azimuth angle of the receiver is between -50 degrees to 50 degrees, where 0 degree represents the line of sight path. We verify that an azimuth angle of 0 degree corresponds to the line of sight path by verifying that the strongest receiver orientation is at this angle.

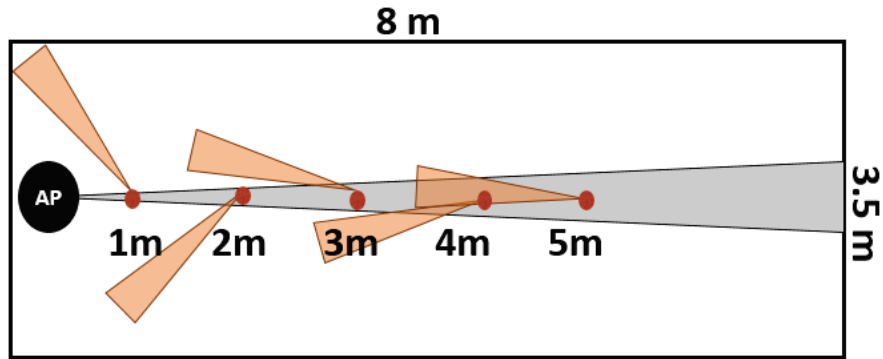


Figure 2.8: Indoor measurements of receiver rotation. The receiver was placed between 1 to 5 meters from the transmitter in steps of 1 meter. *Not drawn to scale.*

We repeat these measurements in 1 meter intervals up to 5 meters away, and then repeat the entire set of measurements with the 20 degrees and 80 degrees antenna horns at the transmitter as well. We always use the 20 degrees antenna horn at the receiver to accurately characterize how the observed angular spread changes for the different setups. Given that the transmitter is always pointed at the receiver, a 360 degrees receiver sweep is not necessary because there are no strong reflectors around the receiver, so the only lobe will be close to the line of sight path.

Afterwards, we perform a separate experiment and measure the variation in signal strength when the receiver is not perfectly centered in the transmitter's beam. We observe this effect by fixing the transmitter-receiver distance to 1 meter and radially translating the receiver around the transmitter as shown in Figure 2.9. The transmitter is always directed along 0 degree, but the receiver is always pointed at the transmitter. This isolates the effect of transmitter-receiver misalignment.

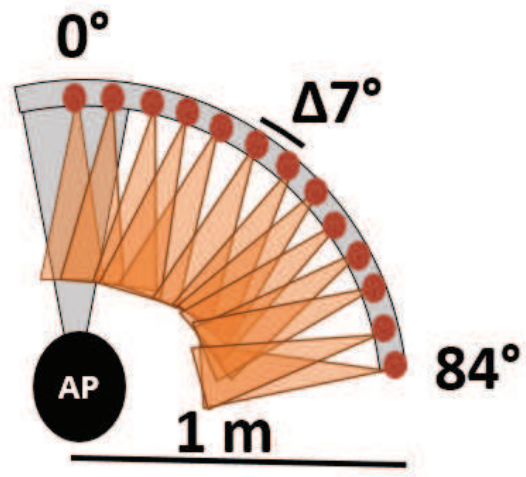


Figure 2.9: Radial translation of the receiver to characterize the effect of transmitter-receiver beam misalignment. The transmitter is fixed at 0 degree azimuth while the receiver moves and constantly points at the transmitter. *Not drawn to scale.*

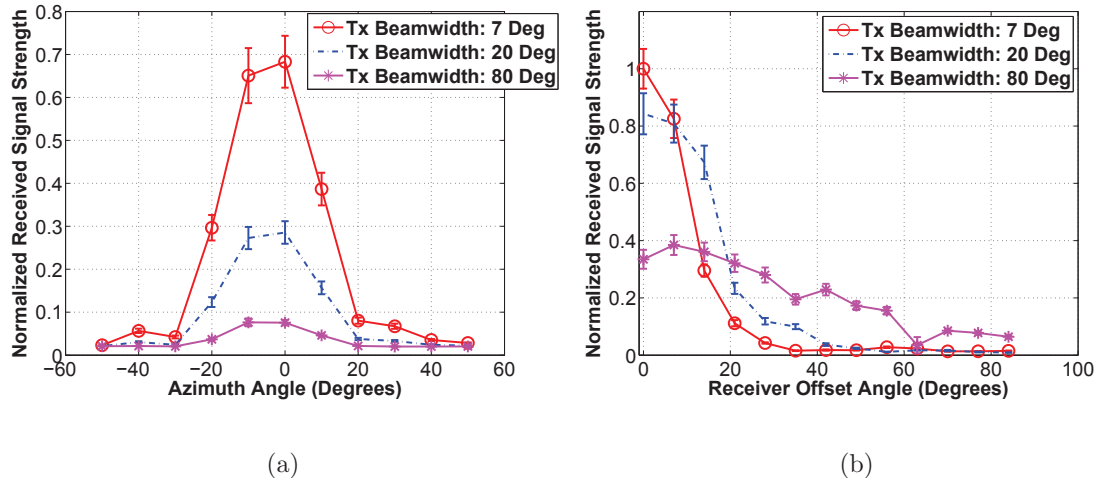


Figure 2.10: (a) Measured signal strength loss when the receiver rotates its beam away from the transmitter while remaining in the center of the transmit beam (2 meter distance). (b) Radial translation of the receiver to characterize the effect of transmitter-receiver beam misalignment. The transmitter is fixed at 0 degree azimuth orientation while the receiver moves and constantly points at the transmitter.

Figure 2.10(a) characterizes signal strength in comparison to the maximum value at perfect orientation as a function of the receiver misalignment angle from perfect

orientation. Moreover, different values of transmit beamwidth are characterized. The figure shows the non-linearity in the relationship between transmit beamwidth and successful reception at rotated receiver antenna. Figure 2.10(b) depicts signal strength at an angle relative to the strength at 0 degree for different transmit beamwidths. As expected, the roll off for 7 degrees is the fastest, but it also has the highest peak. In contrast, 80 degrees has a very slow roll off and wide spread, but the peak value is significantly lower than the other transmitter beamwidths.

#### 2.4.4 Codebook Tree Construction

We construct over 72 5-level codebook trees using the correlation technique presented in [12] with beamwidth levels of 80 degrees, 40 degrees, 20 degrees, 10 degrees and 5 degrees. We construct the codebook trees by linear rotations of the default orientation used in our over-the-air measurements. We estimate the signal strength measurements at the clients for 40 degrees, 10 degrees and 5 degrees by weighted translation of the collected measures for 80 degrees, 20 degrees and 7 degrees. For example, we briefly describe how we estimate the signal strength vector for 10 degrees beamwidth at the AP for a given client location and client orientation. First, we find out the closest beamwidth part of the over-the-air traces which in this case is 7 degrees. This ensures we are not incorporating the measurements of beam patterns widely different from 10 degree. Second, we find out the maximas in signal strength across the AP orientation spanning 360 degrees for the 7 degrees real trace for the same client location and orientation. Then, we place the local maximas for 10 degree at those same AP orientations and utilize the inverse relationship between the signal strength and beamwidth to estimate the signal strength [35, 42].

We perform the above procedure for each codebook tree, codebook level, client location and client orientation. For every codebook tree, we are performing a lin-

ear rotation of the beams from the previous orientation. Therefore, based on our beam misalignment analysis in Section 2.4.3, we need to incorporate an additional misalignment loss into the signal strength estimation. For this purpose, we utilize the misalignment loss function described in [42] that is validated by our results in Section 2.4.3.

We convert the baseband RMS measurements to lie within the received sensitivity range provided in the 802.11ad MCS table [34] for SC-PHY modulation. To achieve this, we map the maximum value in our RMS baseband measurements to the received power of -53 dBm required for the highest data rate of 4.62 Gbps. Accordingly, we select the data rate for a given received power measure using the 802.11ad MCS table.

#### 2.4.5 Monotonicity Analysis

We analyze the monotonicity in the codebook tree traversal using the measurements collected in a typical conference room environment. Let  $\psi(k, c)$  denote the best beam obtained for a client  $c$  at codebook level  $k$  after exhaustive training in that level. Once again, if a client is reachable by a beam, it means the received power measure is greater than the minimum required for data transmission.

**Monotonicity.** We define monotonicity of level  $k$  to level  $k + 1$  as the probability a client can be reached by at least one of the children beams in the codebook tree of its best beam  $\psi(k, c)$  of level  $k$ . Fig. 2.11 shows the monotonicity on the y-axis and the codebook level change on the x-axis. The monotonicity is computed for each level change as an aggregate of all the client locations and orientations. The client orientation in Fig. 2.6b facing the AP is considered as LOS link and the other two orientations as NLOS links. We observe that, for the wider beam levels, the children of the best possible beam at a codebook level do not necessarily provide a higher directivity gain. In fact, for NLOS links, the monotonicity percentage is as low as

16%. These observations validate SDM's additional training conducted using the sibling beams in the codebook tree to address non-monotonicity that is significantly present in realistic indoor environments.

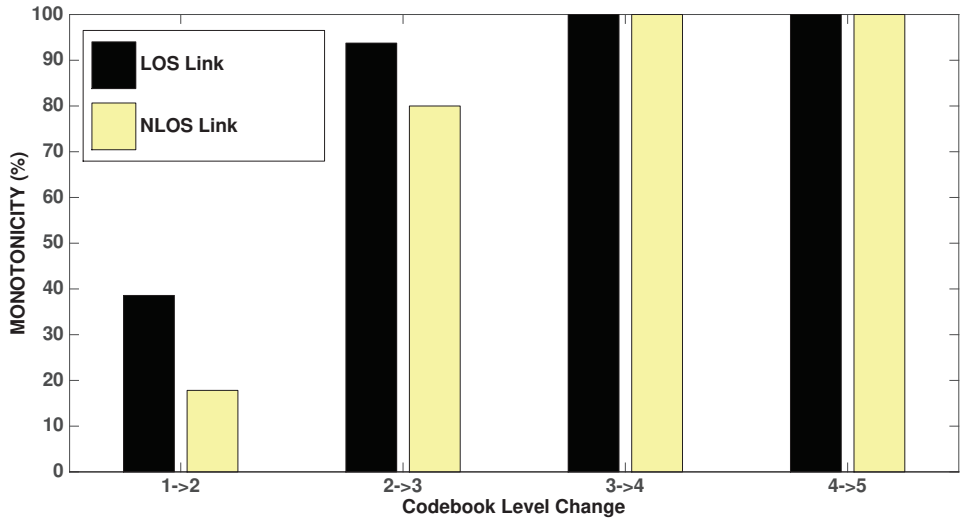


Figure 2.11: Monotonicity.

**Deviation from Best Beam.** Let's consider a client  $c$  is reachable by a child of  $\psi(k, c)$ . Is this child the same as the beam  $\psi(k + 1, c)$ ? In Fig. 2.12, the x-axis is the codebook level change and y-axis is the probability that the child beam reachable at the client and the best beam being equal. We observe that independent of the level change, there is no certainty that we are selecting the best beam at different levels when we traverse using a codebook tree. For the NLOS links, the probability is as low as 12%. The key message here is that in realistic indoor environments due to reflectors and mon-monotonicity inherent in the codebook design, it might be preferable to perform exhaustive search at the finer beam levels than a wide beam level. This is because the deviation from best beam increases with the number of levels trained and we would like to have the finer beams which facilitate higher data rate to have a lower deviation from the best beams in comparison to the wide beams that might lead to a drop in the data rate. These observations validate SDM's training

protocol rationale to begin training from the finest beam level.

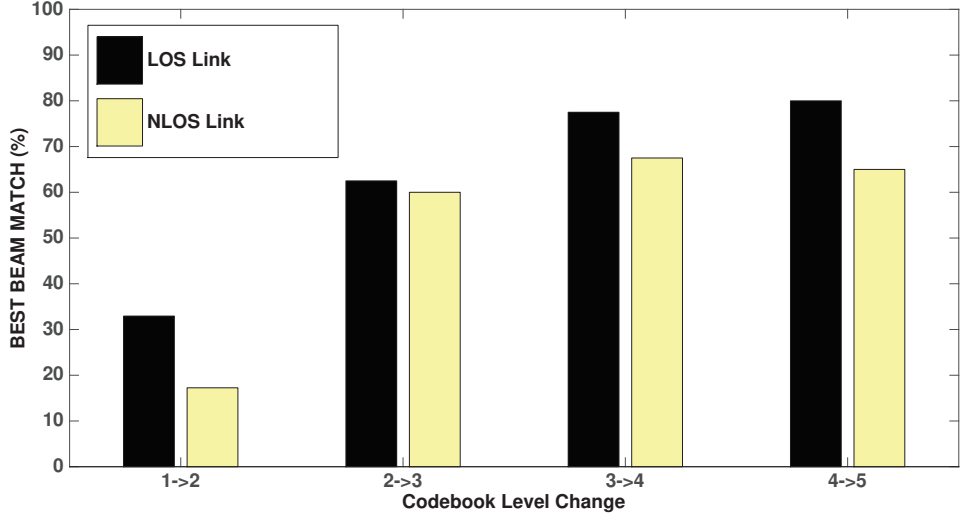


Figure 2.12: Deviation from Best Beam from exhaustive search.

## 2.5 Experimental Evaluation

In this section, we evaluate the performance of SDM’s training protocol and beam group algorithm with the help of our collected measurements. Moreover, we compare its performance against the following baseline models:

- (i) *Exhaustive approach*: This approach performs exhaustive training followed by beam grouping using an exhaustive wide beam search as discussed in Section 2.3;
- (ii) *Only Finest*: This approach performs training only in the finest level followed by beam grouping consisting of only the finest level beams representing a sequential 802.11ad unicast beam generation;
- (iii) *Ascending Order Traversal*: This approach is an extension to the basic traversal discussed in Section 2.2. It performs training starting from the widest beam level and progresses to the finer levels conducting an exhaustive training until every client provides at least one beam pattern in the feedback. Thereafter, it utilizes only the

children of the beams in the feedback for training. For the beam grouping, this approach selects the set of wide beams provided in the feedback that can cover all the clients in the multicast group. In the worst case, all the clients might still be served by the finest level beams if none of the wide beams are such that more than one client is reachable simultaneously by any of them.

Firstly, we analyze the performance in different stages of the multicast timeline (Fig. 2.1(b)) individually. Then, we analyze the throughput performance incorporating the overhead in training and beam group computation. For every experiment analyzed in this section, the x-axis of its corresponding figure is a given number of clients. We collect over a thousand snapshots for every x-axis point. The y-axis in each figure reports the mean and standard deviation of the metric under consideration over all the snapshots. Each snapshot is a combination of:

- (i) *Client Location*: a random client location selection from the 10 locations used in our collected data (Section 2.4);
- (ii) *Client Orientation*: For each client, a random orientation out of the 3 receiver antenna orientations used in our collected data to emulate forced NLOS paths due to blockage;
- (iii) *Codebook Tree*: A random codebook tree out of the 72 codebook trees constructed by our 60 GHz WLAN trace-driven emulator.

We use the same snapshots for the evaluation of our designs in the different stages of the multicast timeline (Section 2.1) including the training, beam grouping and data transmission.

**Scalable Training.** For each snapshot, we conduct training independently using SDM and alternative strategies described earlier in this section. In Fig. 2.13, first, expectedly, exhaustive training has the highest overhead. Second, initially the ascending order traversal strategy has the lowest training overhead as it only uses the

children in the codebook progressing from the widest beam level to the finest beam level. As the multicast group size increases, the number of levels of exhaustive training performed increases before only children are used for training. This is because of the increased probability of at least a single client not being reachable by any of the wide beams. Hence, eventually, for larger multicast group sizes, the training overhead of ascending order traversal is higher than that of the only finest level strategy. Third, SDM has a higher slope than exhaustive training and only-finest level training which have a fixed number of beacons used for training independent of the group size and only the number of feedback packets the AP receives increases with the group size. In contrast, in SDM, not only is the number of feedback packets increasing but the number of beam patterns used increases with the group size resulting in a higher slope. Last, although the gain using SDM in relation to exhaustive training decreases with client size, this represents the scenario when the AP conducts training for all the clients even if a single client failed the beam group quality test. If only the clients that fail the beam group quality test take part in training then the gains would be mainly that of a small client size in Fig. 2.13. *Finding: SDM consistently provides a reduced overhead with up to 44.5% reduction over exhaustive training through its feedback-controlled pruned codebook tree traversal.*

**Scalable Beam Grouping.** Performing an exhaustive beam and client assignment search using exhaustive training information leads to the best beam grouping solution. Therefore, we utilize exhaustive beam grouping as the baseline to compare the performance of SDM and other strategies. To analyze only the performance of beam grouping algorithms with appropriate training inputs, we focus on group throughput during the data transmission period of Fig. 2.1(b) and denote this metric as the *beam grouping efficiency*. For each snapshot, we consider an 8 kB aggregated frame transmitted by each beam of the beam group during a data sweep. We con-

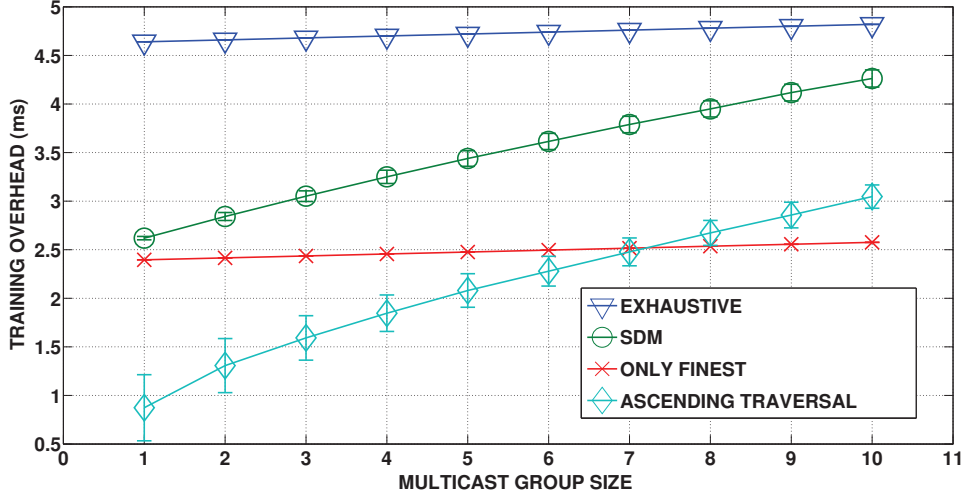


Figure 2.13: Training Overhead.

sider the data transmission period to be the maximum limit of 8.192 ms for transmit opportunity as defined in IEEE 802.11. Therefore, there may be multiple data sweeps during a single data transmission period.

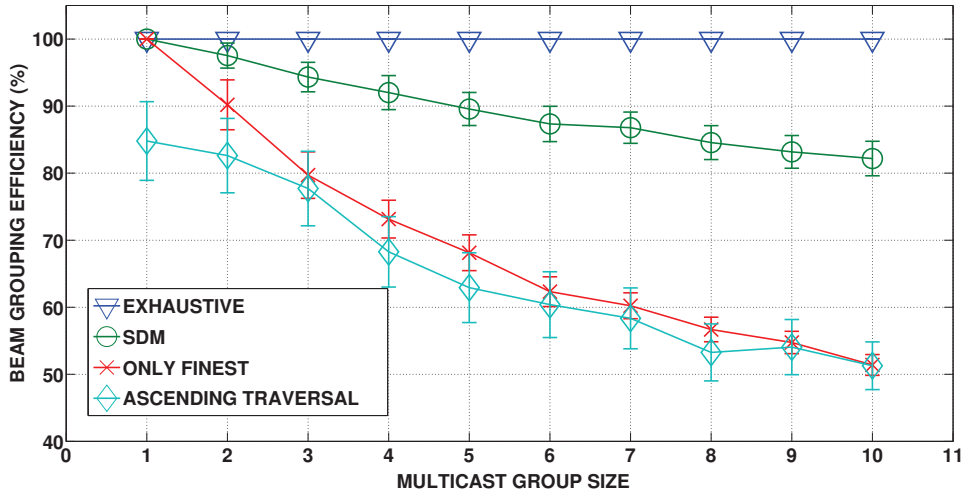


Figure 2.14: Beam Grouping Efficiency.

In Fig. 2.14, first, when there is a single client, all approaches provide the same performance as all use the same finest beam and data rate to serve the client. Second, surprisingly, although the ascending order traversal utilizes wide beams for the beam

grouping, the significant drop in data rate due to the beamwidth-MCS tradeoff leads to a worse performance than even the only finest strategy. Compared to these two strategies, the performance gains of exhaustive strategy and SDM increases with the group size as the diversity in the beam patterns that together minimize the data sweep time increases. Also, the scenario of this figure represents the throughput performance if the beam group quality test (Section 2.1) is a success such that the AP begins data transmission without performing any training and a new beam grouping.

*Finding: SDM’s training and grouping search space although limited in comparison to the exhaustive search yet has a performance within 80% of exhaustive search and grouping solution.*

**Beam Grouping Computation Time.** For each snapshot, we record the computation time taken by the different approaches. We utilize a laptop enabled with quad-core 2 GHz Intel Core i7 processor to record the computation time. As a baseline, we select the only finest strategy solution which is the initial solution for exhaustive search and SDM and consider the mean computation time for this solution to be a nominal value of  $10\mu\text{s}$  when there is a single client. Accordingly, we translate the recorded computation time for our algorithms using this baseline.

In Fig. 2.15, the baseline algorithm expectedly has a negligible increase in computation time with the increase in group size. Second, as the ascending order traversal selects the widest beams that cover all the clients in the multicast group without optimizing over the client assignment and resultant data sweep time of every beam, the beam grouping time for this strategy is only slightly higher in comparison to the only finest strategy. Third, we observe that SDM with its reduced search space for wide beams and using pruned training information, computes its solution in less than 1 ms. This is in comparison to the exhaustive search using exhaustive training information which is heavily slowed down in the wide beam search stage and goes up

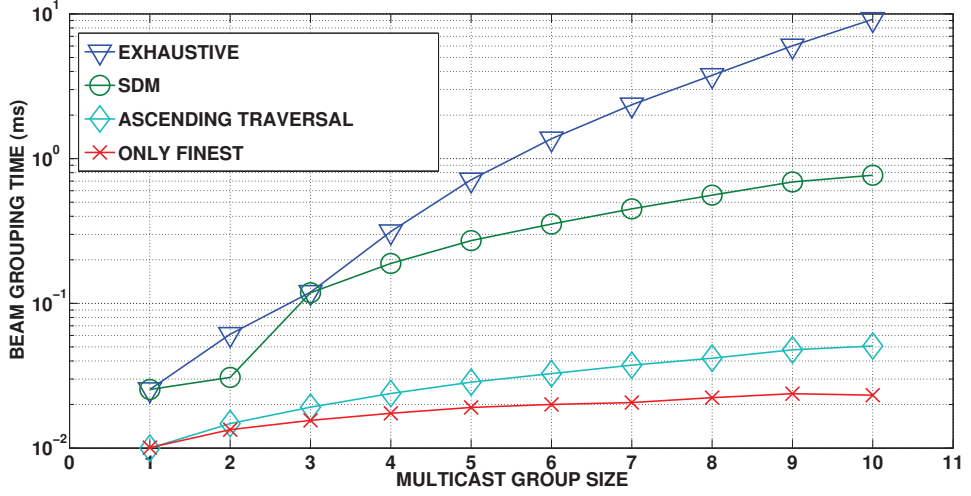


Figure 2.15: Beam Group Computation time.

to 10 ms when the group size is as high as 10.

**Throughput.** Now, we analyze the throughput performance incorporating time overhead for training and beam grouping computation. We analyze the gains provided by SDM if the time saved in training and beam grouping computation was utilized for data transmission. Once again we utilize the exhaustive approach as the baseline.

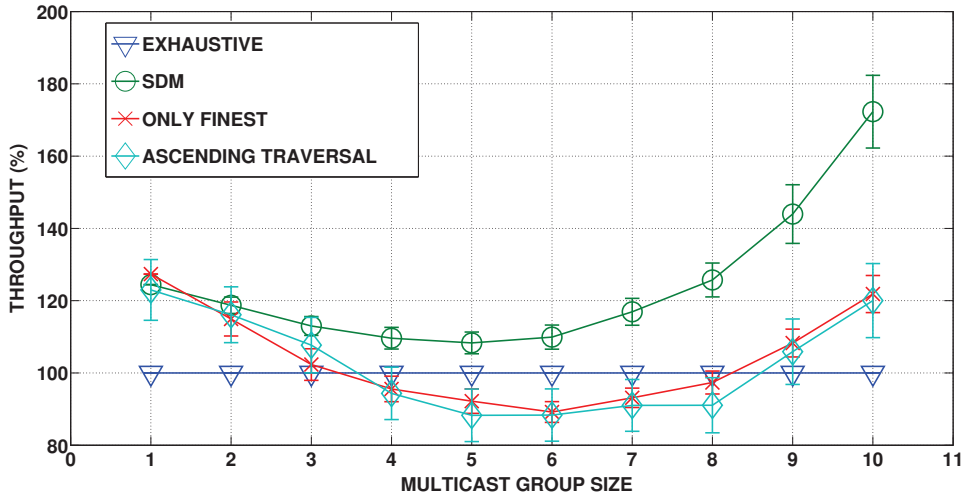


Figure 2.16: Throughput incorporating the overhead in training and beam grouping.

In Fig. 2.16, first, the results indicate that when there is a single client, the ex-

haustive approach is even worse than only finest strategy. This is because of the larger training and beam grouping computation time although the beam group solution is the same for all as shown in Fig. 2.14. Second, as the client size increases, we initially observe a performance drop for all strategies. This is because of the best beam group solution provided by exhaustive approach. Third, with larger group sizes, the performance of all three strategies compared to baseline increases. This is because the increased training time and beam group computation time of the exhaustive approach is better utilized by the other strategies for data transmission. Last, although ascending order traversal and only finest strategies have reduced training and beam grouping computational overhead in comparison to SDM, their significant degradation in data transmission performance as shown in Fig. 2.14 leads to an overall better performance for SDM. *Finding: SDM consistently performs better than the baseline strategies and provides over 80% throughput gains over the exhaustive approach using its scalable codebook tree traversal during the training and beam grouping.*

**Practical Phased-Array Irregularities.** The above experimental evaluation was performed over wireless traces collected using horn antennas as discussed in 2.4. We briefly discuss the impact of irregularities present in consumer-grade phase antenna arrays [43] on SDM’s performance. In [44], the authors analyze the irregularities in the beam patterns of phased antenna array installed in Dell 5000 wireless docking station. For the wide beams, the authors observed deep gaps in the beam pattern that might prevent communication at those specific angles. For the highly-directional beams, the authors observed significant energy from the side lobes -4 to -6 dB compared to main lobe.

SDM’s protocol design naturally takes such irregularities into consideration as the training begins at the finest beams and moves up the codebook

tree to the wider beam levels. Therefore, even if the wide beams cannot be used for communication to a given client either due to low signal strength or deep gaps, the finer beams can still be used for multicast data transmission to that client. In contrast, this strategy would have a negative impact on the Ascending Order Traversal strategy wherein training begins at the widest beam level. With the deep gap irregularity, the probability of performing exhaustive search for all the codebook levels increases in Ascending Order Traversal strategy leading to increased beam training time. As SDM performs a sequential multicast data transmission, there wont be any interference due to the side lobes. The signal energy might be lower in the main lobe due to strong side lobes. This would only affect the SNR and the corresponding MCS used for each beam pattern. This drop in SNR equally affects SDM as well as other alternative strategies considered in this paper for performance comparison.

## LiRa: a WLAN architecture for Visible Light Communication with a Wi-Fi uplink

---

### 3.1 LiRa Architecture

In this section, we present an overview of LiRa’s hardware and software architecture, along with an example deployment scenario and protocol stack.

#### 3.1.1 Hardware and Network Architecture

We design LiRa as an indoor WLAN that dual purposes luminaries for communication. A typical deployment scenario as illustrated in Fig. 3.1 has multiple LED lighting sources used to illuminate a room. The luminaries are typically distributed spatially solely for illumination objectives in order to avoid large shadows associated with a single point source. The LiRa AP controls these LEDs and can either group multiple sources together as a single transmission (e.g., to provide robustness for a high mobility scenario) or divide the coverage area into separate collision domains (e.g., for an auditorium scenario). The latter can be achieved using a variety of techniques including wavelength division (see [45] for a discussion). In either case, the

AP transmits, but does not receive, via VLC, as the LiRa AP is not equipped with photo diodes. For the uplink, the LiRa AP receives via legacy Wi-Fi hardware and custom software as described below.

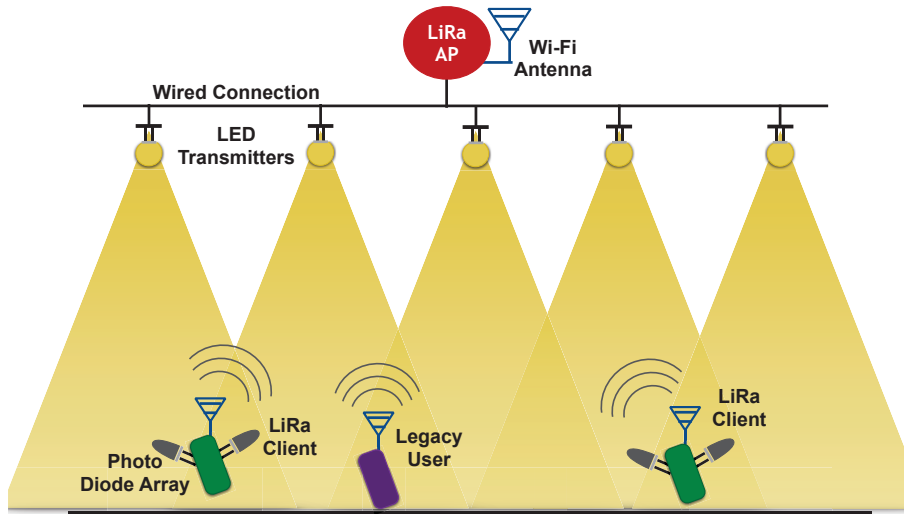


Figure 3.1: Example LiRa scenario.

LiRa clients are equipped with at least one photo diode for reception of VLC signals and preferably have an array of photo diodes on multiple surfaces of the device. The photo diode array provides robustness to device orientation and minimizes the probability of blockage. For example, a device with a single photo diode that is temporarily oriented towards the floor would have a poor reception data rate, receiving only reflected signals, compared to a device that has a photo diode on each surface and can select or combine signals from multiple photo diodes. The LiRa client uses VLC for all downlink data receptions barring outage or failure and uses legacy Wi-Fi hardware and custom software for both uplink control (such as ACKs and channel state reports) and data, and for ACKs of uplink data.

Lastly, as also depicted in the figure, the LiRa AP supports legacy Wi-Fi clients which do not have VLC reception capabilities. A key component of LiRa's design is ensuring that such clients, as well as other nearby Wi-Fi networks (not shown),

obtain a controlled share of air time when interacting with a LiRa network.

Thus, the scenario and hardware architecture target to exploit the inherent coverage of downlink VLC realized by both illumination objectives and low-cost client-side photo diode reception arrays. LiRa does not attempt to realize a robust wide aperture uplink, as to do so would require a client LED transmit array along with transmit power and illumination intensity that would be significantly less than what is viable on the downlink [10, 11]. Instead, LiRa employs a radio uplink.

### 3.1.2 Software and Protocol Stack

LiRa provides a side-by-side light-radio protocol stack integrated via a common IEEE 802.2 interface. Consequently, as illustrated in Fig. 3.2, LiRa provides an abstraction of a single layer-2 hardware interface to higher layers. This approach contrasts with prior work which treats light and radio as separate networks in much the same way mobile clients have both cellular and WLAN interfaces today. The unified interface is critical to realizing both a fast VLC feedback channel and to control the impact of VLC control traffic on legacy Wi-Fi.

From the data flow perspective, *downlink* VLC data originates from the AP only, and the primary functions of the VLC downlink MAC are scheduling, framing, and PHY adaptation. The VLC MAC is not contention based as ambient light sources not controlled by the AP are considered to be interference. The LiRa AP adapts PHY parameters such as the selection of the luminary source(s) and the modulation and coding scheme (MCS), which are impacted by client and environmental mobility as well as interference. The control feedback discussed below provides the required input for this adaptation. LiRa can employ any physical layer, including [6, 5, 46].

The LiRa client receives downlink data via an array of photo diodes. LiRa can also employ any physical layer reception mechanism that is compatible with the transmit-

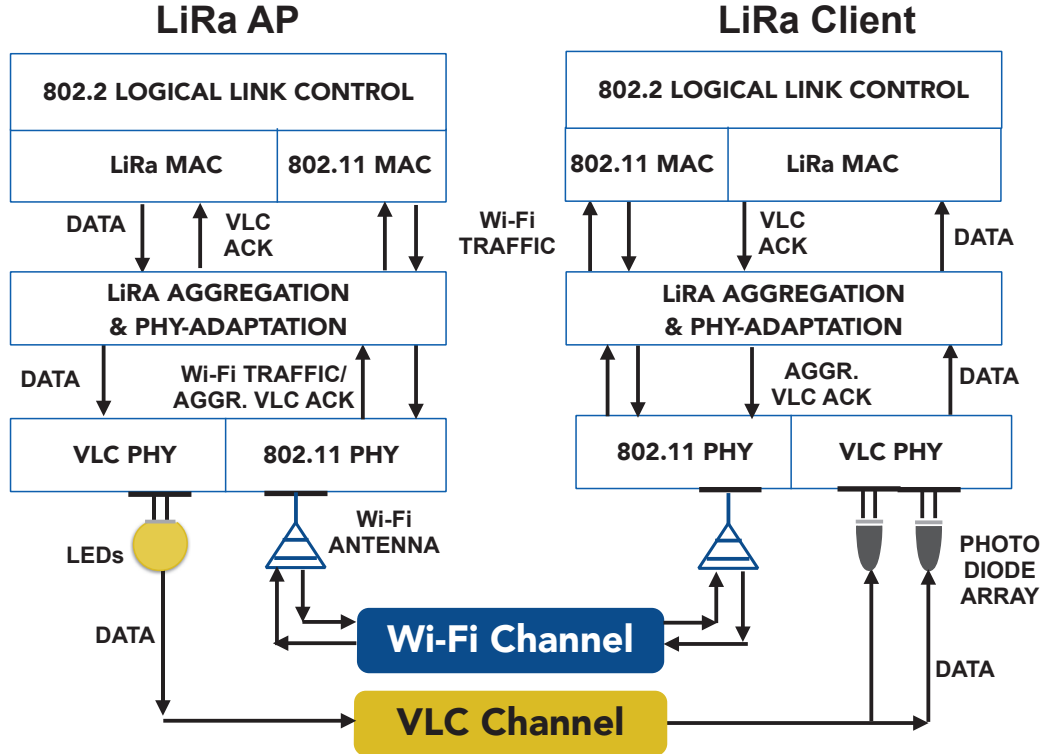


Figure 3.2: LiRa’s protocol stack and data flow.

ter. Frames addressed to the client are processed up the protocol stack as illustrated in the figure.

*Uplink* transmissions can be divided into control frames and data frames. A data frame is transmitted via legacy Wi-Fi in the same way that legacy stations transmit. Moreover, uplink data is acknowledged by the LiRa AP using *Wi-Fi* to maintain backward compatibility and since Wi-Fi already protects the channel for the ACK that follows data. That is, there would be no advantage to using downlink VLC to ACK uplink Wi-Fi data.

Uplink *control* is quite different. Because the VLC and Wi-Fi channels are operating asynchronously, LiRa clients cannot immediately ACK a received VLC frame over Wi-Fi without risking collision or excessively disrupting ongoing traffic. Likewise, if the client contends for Wi-Fi channel access to transmit VLC ARQ feedback,

the delay could be excessive and the feedback load could create heavy contention on the radio channel. Consequently, the AP controls the *time* at which ACKs and other control information are transmitted as described in Section 3.2. Here, we describe the structure of a VLC ARQ feedback: Because client feedback is sent on-demand in response to the AP, we opportunistically aggregate ACK information up to the time that the command is received by the client. When commanded, the client sends an aggregate ACK with a bitmap representation of the frames received along with the sequence number of the first frame. This representation is similar to an 802.11 Block ACK representation [18] with the key difference that the LiRa client does not negotiate a fixed block size with the AP. Instead, this size is opportunistically set by the client at the latest possible instant, in response to the AP’s command. Upon receiving the VLC ARQ feedback, the AP can then perform traditional ARQ. Likewise, we define a field in this same VLC ARQ feedback message to provide hints for the VLC transmitter to adapt its physical layer parameters. The AP can then use a combination of the loss profile (ACK bitmap) and receiver measurements such as SNR for different luminary sources to optimize downlink transmission.

Lastly, we note that with a high data rate in hundreds of Mbps for the VLC downlink and a VLC ARQ feedback delay in the order of tens of milliseconds, the buffering cost at the AP is in the order of a few megabytes. This is a modest overhead given that state-of-the-art APs are equipped with hundreds of megabytes of RAM and gigabytes of flash storage, e.g., Synology RT1900ac router.

### 3.2 A Scalable Feedback Channel for Light

In this section, we present **AP-Spoofed Multi-client ARQ (ASMA)**, a Wi-Fi compatible feedback channel that is triggered by the AP via a spoofed NAV that protects the RF channel for a sufficient time for multiple LiRa clients to send contention-free

feedback. The trigger time is managed to balance the need for timely feedback with the air time that will otherwise be used by legacy Wi-Fi and uplink data.

### 3.2.1 AP Trigger

The VLC downlink transmits multiple frames in succession that can span multiple LiRa clients before reception of acknowledgement feedback to control ARQ. As illustrated in the simplified timeline of Fig. 3.3, VLC downlink frames are transmitted by one luminary or a group of luminaries according to policies as described in Section 2. The AP is shown sequentially transmitting variable sized frames to different LiRa clients as indicated by the depicted numbers. ASMA sets a *feedback trigger timer*: once the timer expires, the AP will aggressively attempt to access the radio channel once it becomes idle in order to transmit an ASMA trigger message.

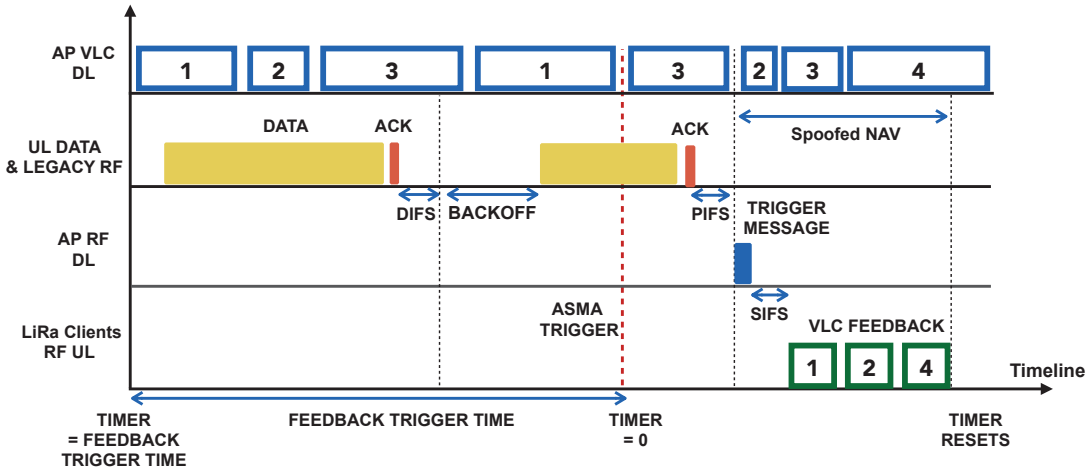


Figure 3.3: Simplified LiRa timeline illustrating the combination of ASMA trigger to the AP, trigger message transmitted by the AP and uplink VLC ARQ feedback transmissions.

The expiration of the feedback trigger timer is also depicted in the figure. In the example, a Wi-Fi transmission was on-going when the timer expired in the figure. Consequently, the AP waits until the transmission completes in order to access the

channel. To minimize the channel access time, the AP employs a prioritized access strategy as follows: When a channel becomes idle, based on the 802.11 standard, each user begins backoff only after the channel becomes idle for DIFS ( $= \text{SIFS} + 2 * \text{SLOT}$ ) duration, where SLOT refers to the length of one backoff counter slot duration. To guarantee that the AP acquires the channel before other users start backoff, the AP sends the ASMA trigger message after the channel becomes idle for PIFS (SIFS + SLOT) time. In case other APs are in range, a less aggressive policy can be used to minimize the chance of collisions of such messages.

### 3.2.2 Spoofed NAV for Control Channel

The objective of the ASMA trigger message is two fold: first, it protects the radio channel for a sufficient duration to enable transmission of the required feedback; second, it provides a transmission schedule for feedback such that multiple clients can send feedback messages without incurring per-client contention and collisions.

We achieve the former objective via the virtual carrier sense mechanism of WiFi in which other stations defer according to the duration contained in the header's Network Allocation Vector (NAV). Namely, the LiRa AP spoofs the NAV: instead of inserting the AP's actual frame transmission duration, it advertises a NAV to enable receipt of the feedback that the AP requires from the stations. This is illustrated in the timeline which depicts the duration field indicating an interval for both the trigger message and the three feedback messages. The trigger message can be realized as a data frame or a CTS-to-self [18] which LiRa clients are programmed to recognize as a trigger message. We employ the latter approach in our implementation. Upon receiving the message, legacy stations will defer and LiRa stations will decode the trigger message.

### 3.2.3 Multi-Client Scheduled Feedback

The second function of the ASMA trigger is to provide a transmission schedule for client feedback messages. In particular, LiRa targets scaling the feedback process by avoiding per-client contention for each feedback message. Consequently, VLC ARQ feedback and channel state information can be efficiently communicated on the uplink in order to guide the AP's ARQ processes and PHY adaptation.

Thus, the trigger message includes an identifier and start time for each LiRa client that the AP requires feedback from. The start time, expressed in mini-slots off-set from the end of the trigger message, enables a group of clients to transmit on the radio uplink sequentially without random access or polling. The figure's timeline illustrates an example in which three clients are commanded by the trigger to transmit feedback, client 1 and 2, which have received data and will feedback both VLC ARQ feedback information and PHY updates, and client 4, which has not received data, but the AP may require other control information from, such as a PHY update to ensure that the client is matched with the best luminary.

### 3.2.4 Balancing LiRa Responsiveness and Control Traffic Air-time

As described above, the feedback trigger time must balance responsiveness for down-link ARQ and PHY adaptation with the air time overhead on the Wi-Fi channel.

Wi-Fi transmissions (legacy RF and LiRa uplink data) following the 802.11 protocol occur for the entire duration of the the feedback trigger time without any use of air-time by LiRa. After the trigger expires, the LiRa AP waits at most the transmission opportunity limit for an ongoing transmission to complete. If the channel was already idle when the timer expires, the AP sends the trigger immediately.

Once the AP accesses the channel to transmit the trigger message after PIFS, the

channel occupancy time includes the time to send the trigger message (denoted as  $T_{tm}$ ) and the time for all LiRa clients to transmit feedback. ASMA includes a SIFS duration between the trigger message and the first LiRa client uplink transmission. This spacing is for the client scheduled first to decode the trigger message preceding its VLC ARQ feedback transmission. Thus, the total time per cycle used for feedback is at most  $PIFS + T_{tm} + SIFS + NT_{fb}$ , in which  $N$  is the number of LiRa stations,  $T_{fb}$  is the maximum per-station feedback time, including PHY preambles and all control fields, and PIFS and SIFS are the same Wi-Fi standard values. Thus, denoting  $T_{ftt}$  as the feedback trigger time, LiRa utilizes no more than a fraction

$$1 - \frac{T_{ftt}}{T_{ftt} + PIFS + T_{tm} + SIFS + NT_{fb}} \quad (3.1)$$

of Wi-Fi air time.

While Equation (3.1) favors a large feedback trigger timer in order to amortize overhead and minimize the impact on legacy and uplink Wi-Fi, a smaller value is favored for ARQ and PHY responsiveness. The maximum delay for feedback is the sum of the trigger time, the maximum Wi-Fi transmission time  $\text{TXOP}_{\max}$ , and the maximum feedback time as given above, i.e.,

$$T_{ftt} + \text{TXOP}_{\max} + PIFS + T_{tm} + SIFS + NT_{fb}. \quad (3.2)$$

Thus, the dominant term in each case is the feedback trigger time with an inverse relationship for fraction of airtime and a linear impact on response delay. We evaluate policies for setting the trigger time in practice in our experimental evaluation.

### 3.3 LiRa Implementation

In this section, we describe our implementation of the key components of LiRa, including a custom VLC platform to collect measurements in a typical indoor environment, and a software-defined radio implementation of LiRa’s RF components.

#### 3.3.1 VLC Downlink Implementation

**VLC AP transmitter.** As described in Section 2, LiRa can employ any VLC physical layer. Here, we repurpose Philips Hue smart-LED lightbulbs [47] that are capable of changing hues and light intensities as transmitters. While the Philips’ hardware and software interfaces do not allow high frequency modulation, the platform enables study of a large set of LiRa performance factors as described below. Most critically, the achievable data rate on a VLC link is a function of the received signal strength at the receiver’s photodiode. This signal strength depends on the luminary’s transmit power, the distance between luminary and photo diode, the incidence angle from the light source, and the irradiation angle at the photodiode. The Philips system along with most other commercial LED luminaries are equipped with diffusers that aid to realizing uniform propagation, thereby minimizing the impact of incidence angle.

**VLC client receiver.** The LiRa VLC receiver depicted in Fig. 3.4, employs Adafruit TSL2591 high dynamic range digital light sensors. We mount the light sensor on top of an Arduino platform that handles serial communication with a computer tasked with data processing. We place the receiver on a transparent holder to reduce undesirable blockage from nearby. This holder is designed to have two concentric acrylic layers that can be rotated 360 degrees relative to each other. This structure is combined with a motion controller [41] that consists of a slider along which the receiver can be linearly moved over 50 cm, and motors that can be controlled via MATLAB to provide desired movements and rotations for the receiver. We further

construct a mobile phone mock-up in order to represent a VLC receiver array used to enhance VLC connectivity as shown in Fig. 3.5.

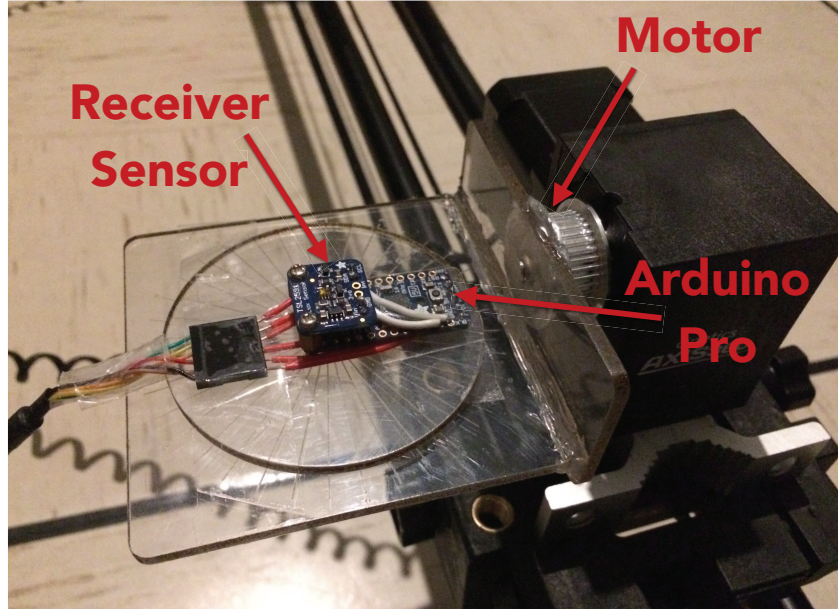


Figure 3.4: VLC single high range sensor.

We further construct a mobile phone mock-up in order to represent a VLC receiver array used to enhance VLC connectivity. As shown in Figure 3.5, we place a photodiode on each edge of a mobile device case, enabling studies the coverage capabilities in the downlink.

**Experimental setup.** Fig. 3.6 illustrates our baseline experimental setup. For all measurements, we hang the smart-LED lightbulb overhead with the help of a stand with an adjustable height. We collect light intensity measurements at locations corresponding to different distances between the LED bulb and receivers spanning over 150 cm. At every location, the receiver's sensor is rotated in steps of 10 degrees, with the sensor's rotation corresponding to the varying irradiance angle that determines the light intensity received. We collect 168 samples of light intensity for every location and every sensor rotation angle. Using this measurement database and

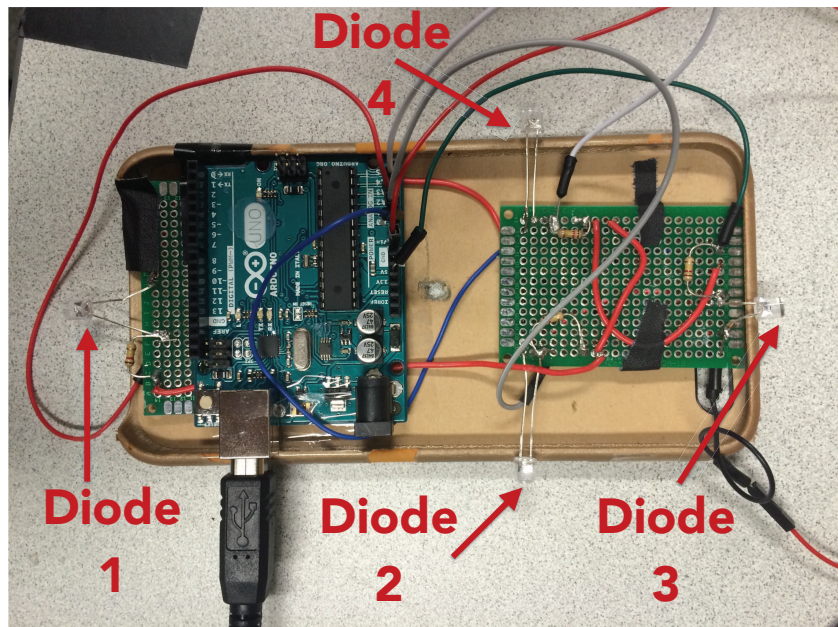


Figure 3.5: VLC receiver array with 4 photo diodes.

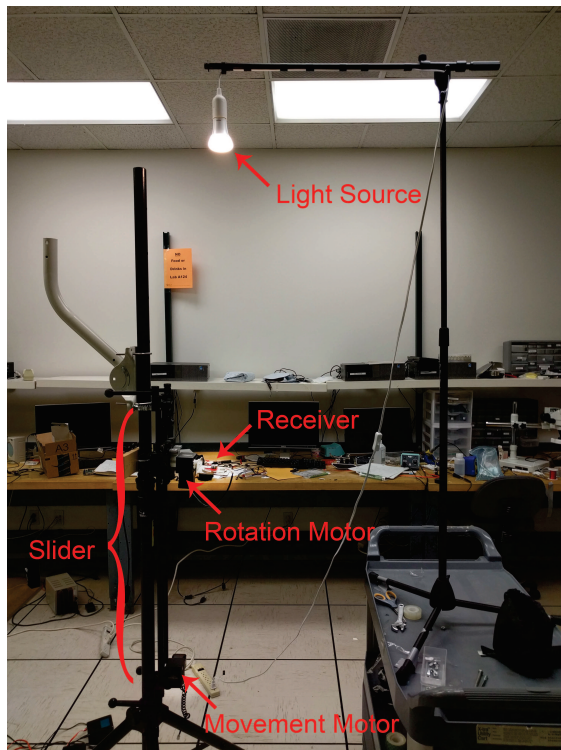


Figure 3.6: Smart LED-based experiment setup.

802.15.7 standard MCS table, we compute the MCS the AP would select for every location and orientation of the sensor.

**Downlink Coverage.** For downlink coverage analysis, we use the same platform setup and methodology. The key difference is that for the receiver, we utilize the phone mock-up design illustrated in Figure 3.5. To study the impact of rotation on downlink coverage, we collect measurements for the roll and pitch axes of rotation, illustrated in Figure 3.7. At each measurement point, we collect 100 samples with an angular granularity of 5 degrees.

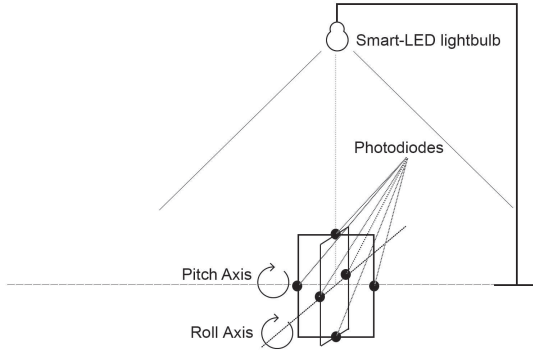


Figure 3.7: Illustration of experimental setup for VLC measurements.

### 3.3.2 Radio Link Implementation

**Implementation.** The hardware setup is illustrated in Fig. 3.8. We utilize WARP v3 [19]. The WARP board exchanges data with a computer via the Ethernet interface and can perform real-time wireless transmission with its WARPNet module. We use the 802.11 reference Design for WARP v3 as the MAC layer design, which is 802.11g compatible. We utilize multiple WARP boards, including 1 AP and different combinations of VLC users and legacy users.

With ASMA, the AP sets the feedback trigger timer after its last reception of feedback and attempts to obtain channel access after the timer expires. During this

period of time, the VLC traffic of LiRa has no impact on the Wi-Fi channel. Once the AP obtains channel access for the trigger, VLC ARQ feedback transmissions are contention free. In our implementation, the AP transmits the trigger message over the air along with the spoofed NAV field. In order to realize the feedback trigger message, the LiRa AP targets to obtain channel access as soon as possible after the channel becomes idle upon expiration of the trigger timer. As specified by ASMA, we replace the DIFS value of the AP with PIFS and set the contention window size to 0 whenever a trigger message should be transmitted.

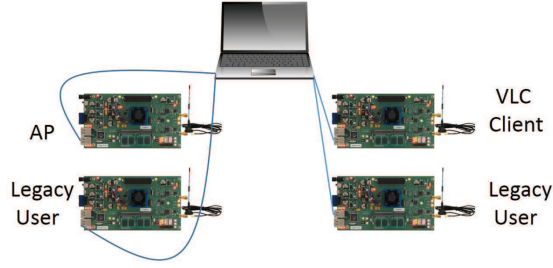


Figure 3.8: Radio link Implementation Setup

The trigger frame’s payload must identify the association ID and time for each of the requested feedback messages. Consequently, we set the trigger frame payload size accordingly.

We implement fully backlog legacy users, which represents the worst case for the AP competing to win contention for the trigger message. We focus on the VLC ACK feedback analysis and therefore do not transmit Wi-Fi uplink data traffic for LiRa clients and instead consider the impact of such traffic to be equivalent to the traffic of other legacy users.

**Experimental Setup.** To evaluate the impact of feedback trigger time, LiRa client size, and legacy user traffic characteristics, we collect over-the-air measurements using the WARP-based LiRa implementation. We couple the above measurements

with computations that utilizes the traces from our VLC downlink measurements as input. We generate 1,000 client locations and assign each client a location and orientation randomly following a uniform distribution of the locations and orientations used in the smart LED bulb measurement study described above. For each location, we compute the per-client MCS that would be selected by the AP for the downlink transmission given the measured signal strength. Then, for different feedback trigger times, we compute the trigger frame payload size for transmission via WARP.

Each experiment run consists of a wall-clock time of 10 seconds in which thousands of legacy user data packets and LiRa feedback messages are transmitted. For analyzing Wi-Fi traffic’s impact on LiRa’s performance, we perform 20 independent reruns spanning several hours given a setting of LiRa trigger time, Wi-Fi operating channel and legacy user traffic flows. We transmit all legacy user data packets via IEEE 802.11g compliant operation and with all frames having length of 1024 bytes with variable MCS unless stated otherwise. The AP has fully backlogged data for the LiRa clients. First, we collect measurements for different feedback trigger times and different trigger frame message sizes corresponding to a unique pairing of feedback trigger time and LiRa client size. Second, we collect measurements for different up-link MCS of the legacy users and the operating Wi-Fi channels to analyze the impact of legacy user traffic on LiRa’s performance. Third, for baseline comparisons, we implement other feedback strategies as described in the next section.

### 3.3.3 Configuration

Unless otherwise noted, all results use the following configuration: First, the ASMA trigger message and the LiRa client’s VLC ARQ feedback is transmitted at the base rate of 6 Mbps and the VLC downlink MPDU (MAC Protocol Data Unit) is 1 kB.

Second, the number of ACKs opportunistically aggregated into a VLC ARQ feed-

---

back transmission depends on the VLC data rate used by the AP to serve the client, as a higher rate yields more ARQ feedback. The VLC downlink rate is dependent on both the PHY architecture of the VLC link as well as environment-dependent factors such as distance. Unless otherwise noted, we map measured signal strength to MCS as specified by 802.15.7, and incorporate all MAC and PHY layer parameters from 802.11 and 802.15.7 standards for the Wi-Fi and VLC links respectively.

Finally, the AP has fully backlogged traffic for downlink transmission to each LiRa client and the legacy users have backlogged traffic for the AP. For scenarios with multiple LiRa clients in the network, the AP conducts the VLC transmission using round-robin scheduling of frames. More sophisticated scheduling [48] and rate adaptation [49] can be applied to improve LiRa performance.

## 3.4 Experimental Evaluation

In this section, we evaluate the performance of LiRa using the above implementation platform. We study VLC coverage, response delay and VLC feedback's impact on legacy Wi-Fi traffic for a broad class of scenarios and configurations.

### 3.4.1 LiRa Coverage

#### 3.4.1.1 Downlink Coverage

Here, we evaluate the coverage provided by VLC luminaries coupled with LiRa's photo-diode receiver array in typical indoor environments. In particular, we study the impact of the receiver's orientation angle on the received signal strength.

In the experiments, we utilize the four diode mobile client depicted in Figure 3.5 in the setup described in Section 4.4. We change the client's orientation angle in  $5$  steps spanning  $360$  and take repeated measurements of signal strength on each photo

diode for each angle.

Figures 3.9(a) and 3.9(b) depict the measured signal strength in the roll and pitch axes of rotation respectively. The figures show the signal strength of the four diodes on the VLC receiver array independently as a function of orientation angle. The results indicate that each photodiode has a non-overlapping 3 dB region of approximately 95 such that in aggregate, the photodiode array can provide 360 coverage for the receiver. Nonetheless, signal strength is not uniform across photodiodes or angles indicating that a feedback channel is required to adapt the VLC transmitter's modulation and coding to its greatest possible value as the device moves.

The measurements also indicate an abrupt drop in signal strength at the 250 mark for diode 2. This is the point where the USB connector is blocking the diode from signal reception. Lastly, while this figure depicts results for a fixed transmitter-receiver distance of 158 cm, other distances yield similar results and hence are not depicted.

### 3.4.1.2 Uplink Coverage

Because LiRa employs a radio uplink, here we evaluate limits of employing *infrared* (or similarly, visible light) as an uplink. In particular, we utilize a commercial system, pureLiFi [17], that, like LiRa, provides downlink coverage via LED light fixtures connected to an AP. However, in contrast to LiRa, pureLiFi's uplink uses infrared instead of radio. The pureLiFi client does not employ an infrared LED transmitter on each of its surfaces; indeed, we expect that due to the relative bulk of LED transmitters (similar to the size of a phone's flash), it would be infeasible to place one on each of the mobile client's surfaces, even in future designs.

PureLiFi enables separate locations for the AP's LED bulb acting as the luminary and downlink transmitter and the AP's photo-diode based infrared receiver. For our purposes of evaluating coverage, we place these two AP components adjacent to

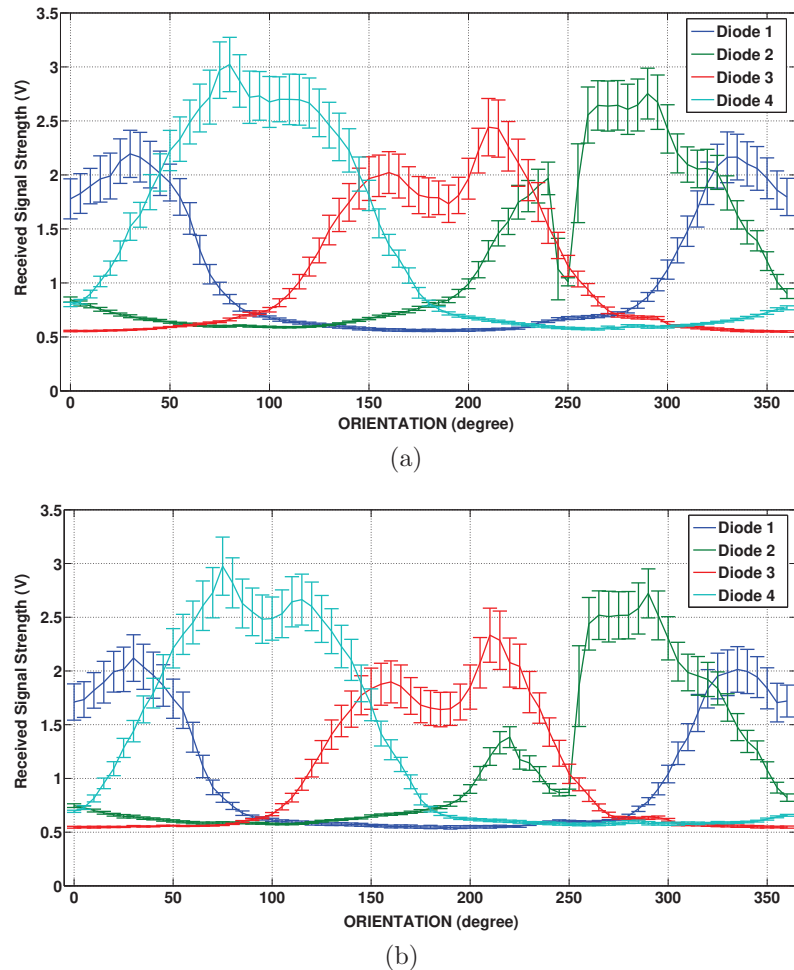


Figure 3.9: Downlink coverage provided by LiRa as a function of client rotation. (a) Roll axis (b) Pitch axis.

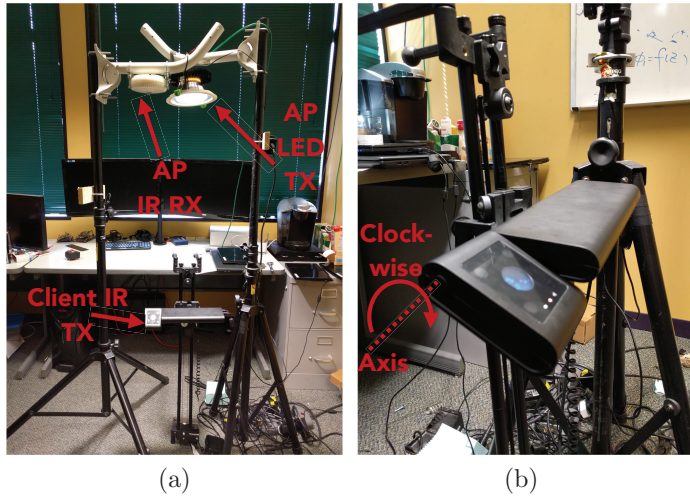


Figure 3.10: Uplink coverage experiments (a) Setup where IR stands for infrared. (b) pureLiFi client unit.

each other and position the client 130 cm below as illustrated in Figure 3.10(a). We study uplink coverage and the impact of the client’s infrared transmitter orientation on uplink throughput and vary the orientation of the client about its edge axis as illustrated in Figure 3.10(b). The orientation is changed in steps of 5° with 0° representing perfect alignment (i.e., the infrared client transmitter is perfectly aligned with the AP’s ceiling mounted photo diode receiver). We perform the rotation in both clockwise and counter-clockwise directions. For each orientation angle, we conduct 10 independent runs and use *iperf* to measure the data transferred in an interval of approximately 10 seconds under TCP protocol with default TCP window size of 85.3 kB.

The results are depicted in Figure 3.11, which shows uplink throughput vs. orientation angle. Negative and positive angles indicate clockwise and counter-clockwise rotations respectively. First, the throughput is close to the peak value at the best alignment and  $\pm 5^\circ$ . Second, with increased rotation of 10°, the throughput remains at 1.2 Mbps in the counter-clockwise direction but reduces to 0.6 Mbps in the clockwise direction. This asymmetry arises due to the increased distance between the trans-

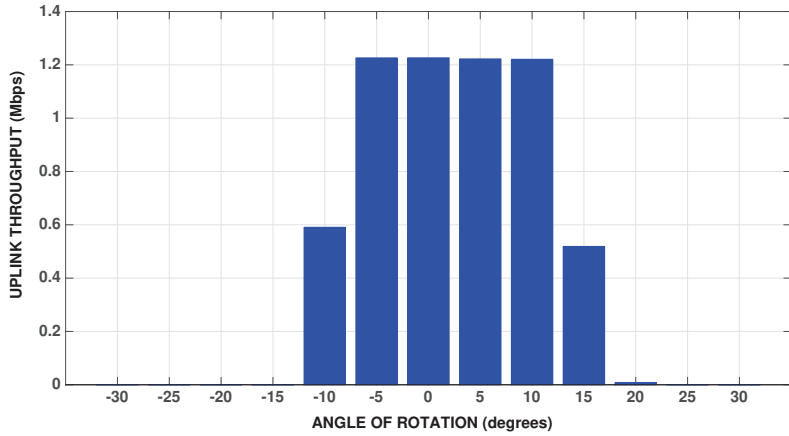


Figure 3.11: Uplink throughput of pureLiFi versus orientation angle.

mitter and receiver in the case of clockwise rotation as the rotation axis is the edge of the client’s device.

*Finding:* At 20 degrees of rotation, we observe negligible throughput of 8.4 kbps, beyond which the link can no longer be established, yielding zero throughput. In contrast, LiRa targets mobile clients and consequently employs radio as an uplink medium, which is not subject to such deep rotational fades and outages.

### 3.4.2 Response Delay Evaluation

Here, we analyze the impact of feedback trigger time, the number of LiRa clients, and interference from Wi-Fi traffic on response delay. The response delay is the duration between when the AP transmits a VLC frame to a particular client and when the AP receives ARQ feedback for that particular frame. The *mean* response delay is an average over all frames and clients, as well as over time with multiple trigger messages. Likewise, the feedback trigger time is the duration of the timer that the AP uses before contending for access to the wireless channel to send the trigger message, as described in Section 3.2.1.

### 3.4.2.1 Clean-Channel Feedback Delay

Here, we isolate the effect of VLC feedback traffic and consider the case of only LiRa feedback on the Wi-Fi link, i.e., without legacy Wi-Fi traffic nor LiRa uplink data traffic. Figure 3.12 depicts the measured mean response delay vs. feedback trigger time. First, for each fixed trigger time, the mean response delay is lower than the corresponding trigger time value. This is because frames transmitted in the latter part of the trigger duration typically have a response delay that is less than the trigger time itself (cf. Figure 3.3).

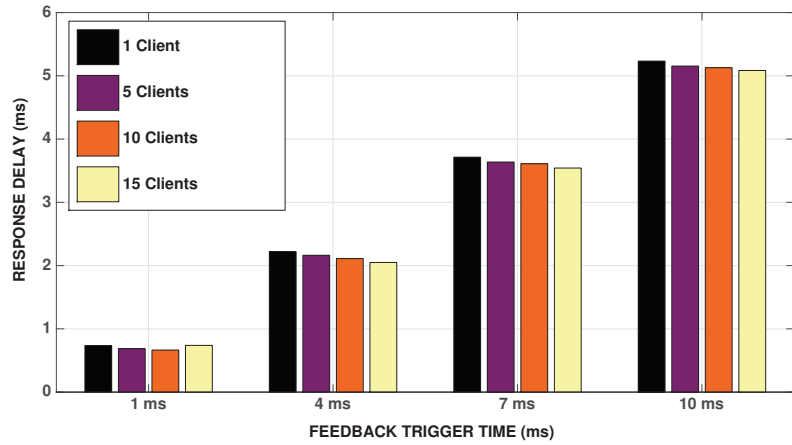


Figure 3.12: ASMA's trigger time impact on response delay.

Second, the response delay is consistently largest when there is a single client in the network, independent of the trigger time. This is because with an increasing number of clients, the time between transmission of consecutive frames to the same client increases. Hence, the time between a frame's transmission and the corresponding VLC ARQ feedback reduces for client size greater than one.

Third, for the smallest feedback trigger time of 1 ms, the response delay is non-monotonic with client size, initially decreasing as described above, but subsequently increasing from 10 to 15 clients. This is because for a low trigger time of 1 ms, the airtime spent in feedback is significant in comparison to the feedback trigger time. For

example, when 15 clients each has the maximum downlink VLC PHY rate 100 Mbps, the airtime required by LiRa’s trigger message and all client VLC ARQ feedback is over 1 ms. This non-monotonicity effect does not occur with higher trigger times since the trigger time would be the dominating factor of the response delay as characterized by Equation (3.2).

### 3.4.2.2 Congested-Channel Feedback Delay

In ASMA, the AP wins channel contention by transmitting the trigger message a duration PIFS after the channel becomes idle. However, the time between ASMA triggering the AP to enqueue the trigger message for transmission and the AP transmitting the trigger message over-the-air depends on the Wi-Fi traffic characteristics which includes uplink and downlink transmissions from legacy stations as well as uplink data from LiRa clients. Moreover, even when a controlled experiment is run with a fixed number of legacy users, there might be interference from legacy users associated with other APs nearby. For this purpose, we analyze the impact of Wi-Fi traffic on ASMA’s response delay in two dimensions: number of Wi-Fi traffic flows and the Wi-Fi operating channel. In our experiments, there are either one or three Wi-Fi traffic flows in the network and we set their uplink PHY data rate to 18 Mbps. We fix the feedback trigger time to 5 ms and the number of LiRa clients to be a high value of 10. We analyze the impact of co-channel interference by conducting the experiments in three different Wi-Fi channels of operation: channels 1 and 14 in the 2.4 GHz band and channel 48 in the 5 GHz band.

Fig. 3.13 depicts mean response delay as a function of the combination of the number of traffic flows and the Wi-Fi operating channel. First, independent of the number of traffic flows and the Wi-Fi channel, the mean response delay is consistently lower than the corresponding trigger time value. This is because frames transmitted

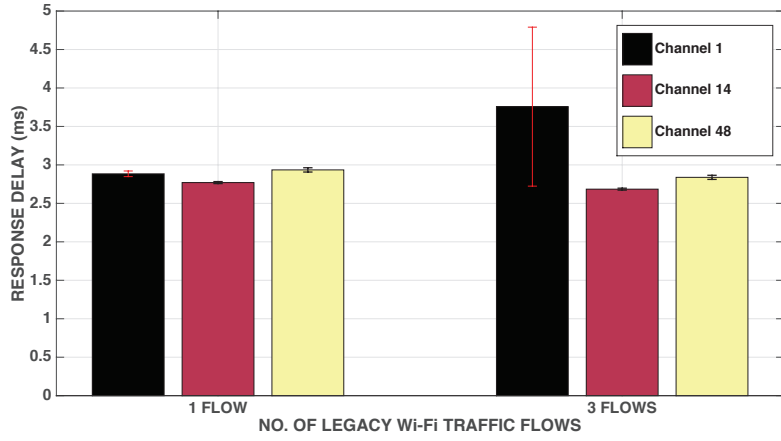


Figure 3.13: Wi-Fi traffic impact on LiRa’s response delay: 1 flow and 3 flows.

in the latter part of the trigger duration typically have a response delay that is less than the trigger time itself (cf. Fig. 3.3). Second, there are differences in response delay across different channels due to uncontrolled Wi-Fi transmissions occurring in the range of the AP. The channels 14 and 48 have negligible variance in response delay because they are not used for commercial Wi-Fi operation in the experiment coverage area. Finally, response delay increases with the number of flows in Channel 1. This is due to the increased probability of the channel being occupied by legacy user transmissions when the trigger timer expires. In our experiments, we observe behavior similar to this figure for varying sets of LiRa client sizes and trigger times spanning from 1 ms (frequent feedback) to 10 ms (less frequent feedback).

*Finding:* The average response delay is lower than LiRa’s feedback trigger time independent of LiRa client size and legacy Wi-Fi traffic.

### 3.4.3 Impact on Wi-Fi Throughput

#### 3.4.3.1 Feedback Channel Airtime Bounds

We next analyze the RF airtime occupied by the AP and LiRa clients for the VLC ARQ feedback transmissions, as this airtime necessarily decreases throughput of Wi-

Fi. The feedback airtime depends on the size of the VLC ARQ feedback messages, which increases with both the feedback trigger time and the the VLC downlink PHY rate, as it requires ARQ feedback for more frames. Nonetheless, a larger trigger time amortizes the fixed feedback overhead such as the header of the AP's trigger message.

To analyze the bounds of airtime utilized by LiRa, we consider scenarios of 1 or 10 LiRa clients each receiving VLC data at either 10 Mbps or 100 Mbps, with 1 kB frame size. As in the analysis of Section 3.2.4, the airtime required includes PIFS, SIFS, the time to send the trigger message, and the time for all LiRa clients to transmit feedback.

Figure 3.14 depicts the computed Wi-Fi airtime required by LiRa feedback vs. feedback trigger time for this scenario. We consider the lower and upper bounds of the channel access delay for the AP's trigger message: Figure 3.14(a) corresponds to zero access delay for the AP so that the AP transmits the trigger message immediately after the message is enqueued, whereas Figure 3.14(b) considers this message to be delayed by the time taken for a 1kB frame to transmit at the Wi-Fi base rate of 6 Mbps. We select this time as the frames of the legacy users in our over-the-air experiments are 1kB size and the longest delay corresponds to the frame transmission at base rate.

Figure 3.14(a) indicates that when there is a single client with VLC downlink data rate 10 Mbps, the feedback airtime is independent of the feedback trigger time because each symbol in 802.11 6 Mbps MCS contains 24 bits. Hence, an ARQ feedback frame containing a single ACK bit and a frame containing 24 ACK bits takes the same time to transmit; likewise for byte boundaries.

In contrast, with 10 VLC clients at 100 Mbps each, client feedback requires significantly more airtime. Consequently, with zero access delay, 1 msec trigger time is undesirable as it would require 0.63 msec of feedback for each 1 msec of Wi-Fi

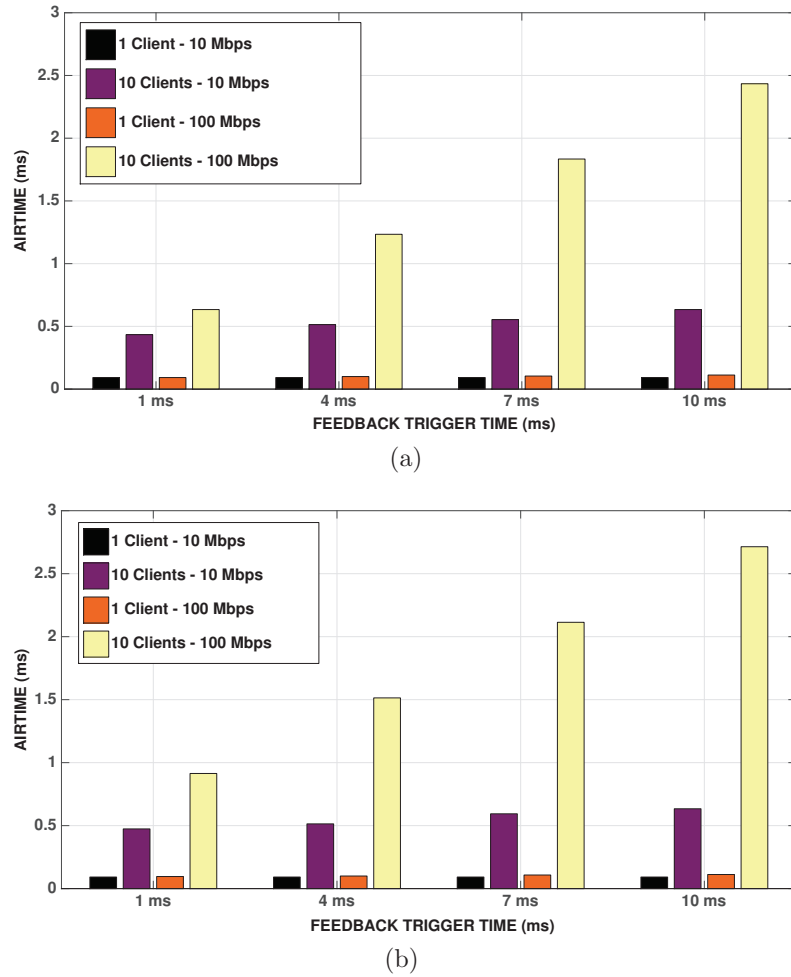


Figure 3.14: Computed airtime used by LiRa for varying access delay between expiration of the trigger timer and transmission of the feedback trigger message: (a) zero delay (b) 1.3 ms delay.

transmissions i.e., up to 39% share of airtime. Hence, with a larger number of LiRa clients, the trigger time must also be increased. Nonetheless, the increase in trigger time is not for free as the required feedback data also increases with trigger time, e.g., the airtime increases 3.84 times as the trigger time increases by 10 times from 1 ms to 10 ms.

Figure 3.14(b) corresponds to the maximum access delay for the trigger message in which the AP must first wait for the transmission time of a 1kB frame in the Wi-Fi channel at the base rate of 6 Mbps. In this case, the airtime required per trigger message is higher in comparison to the corresponding scenarios in Figure 3.14(a) due to the increase in feedback data for the downlink VLC frames received between enqueueing the AP’s trigger message and the AP winning contention. However, this increased airtime does not necessarily lead to increased fraction of airtime in comparison to zero delay case. For example, for 10 clients at 100 Mbps each, a 1 msec trigger time requires 0.91 msec of feedback for each 1 msec of Wi-Fi transmissions i.e., up to 28% of airtime.

### 3.4.3.2 Feedback Trigger Time

Here, we turn from bounds to measurements and vary the feedback trigger time, which not only impacts the airtime reserved for the VLC ARQ feedback transmissions but also the frequency at which the airtime is reserved. We configure a single continuously backlogged uplink Wi-Fi traffic flow with PHY rate configured to 18 Mbps and measure its throughput with and without ASMA.

Figure 3.15 depicts the measured decrease in Wi-Fi throughput vs. the feedback trigger time for varying number of LiRa clients. First, as discussed in Section 3.2, legacy Wi-Fi throughput degradation decreases inversely proportional to feedback trigger time. This is because the airtime required for ARQ feedback messages in-

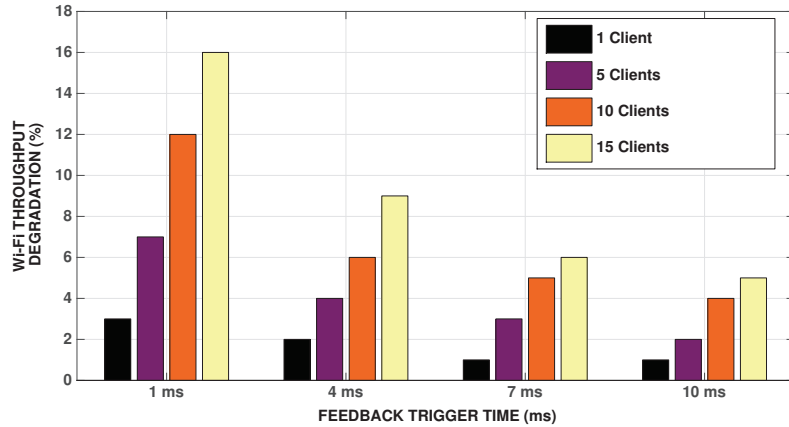


Figure 3.15: LiRa’s feedback trigger time impact on Wi-Fi throughput degradation using over-the-air measurements.

creases at a much slower rate than the increase in trigger time, as only one ACK bit is added for every data packet received in the downlink. For example, with a data rate of 10 Mbps in the VLC downlink, a 1kB frame requires 819.2  $\mu$ sec to transmit. Corresponding to this frame, a single ACK bit added would take 0.17  $\mu$ sec of the Wi-Fi airtime. Second, Wi-Fi throughput degradation increases with the number of LiRa clients independent of the trigger time, with higher variance for short trigger times. This is because with short trigger times, the client feedback time is a significant factor (as high as 92% for 1 msec triggers) in the airtime utilized by LiRa in the Wi-Fi channel and this feedback scales linearly with the number of clients as defined in Equation (3.1).

### 3.4.4 Feedback with Per-Client Contention

To analyze the gains provided by ASMA’s strategies of spoofed NAV and multi-client scheduled feedback, we compare ASMA’s performance with an alternative strategy employing client-driven feedback.

We define *Per-client Contention (PCC)* as a feedback mechanism in which each VLC client *independently* contends via 802.11 to transmit feedback, such that VLC

feedback is treated as an encapsulated Wi-Fi data frame. This approach contrasts with ASMA in that because the AP has not provided a spoofed NAV to allow feedback, the PCC clients providing feedback must contend independently. Consequently, the total feedback contention on the radio channel is once per client vs. once per trigger time. Nonetheless, we do not require PCC clients to contend for each downlink VLC *frame*. Instead, a PCC client begins contention as soon as it has feedback to send to minimize the response delay. Also, each PCC client opportunistically aggregates ARQ feedback up to the time that it obtains channel access for sending the feedback message. Thus, similar to LiRa, PCC uses a bitmap representation with opportunistic aggregation of feedback information up to the time that the client transmits.

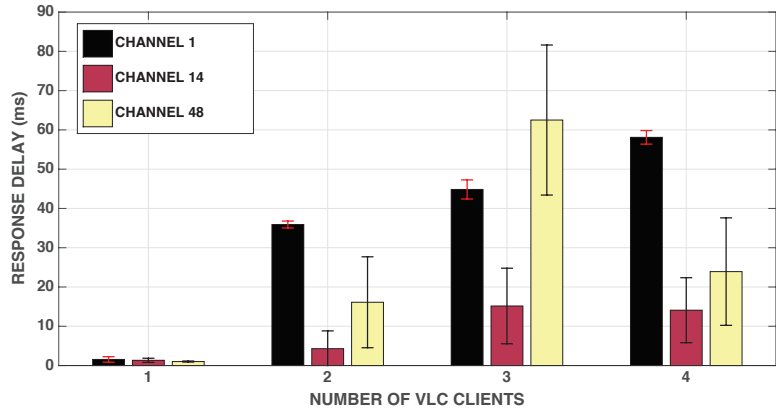


Figure 3.16: Response Delay performance of Per-Client Contention in different Wi-Fi channels.

We configure a single legacy user with fully backlogged traffic for the AP and a varying number of VLC clients. Fig. 3.16 depicts the average response delay of PCC vs. the number of VLC clients in different Wi-Fi channels. First, when there is a single client in the network, the response delay is less than 10 ms in all channels comparable to LiRa’s response delay. When the VLC client size increases to 2, the response delay in channel 1 increases to 35 msec. This is due to the uncontrollable, ongoing transmissions in this channel during this experiment run. In contrast, the

response delay in channels 14 is still below 10 msec. In this channel, not only does the client have negligible interference from other transmissions but also there is a high probability of winning contention as there is just a single legacy user associated to its AP. Second, with an increase in the number of clients, PCC's response delay in all channels increases highlighting the strong impact of contention on the response delay performance of PCC. This increased delay results from the airtime lost in collisions among the PCC feedback and with the uplink data packets of legacy user. Third, increasing from three to four clients results in a decrease in mean response delay for channel 48 and a negligible change in channel 14. This is because although there is increased probability of collisions, there is also increased probability of a VLC client (vs. the legacy user) winning the contention for VLC ARQ feedback transmission. In contrast, channel 1 being used for commercial operation has the additional effect of co-channel interference resulting in an increase in response delay.

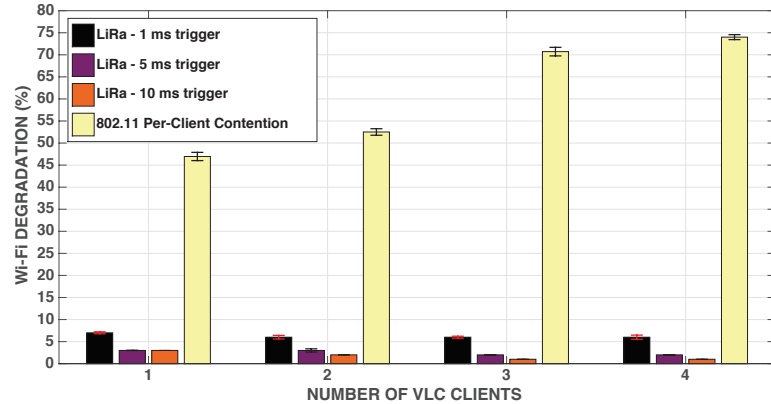


Figure 3.17: Wi-Fi throughput degradation comparison between LiRa and Per-Client Contention model.

Finally, we compare PCC to ASMA and Fig. 3.17 depicts measured Wi-Fi throughput degradation vs. the number of VLC clients. First, as discussed in Section 3.2, for LiRa, legacy Wi-Fi throughput degradation decreases inversely proportional to feedback trigger time. This is because the airtime required for ARQ feedback mes-

sages increases at a much slower rate than the increase in trigger time, as only one ACK bit is added for every data packet received in the downlink. For example, with a data rate of 10 Mbps in the VLC downlink, a 1kB frame requires 819.2  $\mu$ sec to transmit. Corresponding to this frame, a single ACK bit added would take 0.17  $\mu$ sec of the Wi-Fi airtime. Second, for LiRa, Wi-Fi throughput degradation has higher variance for short trigger times. This is because with short trigger times, the client feedback time is a significant factor (as high as 92% for 1 msec triggers) in the air-time utilized by LiRa in the Wi-Fi channel and this feedback scales linearly with the number of clients as defined in Equation (3.1). Third, the results indicate that PCC consistently has over 7 times the degradation of LiRa, independent of the number of VLC clients and LiRa trigger time. When there is a single VLC client, the PCC client attempts to win the channel immediately after receiving the first packet since the last PCC feedback transmission. This leads to 47% degradation of legacy Wi-Fi throughput. As the VLC client size increases, the increased occupancy by the VLC clients for their independent PCC feedback frames and the additional time lost due to collisions leads to 74% degradation in Wi-Fi throughput. In contrast, LiRa has a maximum degradation of 7% when the trigger time is as low as 1 ms. Hence, in contrast to PCC, ASMA provides a responsive and scalable feedback mechanism.

*Finding: With feedback trigger time of 5 msec, LiRa can reduce the response delay by a factor of 15 and reduce the legacy Wi-Fi throughput degradation to 3% from an excessive value of 74%.*

## LiSCAN: Visible Light Uni-Directional Control Channel for Uplink Radio Access

---

### 4.1 Background

In this section, we discuss the contention-free access and packet detection mechanisms in 802.11 standard.

**Point-Coordination Function (PCF).** 802.11 PCF enables the AP capability to provide centralized contention-free access to the sensors. The periods of contention-free service are alternated by the standard random access contention periods. PCF begins with the AP aggressively gaining access to the channel by transmitting a 802.11 beacon PIFS (SIFS + 1 slot time) duration after the channel becomes idle. This beacon includes the maximum possible duration of the current contention-free period. Accordingly, the sensors set their timer to defer from contention-based access. The AP maintains a polling list of associated stations and polls in a *round-robin* manner. For efficiency, acknowledgement for received frames at the AP and polling of immediate next sensor may be combined. If a polled sensor has no backlogged data, the sensor does not transmit any frame and the AP transmits next poll request after

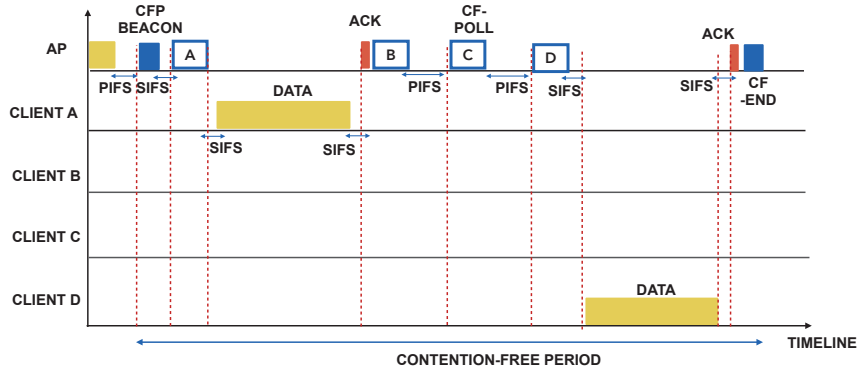


Figure 4.1: 802.11 contention-free period timeline.

PIFS duration ( $25 \mu\text{s}$ ). This PIFS duration includes (a) one slot time ( $9\mu\text{s}$ ) consisting of preamble-based packet detection and (b) SIFS duration ( $16\mu\text{s}$ ) for AP to switch from receive mode to transmit mode. The contention-free period ends when the AP transmits a CF-End management frame leading to the start of a contention period. Figure 4.1 illustrates the functioning of PCF. sensors A and D have backlogged data whereas sensors B and C have no backlogged data.

## 4.2 LiSCAN Architecture

In this section, we present the design principles of LiSCAN’s hardware and software architecture to enable VLC uni-directional control for uplink contention-free access. Moreover, we discuss an example deployment scenario and protocol stack.

### 4.2.1 Hardware and Network Architecture

We design an indoor WLAN [20] that dual purposes luminaries for communication. A typical deployment scenario as illustrated in Fig. 4.2 has multiple LED lighting sources used to illuminate a room. The luminaires are typically distributed spatially solely for illumination objectives in order to avoid large shadows associated with a single point source. To enable maximum reliability of light-poll, the LiSCAN AP

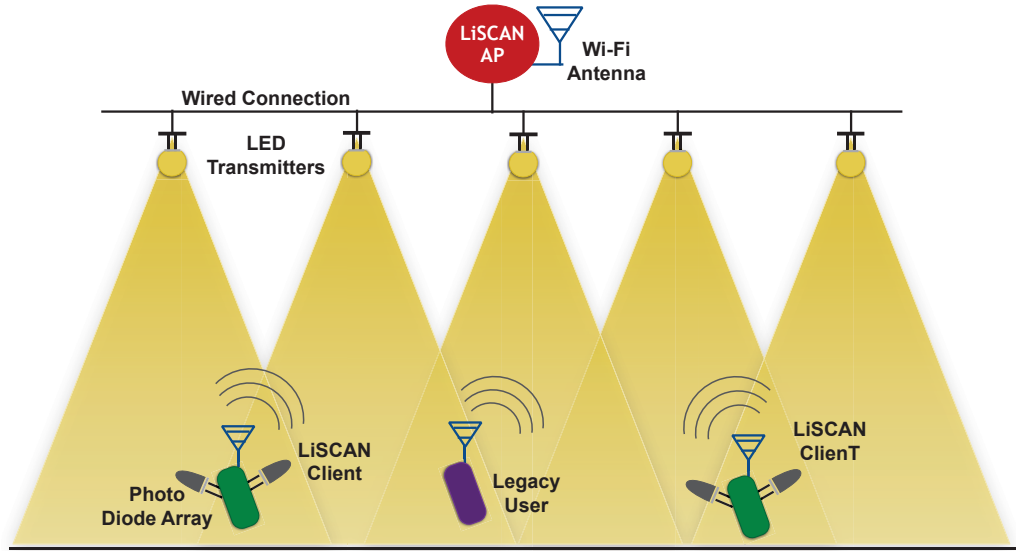


Figure 4.2: Example LiSCAN scenario.

controls these LEDs and groups multiple sources together as a single broadcast transmission. The AP is only required to transmit but not receive via VLC, as the LiSCAN AP need not be equipped with photo diodes. For the downlink data transmission and uplink reception, the LiSCAN AP utilizes legacy Wi-Fi hardware and custom software as described below.

LiSCAN sensors are equipped with a VLC wake-up receiver system [26, 27] for reception of VLC signals. The LiSCAN sensor uses VLC for all downlink polling control barring outage or failure. At the same time, LiSCAN sensor uses legacy Wi-Fi hardware and custom software for uplink control (such as ACKs and channel state reports) and data.

#### 4.2.2 Software and Protocol Stack

LiSCAN provides a side-by-side light-radio protocol stack integrated via a common IEEE 802.2 interface. Consequently, as illustrated in Fig. 4.3, LiSCAN provides an abstraction of a single layer-2 hardware interface to higher layers. The unified inter-

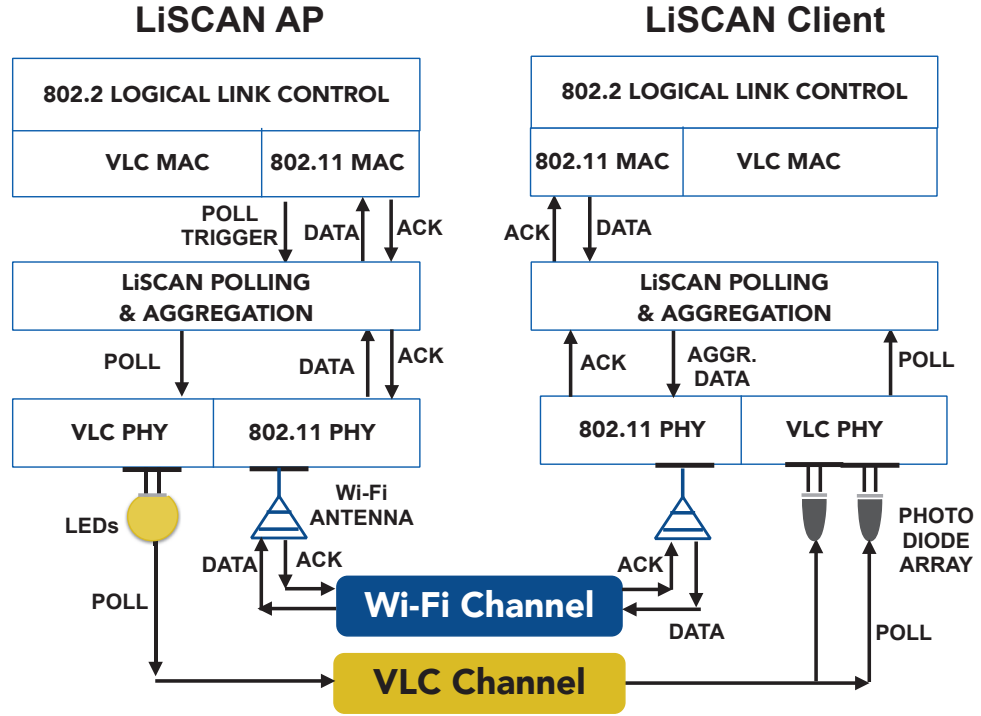


Figure 4.3: LiSCAN architecture and polling traffic flow.

face is critical to realizing a fast VLC control channel for uplink Wi-Fi transmissions.

From the data flow perspective, the polling for LiSCAN sensors is performed over VLC only. The light-polls are transmitted at the base rate similar to a poll transmission over radio. The primary functions of the VLC downlink MAC are scheduling, framing, and PHY adaptation. The VLC MAC is not contention based as ambient light sources not controlled by the AP are considered to be interference. LiSCAN can employ any physical layer, including [6, 5, 46]. Frames addressed to the sensor are processed up the protocol stack as illustrated in the figure.

*Uplink* data frame is transmitted via legacy Wi-Fi in the same way that legacy stations transmit. Moreover, uplink data is acknowledged by the LiSCAN AP using VLC to minimize the radio airtime overhead involved in AP switching from receive mode to transmit mode and back. In this manner, the AP can transmit ACK over VLC as soon as it completes decoding a received data frame over radio.

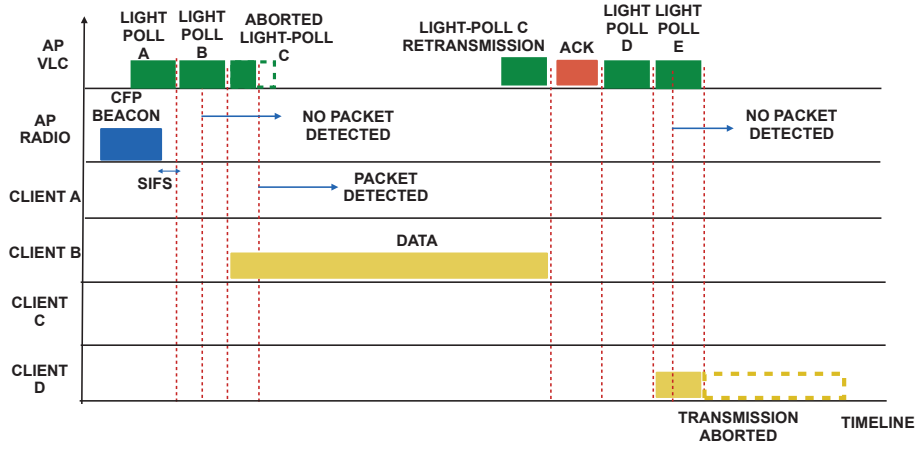


Figure 4.4: LiSCAN contention-free period timeline.

Next, we describe the structure of the uplink data frame. Because the sensor only transmits backlogged data in response to the AP’s light-poll, we employ frame aggregation all the frames forwarded from the 802.11 MAC to the LiSCAN Polling and Aggregation sub-layer. This is in contrast to polling the sensor multiple rounds wherein each round the sensor only transmits a single frame.

### 4.3 LiSCAN Design

Utilizing the virtual full-duplex operation of VLC (transmit mode) and radio (receive mode) at AP, LiSCAN minimizes the radio airtime overhead. In this section, we present the key concepts of LiSCAN’s pipelined VLC polling. Second, we analyze the bounds of overhead reduction achieved by LiSCAN.

#### 4.3.1 LiSCAN’s Pipelined VLC Polling

To realize a scalable contention-free uplink access by polling over VLC, we design LiSCAN whose timeline is illustrated in Figure 4.4. The key strategies of LiSCAN are as follows:

**Initial VLC-RF Alignment.** In LiSCAN, the AP begins CFP by gaining access to both RF and VLC channels. Over RF, similar to 802.11 PCF, AP aggressively transmits a beacon frame PIFS duration after channel becomes idle to broadcast start of CFP. Throughout the contention-free period in LiSCAN, the sensors are solely in transmit mode on Wi-Fi radio and the AP is solely in receive mode over Wi-Fi. This is to eliminate the time spent in switching from transmit mode to receive mode and vice versa. To minimize the airtime lost in RF while transmitting light-poll to first sensor in schedule, our key strategy is to *align* both the transmissions such that light-poll to first sensor in schedule ends SIFS duration after the end of CFP start beacon. This scenario represents CFP start beacon over RF and light-poll to sensors A in Figure 4.4. The additional SIFS duration is required for sensor A to switch from receive to transmit mode.

**Pipelined Polling.** A simple approach (as in 802.11 PCF) to poll the next sensor in schedule is to wait until the occurrence of the following event: (*i*) the end of an ongoing data- ACK exchange or (*ii*) wait for PIFS duration (includes one slot time for packet detection and SIFS duration for AP RX-to-TX switch). Clearly, this can lead to significant polling overhead when only a small percentage of sensors have backlogged data. In LiSCAN’s design, we take advantage of the virtual full-duplex operation of VLC (transmit mode) and radio (receive mode) at AP. Our key strategy is to transmit light-poll to next sensor in schedule immediately after end of light-poll to the current sensor. Also, at the end of a light poll transmission, we begin a packet detection countdown timer that begins from an initial value matching the packet detection time (20  $\mu$ s in IEEE 802.11). Depending on whether the AP detects an uplink transmission or not, LiSCAN behaves in the following manner:

(*a*) *No packet detected.* If the current sensor (sensor A) has no backlogged data, then it won’t transmit any data corresponding to the light-poll it receives. Con-

---

sequently, the AP fully transmits the light-poll for next sensor (sensor B) with no abortion as it does not detect any 802.11 frame. Upon hearing its light-poll, the next sensor can transmit any backlogged data as soon as it decodes the VLC poll. In this scenario, LiSCAN eliminates the overhead involved in waiting for detection of uplink data frame before transmitting next light-poll. This scenario represents light-polls to sensor A and sensor B in Figure 4.4.

(b) *Packet detected.* As soon as the AP detects the current sensor's (sensor B) transmission, it computes the transmission time of the ongoing uplink frame from sensor B. If this transmission time is longer than that of the ongoing light-poll transmission to next sensor (sensor C), the AP will immediately abort the light-poll transmission. As the light poll transmission time is longer than the 802.11 packet detection ( $20\mu s$ ), the light poll to next sensor is not fully transmitted before abortion. In future, if the VLC rate becomes faster, additional payload can be added to ensure the transmission time of light-poll is at least longer than the 802.11 packet detection time. Consequently, the next sensor does not transmit any backlogged data. Through this light-poll abortion, we prevent any uplink collisions at the AP. This scenario represents light-polls to sensors B and C in Figure 4.4.

**ACK over VLC.** In LiSCAN, we utilize VLC instead of radio for ACK transmissions corresponding to successful uplink data reception. This serves two purposes: First, by transmitting over VLC, LiSCAN eliminates the radio airtime lost in AP switching from receive mode to transmit mode for ACK transmission and back to receive mode for future data reception. Second, by transmitting over VLC, the next sensor in schedule can transmit backlogged data over radio concurrently with ACK transmission over VLC. To achieve this, LiSCAN utilizes the PHY header of ongoing uplink data transmission to find out the time at which this transmission ends. As the light-poll to next sensor in schedule was aborted upon hearing the ongoing transmis-

---

sion's preamble, LiSCAN begins the retransmission of next sensor's light-poll to end at the same time as ongoing uplink transmission. In this manner, if the next sensor has backlogged data, it can begin the data transmission as soon as it decodes the light-poll. Concurrently, the AP can transmit the ACK if it successfully receives the uplink data frame. Accordingly, the next light-poll will be transmitted after the ACK transmission. On the other hand, if the AP doesn't receive the frame successfully, then it won't transmit an ACK and the next light-poll in schedule is transmitted immediately after decoding reception failure. In Figure 4.4, we illustrate the alignment of light-poll to sensor C with the end of data transmission from sensor B. After successful decoding of sensor B's data, AP transmits the corresponding ACK over VLC followed by light-poll to sensor D.

**Preemptive Uplink Interference Avoidance.** sensors' uplink transmissions could suffer from channel fading or co-channel interference from neighboring Wi-Fi cells and other co-existing technologies. In 802.11 PCF, when the AP fails to detect the preamble of a sensor's uplink transmission, it waits for PIFS duration before transmitting next poll. If the next sensor has backlogged data and transmits to the AP, it would lead to reception failure at the AP due to the multiple concurrent uplink transmissions. In a saturated traffic scenario, such interference can lead to significant loss in radio airtime. In LiSCAN, for the same scenario of preamble detection failure, the AP assumes there is no data transmission from current sensor and consequently completes the transmission of light-poll to the next sensor without abortion. To prevent collision at the AP, in LiSCAN, the current sensor pre-emptively aborts its ongoing data transmission upon hearing a *fully-transmitted* light-poll to next sensor. In this manner, LiSCAN eliminates collision of uplink data transmissions from multiple sensors due to preamble detection failure. This scenario is represented by the abortion of data transmission from sensor D on hearing the light-poll for sensor

E.

### 4.3.2 Packet Detection Sensitivity

An important component of LiSCAN is the uplink packet detection. When an uplink packet is detected, LiSCAN aborts the light-poll transmission before it is fully transmitted. The physical carrier sensing in 802.11 is conducted by the Clear Channel Assessment module that determines the idle/busy status of the radio channel. OFDM PHY Clear Channel Assessment utilizes the amount of received energy at the Radio-Frequency module and preamble-based detection to detect valid 802.11 signals. The initial part of the preamble consists of ten identical sequences of Short Training Symbols of length 16 samples each of duration  $0.8 \mu\text{s}$  obtained by OFDM modulation of known pseudo-random noise (PN) sequences. The AP can detect the start of an 802.11 packet by correlating the received signal with known PN sequences. The key advantage of a PN sequence is the sharp distinct peak that it provides exactly when the input signal to the correlator matches the PN sequence. The IEEE 802.11 standard mandates that, when a 802.11 receiver senses a 802.11 signal whose energy is above the Clear Channel Assessment threshold of  $-62 \text{ dBm}$ , the preamble detection probability has to be  $\geq 90\%$  in an observation time window of  $4\mu\text{s}$ .

Following the coarse synchronization using preamble detection, the Long Training Symbols in the preamble undergo cross-correlation for channel estimation, fine frequency offset estimation, and fine symbol timing offset estimation. False preamble detection may occur either due to thermal noise or due to devices of co-existing technologies operating in the same radio band. Commercial WLAN devices cope with false packet detection through dynamic adaptation of correlation thresholds for detection and synchronization. Even after the correlation checks, an invalid 802.11 signal would fail the CRC-16 parity check on the PHY header leading to medium

status reset to idle [50]. In our scenario, even when a sensor is transmitting a valid 802.11 frame to the AP, strong interference on the same radio channel might lead to failure in packet detection at the AP. In Section 4.5, we show that LiSCAN’s preemptive interference avoidance helps minimize the performance degradation due to packet detection failure at the AP independent of the interference level.

### 4.3.3 Light-Poll Analysis

In 802.11 PCF, the radio airtime lost in polling a non-backlogged sensor is the sum of poll transmission time and PIFS duration of idle waiting ( $135\mu s$ ). A significant percentage (81.5%) of this lost time is spent in the transmission of poll. In contrast, by transmitting the next light-poll in a pipelined manner can provide significant reductions in overhead. Next, we analyze the overhead reduction brought about by LiSCAN for different scenarios.

Standard Specification	Value
Poll Payload	418 bits
Preamble	124 bits
PHY header	32
Modulation	On-Off Keying
Min. Optical Clock Rate	15 MHz
Lowest data rate	6 Mbps

Table 4.1: 802.15.7 frame timing and data rates.

To compute the poll transmission time over VLC, we utilize the same polling payload size as in 802.11 PCF. We incorporate the rest of the frame components sizes and data rates as defined in the 802.15.7 standard and provided in Table 4.1. The VLC packet preamble consists of a fast locking pattern (64 bits) and four topology dependent patterns (15 bits each). The PHY header consists of 32 bits including information about operating channel, MCS index, optional dimming extension etc. For high rate ON-OFF Keying (OOK) modulation, the PHY header for On-Off Keying

modulation can be sent at one of the following data rates: 6 Mbps, 12 Mbps, 24 Mbps and 48 Mb/s, depending on the selected optical clock rate. The preamble and headers are required by the standard to be transmitted at the lowest data rate for a chosen optical clock rate. Assuming the same rate of 6 Mbps as chosen for 802.11 PCF, the transmission time of a light-poll is equal to  $110\mu s$ . Next, we discuss the range of radio airtime spent idly during light-poll transmission:

(i) *Best case*: This represents the light-poll to sensor C that aligns its end with the end of data transmission from sensor B in Figure 4.4. Therefore, sensor C can transmit any backlogged data immediately resulting in zero airtime lost. When most sensors in the network have fully backlogged traffic, LiSCAN incurs zero radio airtime for light-poll transmissions thus achieving maximum efficiency.

(ii) *Worst case*: This represents the light-poll to sensor B following the light-poll to sensor A in Figure 4.4. As sensor A had no backlogged data, there is no poll reply from sensor A. Therefore, the radio channel is idle during the entire transmission of light-poll to sensor B. In this case, this is equivalent to a poll transmission over RF. However, LiSCAN might still reduce the overhead in case sensor B has no backlogged data. This is because in LiSCAN the light-poll for sensor C immediately follows light-poll for sensor B instead of waiting for PIFS duration as in 802.11 PCF.

(iii) *Interference case*: In case of preamble detection failure of an uplink data frame, the AP doesn't abort the light-poll to next sensor. As that uplink data frame will be aborted after the sensor receives the light-poll for next sensor, this data does not account for successful data received by AP. Therefore, this light-poll transmission to next sensor will be considered as radio airtime overhead and is equivalent to the worst case described previously.

## 4.4 LiSCAN Simulation Framework

To analyze LiSCAN’s performance for varying network conditions and to compare it’s performance against alternative strategies, we utilize ns-3 network simulator [51]. In this section, we briefly describe our ns-3 implementation of LiSCAN and alternative strategies, the traffic generation model at the LiSCAN sensors and radio interference model.

### 4.4.1 Protocol Simulation

To simulate contention-free access in ns-3, we implement a base ns-3 MAC contention-free access model on top of the existing 802.11g Wi-Fi PHY implementation. For channel fading, we utilize the NIST model, an OFDM error rate model that has been validated experimental results from physical-layer testbed [52]. We inherit the base contention-free model to implement the different protocols as follows:

**LiSCAN.** To simulate the uni-directional VLC downlink, we utilize a Wi-Fi channel different from the channel used for the uplink data transmission from the sensors. As cross-channel interference is non-existent in the basic Wi-Fi PHY implementation of ns-3, the VLC downlink and radio uplink are treated as non-interfering bands. In LiSCAN, the radio module is turned on exclusively for the data transmission.

**Contention-free radio access.** In contrast to LiSCAN, in contention-free radio-only strategy, the same Wi-Fi channel is used for transmission of downlink control packets from the AP including poll and ACK and uplink data packets from the sensors. This is simialr to the Contention-free radio access mechanism descibed in Section 4.1. In this strategy, the radio module is turned on when the sensor has backlogged traffic and during the data-ACK exchange.

**Contention-based radio access.** This strategy performs 802.11 contention-based access for uplink data transmissions from the sensors. Similar to contention-

free radio access, the radio module is turned on for contending on the channel for backlogged traffic and data-ACK exchange.

#### 4.4.2 Uplink Data Traffic Model

To simulate realistic Internet traffic, we utilize the Poisson Pareto Burst Process (PPBP) [53] model that has been validated to match the statistical properties of real-life IP networks. This model is based on the overlapping of multiple traffic bursts. The arrival of each traffic burst follows a Poisson distribution. It has been shown that the distribution of the sizes of files transmitted across the Internet is heavy-tailed [54]. Therefore, the burst length is modeled by Pareto distribution with infinite variance resulting in a long-range dependent traffic model. The Pareto distribution is characterized by a Hurst parameter that defines the shape of the distribution. The typical values for this Hurst parameter lie between 0.5 and 0.9.

As our focus is on contention-free access for uplink data transmissions, we consider packets arrive at the uplink MAC queue of each sensor independently following the PPBP model. In LiSCAN, under high traffic conditions, the light-polls are transmitted concurrently with uplink data transmission resulting in a low overhead. To analyze the overhead reduction in comparison to Contention-free radio access, in our simulations, we consider varying mean burst arrival rates at the sensors.

#### 4.4.3 Simulation Setup

Using the models described above, we perform simulations under varying network conditions of sensor size, the percentage of sensors with traffic during the contention-free period and the mean burst arrival rate. We fix the mean burst time length of PPBP process to a value of 10 milliseconds. We consider 10 bytes generated by the burst process model and with a maximum aggregation of 100 bytes for data

---

transmission. For each combination of network conditions, we perform over 1000 runs of 100 ms each separately for LiSCAN and alternative strategies. We consider the polls, light-polls and ACKs are transmitted at the base rate of 6 Mbps. For the uplink data transmission, we consider the sensors can transmit at 54 Mbps. In each contention-free period for both LiSCAN and Contention-free radio access, the polling is performed in a round-robin manner and the schedule is selected randomly using a uniform distribution. For each run, we obtain the following performance metrics:

**Mean channel access delay.** We define channel access delay as the time between a packet arrival to sensor’s uplink MAC queue and corresponding over-the-air transmission. This delay does not include the retransmission delay as our goal is to analyze the delay due to the polling protocol in polling a sensor. When a sensor’s packet fails to be received successfully by the AP, the AP does not transmit any ACK corresponding to that data frame. Accordingly, the failed packet is added back to the transmission queue and is considered a new packet in the queue for our analysis. The mean channel access delay of a contenton free period run is the mean of channel access delay across every uplink data packet transmitted during the run.

**Throughput.** We define the throughput in a contention-free period as the total successful uplink data received by the AP divided by the duration of the contention-free period.

**Energy Consumption.** The mean energy consumption for which the radio module of a sensor is awake. In LiSCAN, the sensor is awake on the radio only for the data transmission. In contrast, in the alternative strategies, the radio is awake whenever there is backlogged traffic and for the data-ACK exchange. For the contention-based access, we utilized the default WiFi Radio Energy model implemented in ns-3. For the energy consumption in contention-free strategies, the power consumption in different states of sensor was modeled utilizing existing research works [55, 56, 57].

## 4.5 LiSCAN Evaluation

With increasing number of sensors generating traffic, we expect negligible change in the polling overhead for LiSCAN and contention-free radio access. This is because the AP is oblivious of the traffic generation at the sensors and therefore includes every sensor in its polling schedule. In contrast, in contention-based access, only the sensors generating traffic take part in the contention procedure. With increasing traffic burst arrival rate at the sensors, we expect the probability of a polled sensor to have backlogged data to increase leading to increased radio channel utilization for contention-free strategies. In this section, we analyze LiSCAN’s performance under varying network conditions and also compare its performance with alternative strategies. Unless stated otherwise, for every figure in this section: (a) each sub-plot corresponds to a particular ratio of the sensors generating any traffic and (b) the x-axis in each sub-plot represents the varying mean burst arrival rate at the sensors generating traffic during a runtime of 100 milliseconds. We define the ratio of sensors generating any traffic during a run as *sensor ratio*.

### 4.5.1 Radio Access Delay

In Figure 4.5, we analyze the impact of the sensor ratio and the traffic arrival rate on the channel access delay. With low traffic burst rates and low sensor ratio, the contention-based access has the lowest access delay as the sensor generating traffic does not suffer from collisions and binary exponential backoff. In contrast, the radio-only contention free strategy has the highest delay as significant airtime is spent in polling sensors with no traffic. With moderate to high traffic burst rates independent of the sensor ratio, contention-based approach incurs a steep increase in access delay. This is because of the increased contention-based collisions and consequent exponential backoff for retransmissions. In contrast, there is only a slight increase for the

contention-free strategies as they do not suffer from collisions. The slight increase in contention-free strategies is due to the increased radio utilization for uplink data transmission.

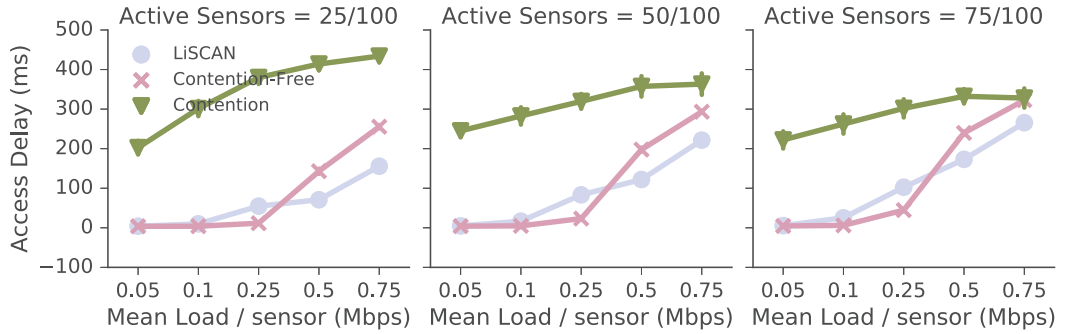


Figure 4.5: Mean channel access delay vs traffic burst arrival rates for varying sensor ratios.

### 4.5.2 Throughput

In Figure 4.6, we analyze the impact of the sensor ratio and the traffic arrival rate on the aggregate uplink throughput at the AP. With low sensor ratio, independent of the traffic burst rate, the contention-based access provides the highest throughput. This is because the contention-based strategies spend significant airtime polling sensors with no backlogged traffic. With moderate to high traffic rates, we observe LiSCAN provides significant improvement in throughput compared to other strategies. Unlike contention-based access, the sensors in LiSCAN do not contend and transmit their data as soon as they receive a light-poll intended for them. Unlike radio-only contention, the increased radio utilization enables LiSCAN to transmit the light-polls and ACKs over VLC concurrently with uplink radio transmissions. In this manner, LiSCAN increases the radio airtime for uplink data transmissions compared to radio-only contention-free strategy.

*Finding:* *LiSCAN's virtual full-duplex operation provides up to 5 times higher*

aggregate throughput over contention-based strategy during high traffic conditions in dense sensor networks.

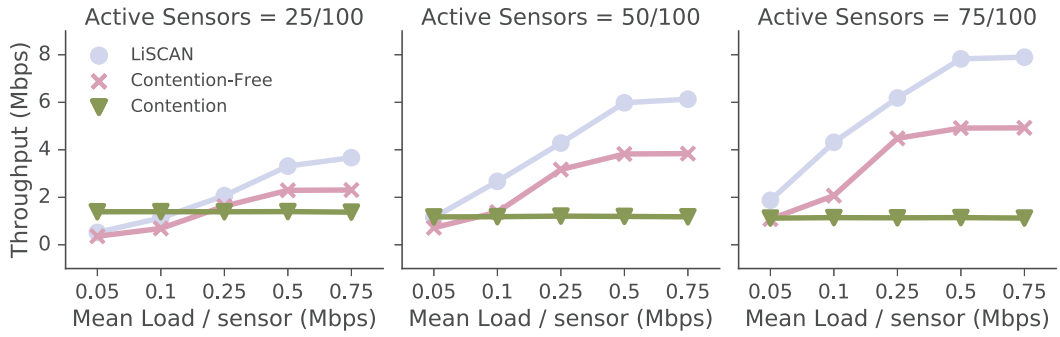


Figure 4.6: Aggregate throughput vs traffic burst arrival rates for varying sensor ratios.

#### 4.5.3 Radio Awake Time

In Figure 4.7, we analyze the impact of the sensor ratio and the traffic arrival rate on the mean time for which the radio is awake in LiSCAN. First, independent of the sensor ratio and traffic rate, the mean awake time of a sensor in LiSCAN is less than 0.5 ms for a contention-free period of 100 ms (less than 0.5%). This low awake time is due to the radio module of a sensor being turned on in LiSCAN only for the uplink data transmission. Even if the sensor has backlogged traffic, the wake up receiver keeps the radio off until receiving a light-poll intended for this sensor. Moreover, the VLC wake-up receiver receives the ACK for a just concluded uplink data transmission instead of the sensor’s radio. Second, for a given traffic ratio, the mean awake time increases with increasing sensor ratio. This is because of the increased number of sensors generating traffic during the contention-free period. Third, with increasing traffic rates, the awake time increases as the data generated by sensors generating any traffic increases.

*Finding:* LiSCAN’s utilization of VLC channel for radio control results in near-

*zero energy consumption on the radio channel.*

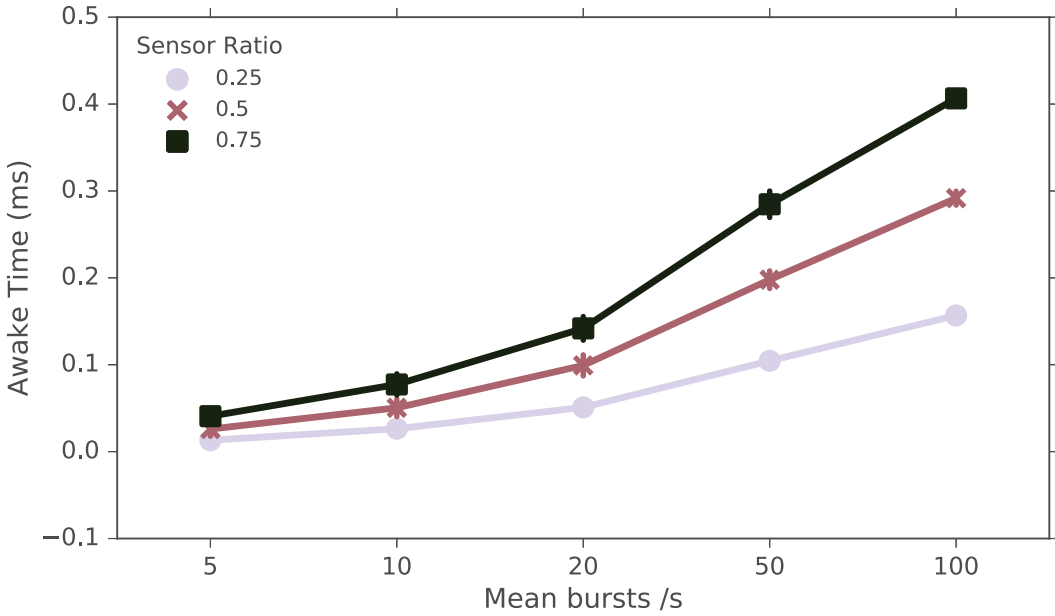


Figure 4.7: Mean energy consumption per active sensor in LiSCAN vs traffic burst arrival rates for varying sensor ratios

In Figure 4.7, we compare the radio awake time of LiSCAN and other strategies for varying traffic rates and sensor ratios. First, compared to LiSCAN, the radio-only strategies have significantly higher awake time. This is because the radio of a sensor is on (a) when it has backlogged traffic, (b) uplink transmission and (c) ACK reception. Second, for low and moderate sensor ratios, the contention-based approach has higher awake time during high traffic rates because of increased waiting time during contention. Third, when the sensor ratio is high and the traffic rate is high, we observe both the contention-based and contention-free strategies converge in their radio awake time. This is because of the increased data generation in the radio only contention-free strategy.

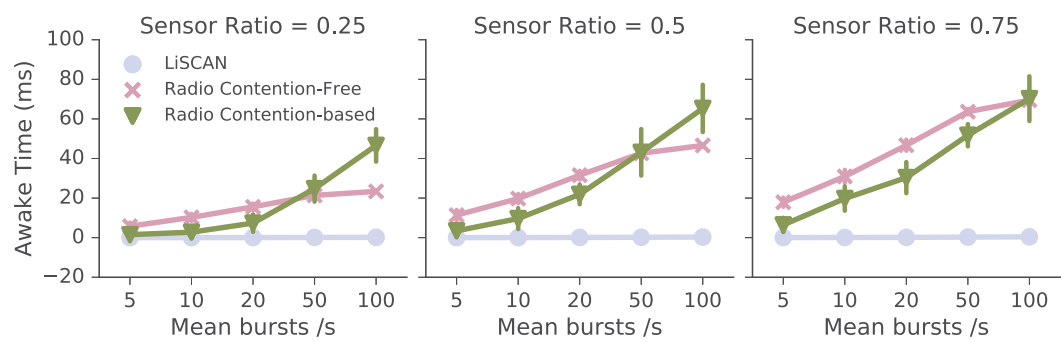


Figure 4.8: Mean energy consumption per active sensor vs traffic burst arrival rates for varying ratios of sensors with traffic.

## Related Work

---

### 5.1 Scalable Directional Multicast at 60 GHz

To the best of our knowledge, this thesis presents the first 60 GHz multicast protocol incorporating the overhead in training and beam grouping.

**Multicast Communication.** Few works have presented algorithms for optimal beam scheduling [58, 59] and beam grouping [60]. With multiple RF chains, users can be localized in distance and angle [60] and beams can be shaped non-symmetrically [58]. In contrast, we focus on multicasting with a single-lobe pattern generation, as it requires only a single RF chain as all state-of-the-art commercial 802.11ad chipsets employ.

**Unicast Beamforming.** A few recent works present solutions to reducing 60 GHz beam training overhead with the objective of establishing a fine beam unicast link. The protocol in [61] optimizes the codewords used in the wider beam levels using signal strength gradient change techniques. In our work, as the training is conducted for all clients at the same time, the gradient changes in the beacon signal strengths could be highly uncorrelated across the different clients thereby preventing gradient-change based optimization. Beamforming techniques are presented in [62] to

---

find a strong unicast link inspite of imperfect quasi-omni patterns. The wider beam training is altogether skipped in [63] by training in legacy Wi-Fi band instead. In our work, the 60 GHz channel gain information even for a wide beam is important in finding an efficient beam group.

**Distributed Multicast.** Distributed peer-to-peer multicast [9, 64, 65] can potentially reduce the transmission time to an order of  $O(\log N)$  where  $N$  is the multicast group size. First, this does not include the quadratic increase in the beam training time as the finest beam level training needs to be conducted between every pair of clients in the multicast group. Second, using all the pairwise beam training information, there is additional complexity involved in the tree construction for the multi-hop multicast scheduling. Third, typically, both the transmission power and number of antennas are lower at the client compared to the AP. Therefore, the AP's antenna gains might not be available for client-to-client communication leading to longer transmission times. Fourth, the latency arising out of random access contention, retransmissions and multi-hop communication might degrade the performance for real-time applications such as high-definition video streaming.

**60 GHz network simulator.** Existing 60 GHz simulation frameworks as in ns-3 [66] do not implement multi-level 60 GHz codebook design and non-linear effects of reflection and blockage. These effects lead to non-monotonicity and unreachability in codebook tree traversal as observed in our measurement study. In contrast, our SDM implementation enables us to incorporate the impact of a multi-level codebook at AP, reflection and blockage effects through our measurements in an indoor conference room environment with several reflective and blockage elements.

## 5.2 Visible Light Communication WLAN with WiFi Uplink

**VLC Only Networks.** A software-defined VLC system including a bi-directional VLC link with On-Off keying modulation is presented in [4]. Likewise, Li-Flame is a commercial VLC system with 10 Mbps downlink up to 3 meters and 10 Mbps uplink via infrared [17]. Moreover, significant progress has been made towards advancing the physical layer of VLC communication for non-laser-based incoherent transmission. For example, the fastest VLC link as of this writing is a custom 3.25 Gbps system based on Single Carrier Frequency Domain Equalization utilizing an RGB LED [67]. Today’s VLC standards such as IEEE 802.15.7 [46] also employ visible light for both the uplink and downlink.

In addition to WLANs, low-power devices with kbps-scale data rate capabilities have been designed for sensor networks and Internet of Things applications. Examples include a novel PHY and VLC MAC layer for energy efficient LED-to-LED communication [3], duplex, battery-free communication using a retro-reflector fabric that backscatters light [68], and OpenVLC, an open source software-based VLC research platform based on BeagleBone [4].

In contrast, LiRa overcomes inherent limitations of infrared or visible light LED-based communication applied to *uplink* WLAN access. Namely, as we experimentally demonstrated in Section 3.4, while the illumination objective of the downlink ensures that the LED transmitters of the AP have wide aperture, large field of view, and high transmit power, LEDs on the client device have none of these benefits [10]. Namely, the limited size, power, and aperture of the mobile client’s LED transmitter can severely constrain field of view, thereby limiting data rate or even breaking the uplink. Consequently, mobility and rotation of user devices might lead to significant

---

throughput reductions or blockages.

**Integrated VLC-RF Networks.** VLC and RF have been jointly used in prior work: VLC was proposed as an additional directional channel to offload RF broadcast traffic in congested networks [69]; load balancing between VLC and RF interfaces was optimized in [70]; horizontal and vertical handover mechanisms between VLC and RF networks were designed in [71]; VLC transmission order was proposed to mirror Wi-Fi transmission order, as the latter will have already resolved contention [72]; routing and address spoofing at the IP layer was demonstrated to integrate VLC and Wi-Fi at layer three [73]. In contrast, LiRa is the first system to integrate VLC and RF at the MAC layer, and hence is the first system to provide a virtual feedback channel for VLC via Wi-Fi. Nonetheless, the aforementioned works are complementary to LiRa and can be used to enhance LiRa at other layers.

**Centralized Scheduling.** In existing centralized scheduling protocols such as 802.11 point coordination function (PCF), the AP polls a single client for data and not the ACK as the ACKs are reserved by the 802.11 mechanism. Also, the AP doesn't have knowledge of clients' backlogged traffic and therefore cannot reserve the channel for fully backlogged traffic from multiple clients. In contrast, in ASMA, the LiRa AP is able to trigger and reserve the channel for the complete duration of fully backlogged VLC feedback transmissions from multiple clients utilizing the downlink VLC scheduling information.

**VLC Services and Devices.** Lastly, there is an emerging body of research on employing VLC for sensing or localization and employing cameras as receivers. For example, a VLC module was designed to locate a user's finger within a workspace with one-centimeter precision [74]. Likewise, a VLC sensing system can reconstruct the 3D human skeleton postures from 2D shadow information [75]. Further, cameras were demonstrated as receivers in [76, 77]. With the addition of photo diode receivers

---

to increase data rate, LiRa can be deployed in parallel with such applications to jointly communicate while also providing such services.

### 5.3 VLC Uni-Directional Control Channel for contention-free radio access

**QoS-aware Scheduling.** Protocols such as Hybrid Coordination Function (HCF) [78] in 802.11e standard have extended 802.11 PCF with QoS-aware scheduling. In such protocols, each traffic flow belongs to a particular traffic category depending on the application and mean QoS requirements. Accordingly, the scheduling is optimized to maximize the QoS metrics. To achieve this QoS-aware scheduling, a separate contention-based period is conducted before the contention-free period to make the AP aware of the sensors' QoS requirements. LiSCAN can work in conjunction with such QoS-aware scheduling algorithms to further improve the contention-free period performance.

**Integrated VLC-RF Networks.** VLC and RF have been jointly used in prior work: VLC was proposed as an additional directional channel to offload RF broadcast traffic in congested networks [69]; load balancing between VLC and RF interfaces was optimized in [70]; horizontal and vertical handover mechanisms between VLC and RF networks were designed in [71]; VLC transmission order was proposed to mirror Wi-Fi transmission order, as the latter will have already resolved contention [72]; routing and address spoofing at the IP layer was demonstrated to integrate VLC and Wi-Fi at layer three [73]. In [20], the authors designed LiRa, the first system to integrate VLC and RF at the MAC layer, and the first system to provide a virtual feedback channel for VLC via Wi-Fi. In contrast, LiSCAN is the first system to design a scalable uni-directional VLC control channel for contention-free RF uplink access. While LiRa

uses VLC for all DL data, LiSCAN does not require this. If the VLC link is slow, then VLC can only be used for fast poll requests. Nonetheless, the aforementioned works are complementary to LiSCAN and can be used to enhance LiSCAN at other layers and other WLAN services.

**VLC Services and Devices.** Lastly, there is an emerging body of research on employing VLC for sensing or localization and employing cameras as receivers. For example, a VLC module was designed to locate a user’s finger within a workspace with one-centimeter precision [74]. Likewise, a VLC sensing system can reconstruct the 3D human skeleton postures from 2D shadow information [75]. Further, cameras were demonstrated as receivers in [76, 77]. With the addition of photo diode receivers to increase data rate, LiSCAN can be deployed in parallel with such applications to jointly communicate while also providing such services.

## CHAPTER 6

# Summary

---

In this thesis, first, I addressed the challenges imposed by directional communication for a scalable multicast service at 60 GHz. I presented SDM, a novel design that includes a scalable training protocol and scalable beam grouping algorithm. Using over-the-air measurements and trace driven simulations, I validated the indoor environment challenges and showed that SDM provides the best performance in comparison to alternative strategies independent of the group size. Second, I presented the design and implementation of LiRa, a WLAN that fuses simplex VLC downlink and bi-directional Wi-Fi on a frame-by-frame basis at the MAC layer. In order for LiRa clients to transmit VLC ARQ feedback via Wi-Fi without excessive contention-based delays, I presented ASMA as a scalable VLC feedback channel over RF. Using over-the-air measurements, I demonstrated limitations of uplink coverage using infrared/VLC. Moreover, I showed that compared to feedback using 802.11-based per-client contention, ASMA's spoofed NAV and multi-client scheduled feedback reduces response delay by a factor of 15 and reduces degradation of Wi-Fi throughput to 3% from 74%. Third, I designed and evaluated LiSCAN, a VLC uni-directional control channel that enables virtual full-duplex contention-free operation of uplink radio access. I showed that LiSCAN utilizes near-zero energy consumption to provide (a)

significant reductions in the radio access delay and (b) 5x improvement in aggregate throughput compared to contention-based radio access.

## References

---

- [1] Y. Zhu, Z. Zhang, Z. Marzi, C. Nelson, U. Madhow, B. Y. Zhao, and H. Zheng, “Demystifying 60GHz outdoor picocells,” in *Proc. of ACM MobiCom*, 2014. 1
- [2] T. S. Rappaport, R. W. Heath Jr, R. C. Daniels, and J. N. Murdock, *Millimeter Wave Wireless Communications*. Pearson Education, 2014. 1
- [3] S. Schmid, J. Ziegler, G. Corbellini, T. R. Gross, and S. Mangold, “Using consumer LED light bulbs for low-cost visible light communication systems,” in *Proc. of the 1st ACM MobiCom workshop on Visible Light Communication Systems*, 2014. 1, 5.2
- [4] Q. Wang, D. Giustiniano, and D. Puccinelli, “OpenVLC: Software-Defined Visible Light Embedded Networks,” in *Proc. of the 1st ACM Workshop on Visible Light Communication Systems*, 2014. 1, 5.2
- [5] G. Cossu, A. M. Khalid, P. Choudhury, R. Corsini, and E. Ciaramella, “3.4 Gbit/s Visible Optical Wireless Transmission Based on RGB LED,” *OSA Optical Express*, vol. 20, no. 26, pp. B501–B506, Dec 2012. 1, 3.1.2, 4.2.2
- [6] D. Tsonev, S. Videv, and H. Haas, “Towards a 100 Gb/s visible light wireless access network,” *OSA Optics Express*, vol. 23, no. 2, pp. 1627–1637, 2015. 1, 3.1.2, 4.2.2
- [7] Y. Ghasempour, C. R. C. M. da Silva, C. Cordeiro, and E. Knightly, “IEEE 802.11ay: Next-Generation 60 GHz Communication for 100 Gb/s Wi-Fi,” *IEEE Communications Magazine*, vol. 55, no. 12, pp. 186–192, December 2017. 1
- [8] M. Choi, G. Lee, S. Jin, J. Koo, B. Kim, and S. Choi, “Link Adaptation for High-Quality Uncompressed Video Streaming in 60-GHz Wireless Networks,” *IEEE Transactions on Multimedia*, vol. 18, no. 4, pp. 627–642, 2016. 1
- [9] J.-H. Kwon and E.-J. Kim, “Asymmetric Directional Multicast for Capillary Machine-to-Machine Using mmWave Communications,” *MDPI Sensors*, vol. 16, no. 4, p. 515, 2016. 1, 5.1

- [10] M. Noshad and M. Brandt-Pearce, “Can visible light communications provide Gb/s service?” *arXiv*, 2013. 1, 1.3, 3.1.1, 5.2
- [11] P. H. Pathak, X. Feng, P. Hu, and P. Mohapatra, “Visible light communication, networking, and sensing: A survey, potential and challenges,” *IEEE Communications Surveys & Tutorials*, vol. 17, no. 4, pp. 2047–2077, 2015. 1, 1.3, 3.1.1
- [12] H.-H. Lee and Y.-C. Ko, “Low Complexity Codebook-Based Beamforming for MIMO-OFDM Systems in Millimeter-Wave WPAN,” *IEEE Transactions on Wireless Communications*, pp. 3607–3612, November 2011. 1.1, 2.1.1, 2.2.2, 2.4.4
- [13] S. Hur, T. Kim, D. Love, J. Krogmeier, T. Thomas, and A. Ghosh, “Multilevel millimeter wave beamforming for wireless backhaul,” in *Proc. of IEEE GLOBECOM*, 2011. 1.1, 2.1.1, 2.2.2
- [14] “Warp project.” [Online]. Available: <http://warpproject.org> 1.1
- [15] IEEE 802.11 Working Group, “IEEE 802.11ad, Amendment 3: Enhancements for Very High Throughput in the 60 GHz Band,” 2012. 1.1
- [16] T. Nitsche, C. Cordeiro, A. B. Flores, E. W. Knightly, E. Perahia, and J. C. Widmer, “IEEE 802.11 ad: directional 60 GHz communication for multi-Gigabit-per-second Wi-Fi,” *IEEE Communications Magazine*, pp. 132–141, Dec 2014. 1.1, 2.2.1
- [17] pureLiFi, “Li-Flame high-speed wireless network solution using VLC.” 1.2, 3.4.1.2, 5.2
- [18] IEEE Computer Society, “IEEE Draft Standard for Local and Metropolitan Area Networks - Specific Requirements - Part 11: Wireless LAN Medium Access Control (MAC) and Physical Layer (PHY),” June 2012. 1.2, 3.1.2, 3.2.2
- [19] A. Khattab, J. Camp, C. Hunter, P. Murphy, A. Sabharwal, and E. Knightly, “WARP: A Flexible Platform for clean-slate Wireless Medium Access Protocol Design,” *ACM SIGMOBILE Mobile Computing and Communications Review*, vol. 12, no. 1, pp. 56–58, 2008. 1.2, 3.3.2
- [20] S. Naribile, S. Chen, E. Heng, and E. Knightly, “LiRa: a WLAN architecture for Visible Light Communication with a Wi-Fi uplink,” in *Proc. of IEEE SECON*, 2017. 1.3, 1.3, 4.2.1, 5.3
- [21] M. A. Al-Maqri, M. Othman, B. M. Ali, and Z. M. Hanapi, “Packet-based Polling Scheme for Video Transmission in IEEE 802.11 e WLANs,” *Elsevier Procedia Computer Science*, vol. 83, pp. 337–344, 2016. 1.3

- 
- [22] R. Viegas, L. A. Guedes, F. Vasques, P. Portugal, and R. Moraes, “A new MAC scheme specifically suited for real-time industrial communication based on IEEE 802.11 e,” *Elsevier Computers & Electrical Engineering*, vol. 39, no. 6, pp. 1684–1704, 2013. 1.3
- [23] A. Jovicic, J. Li, and T. Richardson, “Visible light communication: opportunities, challenges and the path to market,” *IEEE Communications Magazine*, vol. 51, no. 12, pp. 26–32, 2013. 1.3
- [24] J. Chapin and W. Lehr, “Mobile broadband growth, spectrum scarcity, and sustainable competition,” *Proc. of TPRC*, 2011. 1.3
- [25] A. B. Flores, S. Quadri, and E. W. Knightly, “A Scalable Multi-User Uplink for Wi-Fi,” in *Proc. of USENIX NSDI*, 2016. 1.3
- [26] J. S. Ramos, I. Demirkol, J. Paradells, D. Vössing, K. M. Gad, and M. Kasemann, “Towards energy-autonomous wake-up receiver using Visible Light Communication,” in *Proc. of IEEE CCNC*, 2016. 1.3, 4.2.1
- [27] C. Carrascal, I. Demirkol, and J. Paradells, “A novel wake-up communication system using solar panel and Visible Light Communication,” in *Proc. of IEEE GLOBECOM*, 2014. 1.3, 4.2.1
- [28] Y. Ghasempour, N. Prasad, M. Khojastepour, and S. Rangarajan, “Link packing in mmWave networks,” in *Proc. of IEEE ICC*, 2017. 2.1.1
- [29] ——, “Managing Analog Beams in mmWave Networks,” in *Proc. of Asilomar Conference on Signals, Systems and Computers*, 2017. 2.1.1
- [30] J. Zhang, X. Zhang, P. Kulkarni, and P. Ramanathan, “OpenMili: a 60 GHz software radio platform with a reconfigurable phased-array antenna,” in *Proc. of ACM MobiCom*, 2016. 2.1.1
- [31] Y. Ghasempour and E. W. Knightly, “Decoupling Beam Steering and User Selection for Scaling Multi-User 60 GHz WLANs,” in *Proc. of ACM MobiHoc*, 2017. 2.1.1
- [32] N. Instruments, “<http://www.ni.com/white-paper/53095/>.” 2.1.1
- [33] Y. Ghasempour, N. Prasad, M. Khojastepour, and S. Rangarajan, “Novel combinatorial results on downlink mu-mimo scheduling with applications,” in *Proc. of IEEE WONS*, 2017. 2.1.1
- [34] “IEEE Draft Standard for Local and Metropolitan Area Networks - Specific Requirements - Part 11: Wireless LAN Medium Access Control (MAC) and Physical Layer (PHY) Specifications - Amendment 3: Enhancements for Very High Throughput in the 60 GHz Band,” *IEEE P802.11ad/D8.0*, June 2012. 2.1.3, 2.2.2, 2.4.4

- [35] M. K. Haider and E. W. Knightly, “Mobility resilience and overhead constrained adaptation in directional 60 GHz WLANs: protocol design and system implementation,” in *Proc. of ACM MobiHoc*, 2016. 2.1.4, 2.4.4
- [36] S. Sur, V. Venkateswaran, and P. Zhang, X.and Ramanathan, “60 GHz Indoor Networking Through Flexible Beams: A Link-Level Profiling,” in *Proc. of ACM SIGMETRICS*, 2015. 2.1.4
- [37] D. Karabeg and I. Yu, “INF2220: algorithms and data structures Series 9.” 2.3.2
- [38] Vubiq, “V60WGD03 60 GHz Waveguide Development System.” 2.4.1
- [39] N. Anand, E. Aryafar, and E. W. Knightly, “WARPlab: a flexible framework for rapid physical layer design,” in *Proc. of ACM workshop on Wireless of the students, by the students, for the students*, 2010. 2.4.1
- [40] “Analog Devices ADL5565-EVALZ.” 2.4.1
- [41] Cinetics, “Axis360 Pro modular motion control system.” 2.4.1, 3.3.1
- [42] G. Calcev and M. Dillon, “Antenna tilt control in CDMA networks,” in *Proc. of the ACM International Workshop on Wireless Internet*, 2006. 2.4.4
- [43] S. K. Saha, Y. Ghasempour, M. Haider, T. Siddiqui, P. De Melo, N. Somanchi, L. Zakrajsek, A. Singh, O. Torres, D. Uvaydov, J. M. Jornet, E. Knightly, D. Koutsonikolas, D. Pados, and Z. Sun, “X60: A Programmable Testbed for Wideband 60 GHz WLANs with Phased Arrays,” in *Proc. of ACM WinTECH*, 2017. 2.5
- [44] T. Nitsche, G. Bielsa, I. Tejado, and J. Loch, A.and Widmer, “Boon and bane of 60 GHz networks: Practical insights into beamforming, interference, and frame level operation,” in *Proc. of the ACM CoNEXT*, 2015. 2.5
- [45] T. A. Khan, M. Tahir, and A. Usman, “Visible light communication using wavelength division multiplexing for smart spaces,” in *Proc. of IEEE Consumer Communications and Networking Conference (CCNC)*, 2012. 3.1.1
- [46] IEEE Computer Society, “IEEE Standard for Local and Metropolitan Area Networks - Part 15.7: Short-Range Wireless Optical Communication Using Visible Light,” September 2011. 3.1.2, 4.2.2, 5.2
- [47] Philips, “Hue White and Color bulb kit.” 3.3.1
- [48] X. Li, R. Zhang, J. Wang, and L. Hanzo, “Cell-Centric and User-Centric Multi-User Scheduling in Visible Light Communication aided networks,” in *Proc. of IEEE ICC*, 2015. 3.3.3

- [49] J. Zhang, X. Zhang, and G. Wu, “Dancing with light: Predictive in-frame rate selection for visible light networks,” in *Proc. of IEEE INFOCOM*, 2015. 3.3.3
- [50] L. Scialia, J. Widmer, and I. Aad, “On the side effects of packet detection sensitivity in IEEE 802.11 interference management,” in *[Proc. of IEEE WoWMoM*, 2010. 4.3.2
- [51] T. R. Henderson, M. Lacage, G. F. Riley, C. Dowell, and J. Kopena, “Network simulations with the ns-3 simulator,” *SIGCOMM demonstration*, vol. 14, no. 14, p. 527, 2008. 4.4
- [52] G. Pei and T. R. Henderson, “Validation of OFDM error rate model in ns-3,” *Boeing Research Technology*, pp. 1–15, 2010. 4.4.1
- [53] D. Ammar, T. Begin, and I. Guerin-Lassous, “A new tool for generating realistic internet traffic in ns-3,” in *Proc. of 4th International Conference on Simulation Tools and Techniques*, 2011. 4.4.2
- [54] M. E. Crovella and A. Bestavros, “Self-similarity in World Wide Web traffic: evidence and possible causes,” *IEEE/ACM Transactions on Networking*, vol. 5, no. 6, pp. 835–846, 1997. 4.4.2
- [55] J. M. Molina, J. Haase, and C. Grimm, “Energy consumption estimation and profiling in wireless sensor networks,” in *Proc. of VDE ARCS*, 2010. 4.4.3
- [56] M. Abo-Zahhad, M. Farrag, A. Ali, and O. Amin, “An energy consumption model for wireless sensor networks,” in *Proc. of IEEE ICEAC*, 2015. 4.4.3
- [57] W. Du, F. Mieyeville, and D. Navarro, “Modeling energy consumption of wireless sensor networks by systemc,” in *Proc. of IEEE ICSNC*, 2010. 4.4.3
- [58] K. Sundaresan, K. Ramachandran, and S. Rangarajan, “Optimal Beam Scheduling for Multicasting in Wireless Networks,” in *Proc. of ACM MobiCom*, 2009. 5.1
- [59] H. Zhang, Y. Jiang, K. Sundaresan, S. Rangarajan, and B. Zhao, “Wireless multicast scheduling with switched beamforming antennas,” *IEEE/ACM Transactions on Networking*, vol. 20, no. 5, pp. 1595–1607, 2012. 5.1
- [60] H. Park, S. Park, T. Song, and S. Pack, “An Incremental Multicast Grouping Scheme for mmWave Networks with Directional Antennas,” *IEEE Communications Letters*, pp. 616–619, March 2013. 5.1
- [61] B. Li, Z. Zhou, W. Zou, X. Sun, and G. Du, “On the Efficient Beam-Forming Training for 60GHz Wireless Personal Area Networks,” *IEEE Transactions on Wireless Communications*, pp. 504–515, February 2013. 5.1

- [62] K. Hosoya, N. Prasad, K. Ramachandran, N. Orihashi, S. Kishimoto, S. Rangarajan, and K. Maruhashi, “Multiple sector id capture (midc): A novel beamforming technique for 60-ghz band multi-gbps wlan/pan systems,” *IEEE Transactions on Antennas and Propagation*, pp. 81–96, Jan 2015. 5.1
- [63] T. Nitsche, A. B. Flores, E. W. Knightly, and J. Widmer, “Steering with Eyes Closed: mm-Wave Beam Steering without In-Band Measurement,” in *Proc. of IEEE INFOCOM*, 2015. 5.1
- [64] S. Guo, O. W. Yang, and V. Leung, “Tree-based distributed multicast algorithms for directional communications and lifetime optimization in wireless ad hoc networks,” *EURASIP Journal on Wireless Communications and Networking*, vol. 2007, no. 1, pp. 20–20, 2007. 5.1
- [65] J. Wang, M. Song, and Y. Zhao, “Interference-aware multicast in wireless mesh networks with directional antennas,” in *Proc. of IEEE NAS*, 2010. 5.1
- [66] H. Assasa and J. Widmer, “Implementation and Evaluation of a WLAN IEEE 802.11 ad Model in ns-3,” in *Proc. of ACM Workshop on Ns-3*, 2016. 5.1
- [67] Y. Wang, R. Li, Y. Wang, and Z. Zhang, “3.25-Gbps visible light communication system based on single carrier frequency domain equalization utilizing an RGB LED,” in *Proc. of OSA Optical Fiber Communication Conference*, 2014. 5.2
- [68] J. Li, A. Liu, G. Shen, L. Li, C. Sun, and F. Zhao, “Retro-VLC: Enabling battery-free duplex visible light communication for mobile and iot applications,” in *Proc. of ACM HotMobile*, 2015. 5.2
- [69] M. Rahaim, A. Vegni, and T. Little, “A Hybrid Radio Frequency and Broadcast Visible Light Communication System,” in *Proc. of IEEE GLOBECOM Workshop on Optical Wireless Communications*, 2011. 5.2, 5.3
- [70] X. Li, R. Zhang, and L. Hanzo, “Cooperative Load Balancing in Hybrid Visible Light Communications and WiFi,” *IEEE Transactions on Communications*, vol. 63, no. 4, pp. 1319–1329, 2015. 5.2, 5.3
- [71] X. Bao, X. Zhu, T. Song, and Y. Ou, “Protocol Design and Capacity Analysis in Hybrid Network of Visible Light Communication and OFDMA Systems,” *IEEE Transactions on Vehicular Technology*, vol. 63, no. 4, pp. 1770–1778, 2014. 5.2, 5.3
- [72] W. Guo, Q. Li, H. Yu, and J. Liu, “A parallel transmission MAC protocol in hybrid VLC-RF network,” *Journal of Communications*, vol. 10, no. 1, 2015. 5.2, 5.3
- [73] S. Shao, A. Khreishah, M. Ayyash, M. B. Rahaim, H. Elgala, V. Jungnickel, D. Schulz, T. D. C. Little, J. Hilt, and R. Freund, “Design and Analysis of a

- Visible-Light-Communication Enhanced WiFi system,” *OSA Journal of Optical Communications and Networking*, vol. 7, no. 10, pp. 960–973, 2015. 5.2, 5.3
- [74] C. Zhang, J. Tabor, J. Zhang, and X. Zhang, “Extending Mobile Interaction Through Near-Field Visible Light Sensing,” in *Proc. of ACM MobiCom*, 2015. 5.2, 5.3
- [75] T. Li, C. An, Z. Tian, A. T. Campbell, and X. Zhou, “Human Sensing Using Visible Light Communication,” in *Proc. of ACM MobiCom*, 2015. 5.2, 5.3
- [76] R. D. Roberts, “A MIMO protocol for camera communications (CamCom) using undersampled frequency shift ON-OFF keying (UFSOOK),” in *Proc. of IEEE Globecom Workshop on Optical Wireless Communications*, 2013. 5.2, 5.3
- [77] S. Schmid, L. Arquint, and T. R. Gross, “Using Smartphones as Continuous Receivers in a Visible Light Communication System,” in *Proc. of 3rd ACM Workshop on Visible Light Communications Systems*, 2016. 5.2, 5.3
- [78] S. Mangold, S. Choi, P. May, O. Klein, G. Hiertz, and L. Stibor, “IEEE 802.11 e Wireless LAN for Quality of Service,” in *Proc. European Wireless*, vol. 2, 2002, pp. 32–39. 5.3

## Appendix

---

### 7.1 Appendix A

We consider a set of  $B$  wide beams,

$$G = \{(\psi(i_1, j_1)), \dots, (\psi(i_B, j_B))\}, \text{ such that}$$

(i) *Disjoint Client Assignment*: No two beams  $\in G$  have a common client serving set. Mathematically,  $C_{th}(i_a, j_a) \cap C_{th}(i_b, j_b) = \emptyset, 1 \leq a, b \leq B$ ,

(ii) *Multicast Group subset*: The combined set of clients served by the beams  $\in G$  is a subset of the multicast group. Mathematically,  $U_G = \cup_{a=1}^B C_{th}(i_a, j_a) \subseteq \mathbb{U}$ .

We denote the set of clients not served by any of the beams  $\in G$  by  $U_f = \mathbb{U} \setminus U_G$  and they will be served only by the finest beams.

The data sweep time of the sequential unicast can be expressed as

$$\begin{aligned}
T_f &= \sum_{u \in \mathbb{U}} \frac{1}{R(i_u, K)} \\
&= \left( \sum_{a=1}^B \sum_{u \in C_{th}(i_a, j_a)} \frac{1}{R(i_u, K)} \right) + \sum_{u \in U_f} \frac{1}{R(i_u, K)},
\end{aligned} \tag{1}$$

where  $R(i_u, K)$  corresponds to the data rate corresponding to the primary beam  $\psi(i_u, K)$  at  $K$ th (finest) level for client  $u$ . Similarly, for a beam  $\psi(i, j) \in G$ , let the beam group formed when this is the only beam added to  $\mathbb{I}$  along with removal of finest beams that were serving clients  $\in C_{th}(i, j)$ , be denoted by  $\mathbb{B}$ . The data sweep of this beam group is given by

$$T(\mathbb{B}) = \frac{1}{R(i, j)} + \sum_{u \in \mathbb{U} \setminus C_{th}(i, j)} \frac{1}{R(i_u, K)}. \tag{2}$$

Using Equations (1) and (2), we denote the data sweep time difference between the beam group  $\mathbb{B}$  corresponding to the wide beam  $\{\psi(i, j)\}$  and the sequential unicast solution by

$$\begin{aligned}
\delta(\psi(i, j)) &= T_f - T(\mathbb{B}) \\
&= \left( \sum_{u \in C_{th}(i_a, j_a)} \frac{1}{R(i_u, K)} \right) - \frac{1}{R(i, j)}.
\end{aligned} \tag{3}$$

Let  $\text{WIR}(\{\psi(i, j)\})$  be the wide beam improvement ratio of the beam group with a wide beam set consisting of a single wide beam  $\psi(i, j)$ . Then, the data sweep time difference can also be expressed as

$$\begin{aligned}
\delta(\psi(i, j)) &= T_f - T(\mathbb{B}) \\
&= T_f \left( 1 - \frac{1}{\text{WIR}(\{\psi(i, j)\})} \right)
\end{aligned} \tag{4}$$

Now, we would like to calculate the resultant WIR of a beam group  $G^*$  containing all the beams  $\in G$  to serve the client subset  $U_G$  and finest beams to serve  $U_f$ . Firstly, the data sweep time of  $G^*$  is given by

$$T(G^*) = \left( \sum_{a=1}^B \frac{1}{R(i_a, j_a)} \right) + \sum_{u \in U_f} \frac{1}{R(i_u, K)}. \tag{5}$$

Using the Equations (3) and (4), the difference  $\delta(G)$  between the data sweep time of the sequential unicast and  $G^*$  is given by

$$\begin{aligned}
\delta(G^*) &= T_f - T(G^*) \\
&= \sum_{a=1}^B \left( \left( \sum_{u \in C_{th}(i_a, j_a)} \frac{1}{R(i_u, K)} \right) - \frac{1}{R(i_a, j_a)} \right) \\
&= \sum_{a=1}^B \delta(\psi(i_a, j_a)) \\
&= T_f \sum_{a=1}^B \left( 1 - \frac{1}{\text{WIR}(\{\psi(i_a, j_a)\})} \right)
\end{aligned} \tag{6}$$

Using Equation (6), the WIR of  $G^*$  can be expressed as

$$\begin{aligned}
\text{WIR}(G^*) &= \frac{T_f}{T(G^*)} \\
&= \frac{1}{1 - \sum_{a=1}^B \left( 1 - \frac{1}{\text{WIR}(\{\psi(i_a, j_a)\})} \right)} \\
&= \frac{1}{\left( \sum_{a=1}^B \frac{1}{\text{WIR}(\{\psi(i_a, j_a)\})} \right) - (B-1)}
\end{aligned} \tag{7}$$